Biogeochemical controls on ammonium accumulation in the surface layer of the Southern Ocean

Shantelle Smith

A dissertation submitted for the degree of
Master of Science (M.Sc.)
in the Department of Oceanography,
University of Cape Town

Supervisor:	Co-Supervisor:
Dr Katye Altieri	Dr Sarah Fawcett

December 2021

Declaration

I know the meaning of Plagiarism and I declare that this dissertation is my own original work with sources being cited using the Harvard referencing system. No part of this dissertation has been submitted in the past, or is being submitted, for a degree or examination at another university.

The majority of the content of this dissertation has been published as:

> Smith, S., Altieri, K.E., Mdutyana, M., Walker, D.R., Parrott, R.G., Gallie, S., Spence, K.A.M., Burger, J.M., Fawcett, S.E. Biogeochemical controls on wintertime ammonium accumulation in the surface layer of the Southern Ocean. In review, *Biogeosciences Discussions* [preprint], 10.5194/bg-2021-149 (2021).

Permission to use the content of this publication has been provided by the deputy dean for postgraduate studies in the Science faculty at the University of Cape Town and all co-authors support the inclusion of this work in this dissertation.

Supervisor

Dr Katye Altieri (Department of Oceanography University of Cape Town, South Africa)

Co-Supervisor

Dr Sarah Fawcett (Department of Oceanography University of Cape Town, South Africa)

Acknowledgements

I owe my success and submission of this dissertation to those closest to me, without whom I would not have endured the last five years of my postgraduate studies. To my partner in everything, Ruan, you are my favourite and I am so grateful for your unwavering love, joking, and cheerleading. I would not be here without you. To my parents, Dawn and Gert, I am eternally in awe of your unfaltering love and readiness to support anything I have decided to take on. To the other members of my and Ruan's families, especially Iris, Jim, Elaine, and Charné, thank you so much for all of your kind words and distractions when I needed it. To my closest friend, Michelle, I am so glad that, whenever I needed you, you were there.

To my supervisor, Dr Altieri, thank you for guiding me throughout my time in your lab. You have been a kind and understanding mentor and fantastic researcher to learn from.

To my co-supervisor, Dr Sarah Fawcett, I would not have achieved a large portion of my research or professional development without you. I am so grateful for your dedication to helping me get this work published.

To my lab mates, especially Kurt, Jessica, Raquel, Riesna, Heather, Sina, Mhlangabezi, and Mishka, I am so grateful for your friendship and support in the office, lab, and, most of all, at sea.

To the administrative officer at the Department of Oceanography, Cashifa Karriem, you were always ready to go above and beyond to help me with any funding issues or shipping of samples and I'm endlessly grateful. To Hazel Little, for always being ready to help with orders and lab admin.

I am endlessly grateful for the efforts of the captains and crew of the R/V *SA Agulhas II* during the 2017 Winter Cruise, SANAE58 relief voyage, and 2019 SCALE cruises, especially those of Captain Knowledge Bengu.

To Tahlia Henry, other CTD operators, and Sea Technology Services, as well as the chief scientists during all of the cruises I was a part of, Prof. Marcello Vichi, Hermann Luyt, and Thomas Ryan-Keogh, I am grateful for your hard work.

To the R and Python communities online, this project would have been completed in ten+ years without you, and to the food delivery industry in Cape Town, I would have been a very unhappy student without your efforts.

Lastly, I would like to acknowledge the National Research Foundation (NRF) for the funding of my research through an Innovation Scholarship (120105). In addition, I would like to thank

the University of Cape Town, South African Weather Service, NRF South African National Antarctic Programme, and South African Department of Environmental Affairs and Department of Science and Innovation (formerly Department of Science and Technology), for their funding of cruises (R/V *SA Agulhas II*), equipment, and other resources that have made my research possible.

TABLE OF CONTENTS

TABLE OF ABBREVIATIONS

Chemical formulas	
CO_2	Carbon dioxide
NH_3	Ammonia
NH_4^+	Ammonium
$NH_4^{+}{}_{(aq)}$	Aqueous ammonium
$NH_4^{+}{}_{(p)}$	Ammonium aerosol
NO_2^-	Nitrite
NO_3^-	Nitrate
PO_4^{3-}	Phosphate
$Si(OH)_4$	Silicic acid
SiO_4^{4-}	Silicate
Oceanographic terms	
AAIW	Antarctic Intermediate Water
ACC	Antarctic Circumpolar Current
AF	Agulhas Front
ARC	Agulhas Return Current
AZ	Antarctic Zone
Bulk	Cells >0.3 µm in diameter
Chl-a	Chlorophyll-a
MIZ	Marginal Ice Zone
MLD	Mixed Layer Depth
N	Nitrogen
Nano+	Cells >2.7 µm in diameter
$NH_4^{+}{}_{ox}$	Ammonium oxidation rate
NPP	Net Primary Production
OAZ	Open Antarctic Zone
PAZ	Polar Antarctic Zone
PF	Polar Front
PFZ	Polar Frontal Zone
Pico	Cells 0.3-2.7 µm in diameter
POC	Particulate Organic Carbon
PON	Particulate Organic Nitrogen
SACCF	Southern Antarctic Circumpolar Current Front
SAF	Subantarctic Front
SAMW	Subantarctic Mode Water
SAZ	Subantarctic Zone
SB	Southern Boundary
SPF	Southern Polar Front
SST	Sea Surface Temperature
STF	Subtropical Front
STZ	Subtropical Zone
VX	Specific uptake rate of nutrient X
$\delta^{15}N$-*PON*	Stable nitrogen isotopic ratio of particulate organic nitrogen
ρX	Transport rate of nutrient X
C	Carbon

ABSTRACT

The production and assimilation of ammonium (NH_4^+) are essential upper-ocean nitrogen (N) cycle pathways. However, in the Southern Ocean where the alternation between biological nitrate drawdown in summer and physical nitrate resupply in winter is central for setting atmospheric CO_2, the active cycling of NH_4^+ in the seasonally-varying mixed layer remains poorly understood. On a cruise from Cape Town (33.9°S) to the Marginal Ice Zone (MIZ; 61.4°S) in winter 2017, surface samples were collected and analysed for nutrient concentrations, planktonic community composition, size-fractionated rates of net primary production and N (as NH_4^+, urea, and nitrate) uptake, and rates of NH_4^+ oxidation. NH_4^+ concentrations, measured every four hours, were five-fold higher than is typical for summer, and lower north than south of the Subantarctic Front (SAF; 0.01–0.26 µM versus 0.19–0.70 µM). Thus, showing that NH_4^+ accumulates in the Southern Ocean's winter mixed layer, particularly in polar waters. NH_4^+ uptake rates were highest near the Polar Front (PF; 12.9 ± 0.4 nM day^{-1}) and in the Subantarctic Zone (10.0 ± 1.5 nM day^{-1}), decreasing towards the MIZ (3.0 ± 0.8 nM day^{-1}) despite the high ambient NH_4^+ concentrations, likely due to the low temperatures and limited light. By contrast, rates of NH_4^+ oxidation were higher south than north of the PF (16.0 ± 0.8 versus 11.1 ± 0.5 nM day^{-1}), perhaps due to the lower light and higher iron concentrations characteristic of polar waters. Additional NH_4^+ concentration measurements spanning the 2018/2019 annual cycle suggest that mixed-layer NH_4^+ accumulation south of the SAF is due to sustained heterotrophic NH_4^+ production in late summer through winter that outpaces NH_4^+ removal by temperature-, light, and iron-limited microorganisms. The contribution by heterotrophic prokaryotes is supported by observations from winter 2017, where lower ratios of photosynthetic-to-heterotrophic cells were associated with maxima in NH_4^+ concentrations. These observations imply that the Southern Ocean becomes a biological source of CO_2 to the atmosphere in autumn and winter, not only because nitrate drawdown is weak, but also because the ambient conditions favour net heterotrophy and NH_4^+ accumulation. High wintertime surface NH_4^+ concentrations, and the drivers of biological NH_4^+ cycling, may also have implications for nitrate uptake, through inhibition, and for the air-sea flux of ammonia gas, with the latter influencing the formation of aerosols, clouds, and climate.

1 INTRODUCTION

1.1 BACKGROUND

Ammonium (NH_4^+) is an integral component of nitrogen (N) cycling in the ocean's mixed-layer, functioning as an important nutrient for many microorganisms. However, NH_4^+ cycling in the Southern Ocean mixed layer is not yet well understood, particularly in winter – a season assumed to be largely biologically dormant (e.g., Arrigo et al., 2008; Schaafsma et al., 2018) and for which NH_4^+ cycle data are scarce. In contrast to nitrate (NO_3^-), NH_4^+ (and other reduced forms of N) requires less energy by phytoplankton to be assimilated, thus it is often the preferred source of N and is rapidly depleted in the surface ocean to nanomolar concentrations. As a result, surface NH_4^+ concentrations in the Southern Ocean are thought to decrease rapidly following the late summertime peak that results from heterotrophic NH_4^+ production which follows the summertime growing season (e.g., Becquevort et al., 2000; Sambrotto & Mace, 2000). Despite this canonical expectation, there are observations of elevated NH_4^+ concentrations in winter (Bianchi et al., 1997; Philibert et al., 2015; Mdutyana et al., 2020). There are several possible implications for elevated NH_4^+ concentrations in the surface Southern Ocean, including (partial) inhibition of NO_3^- uptake. Additionally, a more thorough characterisation of the NH_4^+ seasonal cycle, and drivers thereof, may aid interpretations of palaeoceanographic records and of ammonia (NH_3) cycling between the surface ocean and lower atmosphere, with the latter having implications for aerosol composition and climate.

1.2 SCOPE OF PROJECT

This dissertation includes data from samples collected during four cruises between Cape Town (33.9°S) and Antarctica (~72°S) (See Sections 3.1 and 3.3). The first of which was conducted in June-July 2017 from Cape Town to the Marginal Ice Zone (61.4°S; MIZ), and, with surface samples that were collected and analysed for nutrient concentrations, planktonic community composition, size-fractionated rates of net primary production and N (as NH_4^+, urea, and NO_3^-) uptake, and rates of NH_4^+ oxidation. These data are used to confirm that NH_4^+ concentrations are high in winter south of the PF, and to investigate the possible causes of wintertime NH_4^+ accumulation. The other three cruises were conducted in 2018-2019 along the Good Hope monitoring line, spanning one full seasonal cycle (a dataset that is the first of its kind in the region). Only the surface NH_4^+ concentrations are shown in this dissertation and they are used to supplement the winter 2017 data and to support the related arguments.

1.3 THESIS AIM

The aim of this dissertation is to use *in situ* data to evaluate a number of potential causes of NH_4^+ accumulation, including a contribution from the residual late-summer NH_4^+ pool, sustained NH_4^+ production in the autumn/winter, and limited NH_4^+ uptake and/or oxidation in winter. The possible drivers and implications of each of these scenarios are then considered. Finally, a hypothesis for the seasonal evolution of the mixed-layer NH_4^+ pool south of the SAF is presented, using *in situ* data collected during a single seasonal cycle.

2 LITERATURE REVIEW

2.1 SOUTHERN OCEAN ZONES

The Southern Ocean impacts the Earth system through its role in global thermohaline circulation, which drives the exchange of heat and nutrients between the Southern Ocean and other major ocean basins (Frölicher et al., 2015; Popp et al., 1999; Sarmiento et al., 2004). The Southern Ocean also plays an integral role in mediating Earth's climate, by transferring carbon to the deep ocean via its biological and solubility pumps (Sarmiento & Orr, 1991; Volk & Hoffert, 1985) and through the release of deep-ocean CO_2 to the atmosphere during deep-water ventilation (i.e., CO_2 leak; Broecker & Peng, 1992; Lauderdale et al., 2013; Sarmiento & Toggweiler, 1984). Upper Southern Ocean circulation is dominated by the eastward-flowing Antarctic Circumpolar Current (ACC) that consists of a series of broad circumpolar bands ("zones") separated by oceanic fronts. Fronts are regions of deep-flowing, highly turbulent jets, including meanders and eddies, and are characterised by large zonal gradients in temperature, salinity, and sea-surface height (Carter et al., 2008; Chapman et al., 2020). Southern Ocean fronts can drive water mass formation (Ito et al., 2010) and upwelling of nutrients that support elevated biological activity (Longhurst, 1998; Sokolov & Rintoul, 2007).

The Agulhas Front (AF) forms at the southern edge of the Agulhas Return Current (ARC) in the Subtropical Zone (STZ) and spans ~15-70°E (Fig. 1; Belkin & Gordon, 1996; Lutjeharms, 1985; Lutjeharms & van Ballegooyen, 1988; Lutjeharms & Ansorge, 2001). High mesoscale activity in the STZ between the AF and Subtropical Front (STF) (Lutjeharms & Valentine, 1988) has been observed to drive elevated levels of biological activity that declines to a minimum in winter (Machu & Garçon, 2001). South of the STF, the Subantarctic Zone (SAZ) is a region of subduction where Subantarctic Mode Water (SAMW) forms (McCartney, 1979). The SAZ is bordered at its southern edge by the Subantarctic Front (SAF) that also forms the northern boundary of the Polar Frontal Zone (PFZ) (Orsi et al., 1995; Tréguer & Jacques, 1992). Antarctic Intermediate Water (AAIW) is formed in the PFZ and subducts at the SAF (Sloyan & Rintoul, 2001). The subduction of SAMW and AAIW is critical for the solubility pump (Daly et al., 2001) and global ocean fertility, with SAMW supplying nutrients to the low-latitude thermocline that support 33-75% of net community production north of 30°S (Marinov et al. 2006; Palter et al., 2010; Sarmiento et al., 2004).

a)

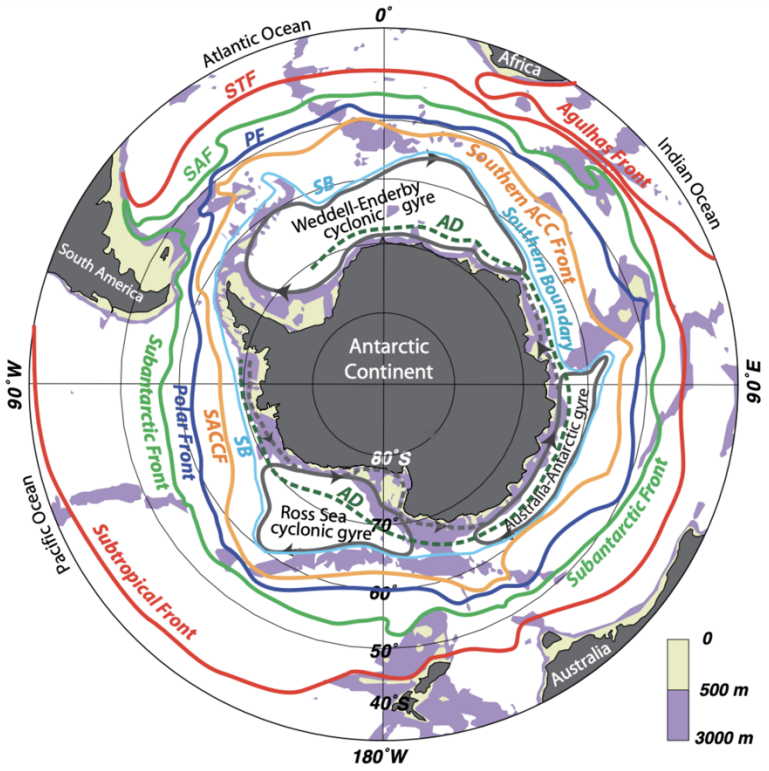

b)

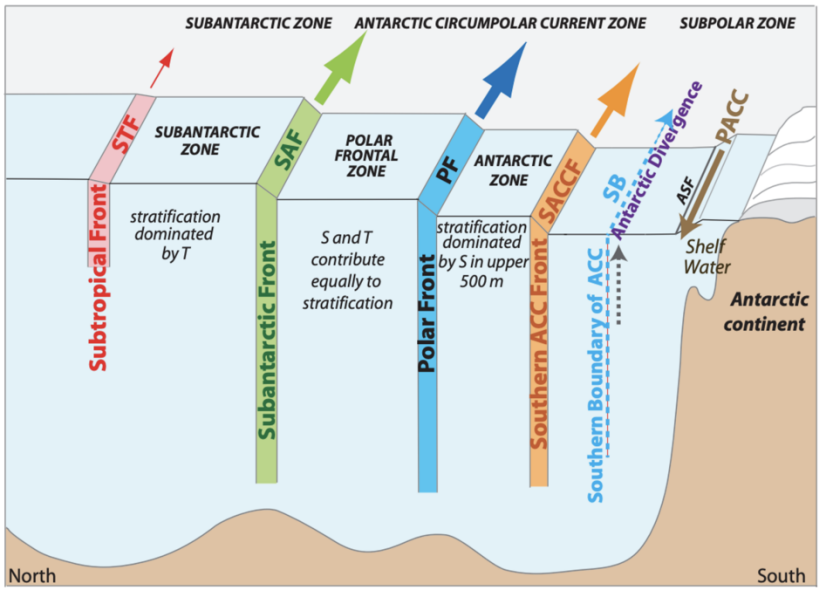

Figure 1: Frontal structure of the Southern Ocean. a) Climatological fronts obtained from selected contours of mean dynamic height from satellite altimetry between 1993-1999. The altimeter products were produced and distributed by Aviso+ (https://www.aviso.altimetry.fr/), as part of the Ssalto ground processing segment. b) Vertical-latitudinal cross section of the Southern Ocean depicting the frontal structure and zones. The Antarctic Slope Front (ASF) and Periantarctic Coastal Current (PACC) are not discussed in this dissertation. Figures taken from Fig. 2-20 and 2-21 from Fieux (2017).

The PFZ is a transition zone between Antarctic and Subantarctic waters and is characterised by high physical variability that results in the formation of eddies (Fig. 1; Emery, 1977; Gordon et al., 1977). The highly turbulent Polar Front (PF), which constitutes the southern boundary of the PFZ, can meander considerably, merging at times with the SAF (e.g., Langlais et al., 2011; Sokolov & Rintoul, 2009) and splitting in some regions into two separate fronts, the PF and the South Polar Front (SPF) (Moore et al., 1999; Pollard et al., 2002). The PF (or SPF in the case of branching) is the northern boundary of the Open Antarctic Zone (OAZ), the northern domain of the Antarctic Zone (AZ) that remains ice-free year round (Orsi et al., 1995). The PF and AZ are particularly important regions for Southern Ocean biogeochemistry where nutrient-rich deep waters upwell, providing nutrients to surface biology (Anderson et al., 2009; Marinov et al., 2006). Maximum upwelling occurs at the Antarctic Divergence due to the interface between the westerly and easterly winds (Fieux, 2017). As a result, the PF and waters near its southern edge, are areas of elevated phytoplankton biomass and chlorophyll-a concentrations (chl-a; >1 μg L^{-1}) throughout the year (Brandini et al., 2000; Tréguer & Jacques, 1992).

The OAZ is bounded to the south by the Southern ACC Front (SACCF), which constitutes the southern edge of the ACC core and is the only front that is not a boundary between distinct surface water masses (Fig. 1; Orsi et al., 1995). South of the SACCF is the southern domain of the AZ, the Polar Antarctic Zone (PAZ). In the west Indian sector of the Southern Ocean, the PAZ encompasses the easternmost reaches of the Weddell Gyre and the MIZ (Orsi et al., 1995), where the latter lies south of the Southern Boundary (SB) of the ACC and is a biologically-active zone of partial sea-ice cover (e.g., Squire, 1998).

2.2 NUTRIENTS AND BIOLOGY IN THE SOUTHERN OCEAN

Concentrations of the essential macronutrients, NO_3^- and phosphate (PO_4^{3-}), are perennially high in Southern Ocean surface waters due to a combination of light and dissolved iron (and at times, silicic acid ($Si(OH)_4$)) limitation of phytoplankton (Hutchins et al., 2001; Martin et al., 1990; Sunda & Huntsman, 1997). Surface NO_3^- and PO_4^{3-} concentrations decrease sharply from south to north across the SAF, while the strongest decline in the silicate (SiO_4^{4-}) concentration occurs further south, near the PF (Brzezinski et al., 2001; Sarmiento et al., 2004; Henley et al., 2020). The decoupling of NO_3^-/PO_4^{3-} and SiO_4^{4-} cycling occurs because heavily-silicified diatoms consume $Si(OH)_4$ and NO_3^- in an anomalously high ratio (>>1:1) south of the PF, which has been attributed to iron limitation (Franck et al., 2000; Takeda, 1998) and/or heavy grazing pressure (Assmy et al., 2013; Smetacek et al., 2004), with a possible contributing role

for the different remineralization length-scales of NO_3^-/PO_4^{3-} (recycled in the shallow subsurface) versus SiO_4^{4-} (regenerated via dissolution from particles rapidly exported to greater depths) (Holzer et al., 2014). As a result, the PFZ separates two distinct communities – carbonate-shell coccolithophores to the north and highly silicified-shell diatoms to the south (Honjo, 2004; Trull et al., 2001).

Primary productivity in the Southern Ocean is limited by numerous (often overlapping) factors, including temperature, light, micronutrient concentrations, and grazing pressure (e.g., Boyd et al., 2001; Martin et al., 1990; Reay et al., 2001; Smith Jr & Lancelot, 2004). These limitations vary with Southern Ocean sector (i.e., longitude), zone (i.e., latitude), and season, resulting in spatial and seasonal variations in chlorophyll-a concentrations, primary production, community composition, and N uptake regime (Arrigo & McClain, 1994; Shadwick et al., 2015; Thomalla et al., 2011; Mengesha et al., 1998; Mdutyana et al., 2020). Sectors and zones can differ in their biogeochemical properties due to the influence of local features (e.g. Drake Passage, islands, hydrothermal vents, sea-ice; e.g. Allison et al., 2010) that provide nutrient inputs or changes to ocean circulation. For example, the AZ is characterized by sparser phytoplankton populations than the PFZ (Mengesha et al., 1998), although AZ spring blooms generally host higher diatom abundances than the blooms of the SAZ and PFZ (Kopczyńska et al., 2007). There is strong seasonality due to large changes in temperature and light availability, resulting from deep mixing, low incident radiation, and cloudiness in winter lowering surface temperatures and light availability (Rintoul & Trull, 2001).

Sub-optimal wintertime conditions severely impede biological activity but deep wintertime mixing is also necessary to replenish nutrients required for the spring/summer bloom period (i.e., wintertime recharge). Once the surface layer stratifies and the mixed layer shoals in spring and summer, phytoplankton begin to consume the available nutrients until some form of limitation (usually iron; Mtshali et al., 2019; Nelson et al., 2001) sets in. This balance between wintertime nutrient recharge and summertime nutrient drawdown is central to the role of the Southern Ocean in setting atmospheric CO_2 (Sarmiento & Toggweiler, 1984) since CO_2 is lost to the atmosphere during the ventilation of vertically-mixed subsurface waters in winter and removed again by photosynthesis in spring and summer. Similarly, SiO_4^{4-} concentrations are at a maximum in winter, although to a larger extent than NO_3^- and PO_4^{3-} concentrations (Pondaven et al., 2000; Weir et al., 2020), which may derive from a seasonal shift in the diatom community composition (Baines et al., 2010), environmental conditions (e.g. temperature;

Lomas et al., 2019), and/or alleviated trace metal limitations which lowers the ratio of silicate-to-nitrate uptake rates (Franck et al., 2000; Takeda, 1998; Timmermans et al., 2004).

As the growing season progresses, iron limitation causes phytoplankton to increase their dependence on recycled NH_4^+ (Timmermans et al., 1998) since NO_3^- assimilation has a significant iron requirement (Morel et al., 1991; Price et al., 1994). The extent to which phytoplankton rely on NO_3^- versus NH_4^+ as their primary N source (i.e., the N uptake regime) has implications for Southern Ocean CO_2 removal since phytoplankton growth fuelled by upwelled NO_3^- (i.e., "new production") must be balanced on an annual basis by the export of sinking organic matter (Dugdale & Goering, 1967), which drives CO_2 sequestration (i.e., the biological pump; Volk & Hoffert, 1985). By contrast, phytoplankton growth on NH_4^+ or other recycled N forms (i.e., "regenerated production") yields no net removal of CO_2 to the deep ocean (Dugdale & Goering, 1967; Eppley & Peterson, 1979). To-date, considerable Southern Ocean research has focused on NO_3^- cycling in the mixed layer because of its importance for the biological pump (e.g., DiFiore et al., 2006; Francois et al., 1992; Johnson et al., 2017; Mdutyana et al., 2020; Primeau et al., 2013; Sarmiento & Toggweiler, 1984; Sigman & Boyle, 2000) and global ocean nutrient distributions (Fripiat et al., 2021; Sarmiento et al., 2004). As a result, the active cycling of regenerated N within the seasonally-varying mixed layer – including the production of NH_4^+ and its consumption via phytoplankton uptake and nitrification – remains poorly understood.

2.3 AMMONIUM AND ITS ROLE IN THE SURFACE OCEAN NITROGEN CYCLE

NH_4^+ is produced in the euphotic zone as a by-product of heterotrophic metabolism (i.e., ammonification; Herbert, 1999) and as a consequence of grazing by zooplankton (through egestion, excretion, and messy feeding; Lehette et al., 2012; Steinberg & Saba, 2008), and is removed by phytoplankton uptake (in euphotic waters) and nitrification (mainly in aphotic waters) (See also Section 5.1). Heterotrophic bacteria can also directly consume NH_4^+ (Kirchman, 1994) and have been hypothesized to do so at significant rates in the Southern Ocean mixed layer in winter (Cochlan, 2008; Mdutyana et al., 2020). NH_4^+ assimilation by phytoplankton, in contrast to NO_3^- consumption, requires relatively little energy (Dortch, 1990) such that NH_4^+ is usually consumed in the surface ocean as rapidly as it is produced (Glibert, 1982; La Roche, 1983), resulting in very low open-ocean NH_4^+ concentrations (<0.2 μM) (Brzezinski, 1988; Paulot et al., 2015). NH_4^+ is often the preferred N source to phytoplankton communities dominated by smaller species, while larger phytoplankton such as diatoms that

invest more energy in nutrient consumption specialize in the assimilation of NO_3^- (e.g., Chisholm, 1992; Fawcett & Ward, 2011). The phytoplankton community typically shifts towards smaller species when iron and/or light are limiting (Pearce et al., 2010; Tagliabue et al., 2014), since a higher cellular surface area-to-volume ratio renders small phytoplankton less vulnerable to diffusion limitation (Hudson & Morel, 1993; Mei et al., 2009; Munk & Riley, 1952) and a larger cell volume limits light absorption efficiency (Finkel et al., 2004; Fujiki & Taguchi, 2002).

In addition to the consequences for small versus large phytoplankton abundance, which has implications for higher trophic levels in the Southern Ocean (Venkataramana et al., 2019), determining the dominant N source to phytoplankton provides a means of estimating their capacity for CO_2 removal, as per the new production paradigm (Dugdale & Goering, 1967). The N isotopic composition ($\delta^{15}N$, in ‰ vs. N_2 in air, = $(^{15}N/^{14}N_{sample}/^{15}N/^{14}N_{air} - 1) \times 1000$) of particulate organic N (PON) can be used to infer the dominant N source to phytoplankton (Altabet, 1988; Lourey et al., 2003; Fawcett et al., 2011; Smart et al., 2020) since the assimilation of subsurface NO_3^- ($\delta^{15}N$ ~5‰; Sigman et al., 2000) yields PON that is higher in $\delta^{15}N$ than that fuelled by recycled NH_4^+ (the $\delta^{15}N$ of which is inferred from the isotopic fractionations associated with its production (e.g., deamination) to be -5 to 0‰; Macko et al., 1986; Silfer et al., 1992; Checkley & Miller, 1989). The $\delta^{15}N$ of PON yields an integrated view of the autotrophic N uptake regime (Fawcett et al., 2011), at times complicated by overlapping processes such as bacterial degradation (Möbius, 2013), while ^{15}N tracer-derived N uptake rates provide an instantaneous measure, often poorly-suited to extrapolation, of the extent of phytoplankton reliance on new versus regenerated N.

During the first step of nitrification, NH_4^+ is oxidised to nitrite (NO_2^-) by chemoautotrophic archaea and bacteria. Nitrification was historically considered unimportant in euphotic zone waters due to the evidence for light inhibition of nitrifiers (Hooper & Terry, 1974; Horrigan & Springer, 1990; Olson, 1981; Schön & Engel, 1962) and competition with phytoplankton for NH_4^+ (Smith et al., 2014; Ward, 1985; Ward, 2005; Zakem et al., 2018). However, this view has been challenged in numerous oceanic regions (e.g., Yool et al., 2007) including the Southern Ocean (Smart et al., 2015; Cavagna et al., 2015; Fripiat et al., 2015), with elevated rates of NH_4^+ oxidation recently observed throughout the winter mixed layer in all major zones of the Southern Ocean (Mdutyana et al., 2020). Wintertime upper-ocean NH_4^+ dynamics thus have implications for annual estimates of carbon export potential, insofar as NO_3^- produced by nitrification in the winter mixed layer that is subsequently supplied to spring/summer

phytoplankton communities constitutes a regenerated rather than a new source of N on an annual basis (Yool et al., 2007; Mdutyana et al., 2020).

Surface concentrations of NH_4^+ and other reduced N forms are often near or below detection in spring and early/mid-summer in the Southern Ocean (e.g., Mdutyana et al., 2020; Daly et al., 2001; Sambrotto & Mace, 2000; Savoye et al., 2004) as NH_4^+ is readily consumed by phytoplankton. In late summer, a peak in NH_4^+ concentration has been observed (Mengesha et al., 1998; Sambrotto & Mace, 2000) and attributed to enhanced bacterial and zooplankton activity following elevated phytoplankton growth (e.g., Becquevort et al., 2000; Dennett et al., 2001; El-Sayed, 1984; Sambrotto & Mace, 2000). One might expect this high-concentration NH_4^+ pool to be quickly depleted given the capacity of phytoplankton for rapid NH_4^+ uptake, leaving the winter mixed layer NH_4^+-deplete. However, the limited available observations suggest that winter mixed-layer NH_4^+ concentrations in the open Southern Ocean are high (often >1 μM), particularly south of the SAF (Bianchi et al., 1997; Philibert et al., 2015; Mdutyana et al., 2020; Henley et al., 2020). If ambient NH_4^+ is not depleted following the late summer peak in its concentration despite the high rates of NH_4^+ uptake and oxidation that have been measured in autumn and winter (Bianchi et al., 1997; Thomalla et al., 2011; Philibert et al., 2015; Mdutyana et al., 2020), then NH_4^+ regeneration must be occurring at an elevated rate, either coincident with wintertime NH_4^+ consumption and/or prior to this in late summer and/or autumn. Under these conditions, the Southern Ocean mixed layer may become net heterotrophic and thus a biological source of CO_2 to the atmosphere.

3 METHODS

3.1 2017 WINTER CRUISE TRACK AND SAMPLE COLLECTION

Samples were collected on the southward (S) and northward (N) legs of a winter cruise between Cape Town, South Africa, and the MIZ of the Southern Ocean onboard the R/V *SA Agulhas II* (VOY25; 28 June to 13 July 2017) (Fig. 2). Leg S crossed the Atlantic sector of the Southern Ocean while leg N bordered the Atlantic and Indian sectors (30°E; WOCE IO6 line). Due to logistical constraints, leg S had only surface underway collections, and leg N consisted of eight conductivity-temperature-depth (CTD) hydrocast stations. Frontal positions were determined using the ship's hull-mounted thermosalinograph and supported by temperature, salinity, and oxygen concentration data from CTD measurements made during leg N. The salinity and oxygen sensors were calibrated against seawater samples that were analyzed for salinity using a Portasal 8410A salinometer and for dissolved oxygen by Winkler titration (Strickland &

Parsons, 1972). The criteria for determining frontal positions included identifying sharp gradients in potential temperature, salinity, potential density, and oxygen concentrations (Belkin & Gordon, 1996; Lutjeharms & Valentine, 1984; Orsi et al., 1995; Park et al., 1993; Pollard et al., 2002 ; Read et al., 2002). For leg N, the mixed layer depth (MLD) was determined for each Niskin (up)cast as the depth between 10 m and 400 m at which the Brunt Väisälä Frequency squared, N^2, reached a maximum (Carvalho et al., 2017).

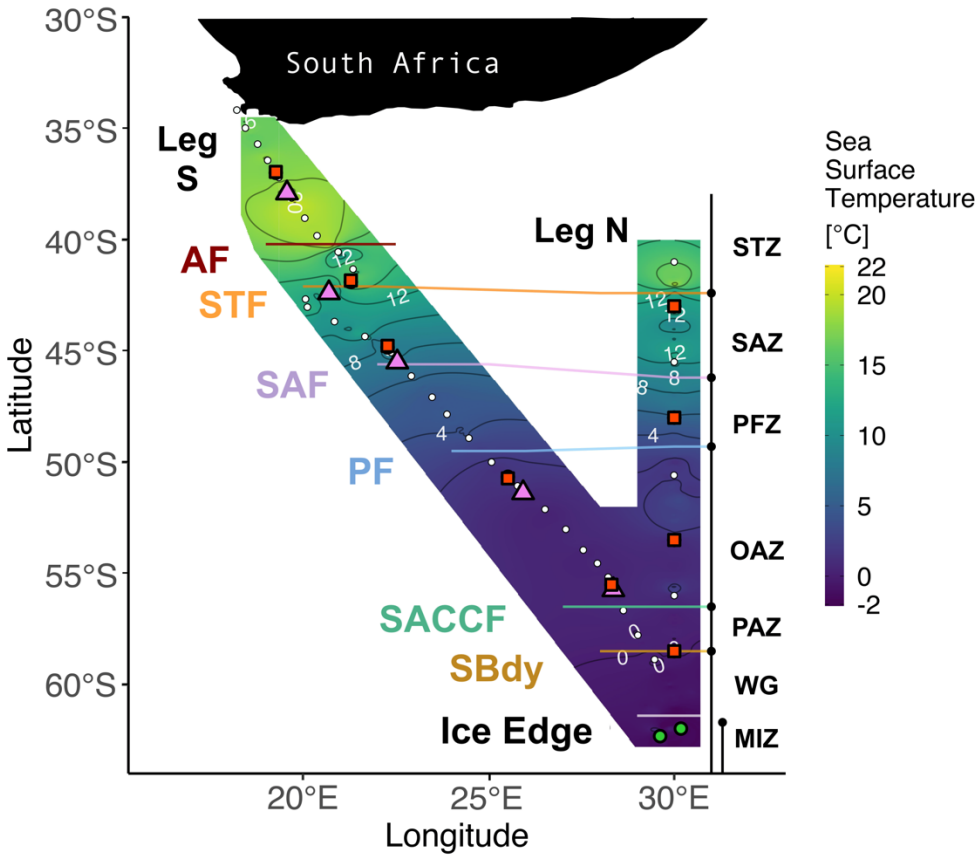

Figure 2: Winter 2017 cruise track overlaid on sea surface temperature (SST) measured by the hull-mounted thermosalinograph. The underway (Leg S) and CTD (Leg N) stations are indicated by white circles. Stations at which net primary production (NPP), nitrogen uptake, and ammonium oxidation experiments were conducted are denoted by red squares. The pink triangles indicate stations where only NPP experiments were conducted while the green circles show stations where only ammonium oxidation was measured. Solid lines indicate the positions of the fronts, identified using temperature and salinity, measurements. Abbreviations for fronts: AF – Agulhas Front (~40.2°S); STF – Subtropical Front (~42.1°S); SAF – Subantarctic Front (~45.6°S); PF – Polar Front (~49.5°S); SACCF – Southern Antarctic Circumpolar Current Front (~56.5°S); SBDY – Southern Boundary (~58.5°S). Abbreviations for zones: STZ – Subtropical Zone; SAZ – Subantarctic Zone; PFZ – Polar

Frontal Zone; OAZ – Open Antarctic Zone; PAZ – Polar Antarctic Zone; WG – Weddell Gyre; MIZ – Marginal Ice Zone. Figure produced using the package ggplot2 (Wickham, 2016).

During leg S, samples were collected every four hours from the ship's underway system (~7 m intake; "underway stations") while samples on leg N were collected from surface (~10 m, approximately 55% light depth) Niskin bottles mounted on the CTD rosette ("CTD stations"). NH_4^+ samples were also taken at 13 depths over the upper 500 m at all CTD stations. At all stations (underway + CTD), ~40 mL of unfiltered seawater was collected for the analysis of NH_4^+ concentrations in duplicate 50 mL high density polyethylene (HDPE) bottles that had been stored ("aged") with orthophthaldialdehyde (OPA) working reagent. Unfiltered seawater was collected in 50 mL polypropylene centrifuge tubes, for the analysis of macronutrients including urea, in duplicate for nitrite (NO_2^-) and PO_4^{3-} and single replicates for NO_3^- and urea. Immediately following collection, NH_4^+ and nutrient samples were stored at -20°C.

Duplicate size-fractionated chlorophyll-a samples were collected by filtering seawater (500 mL) through 25 mm-diameter glass fibre filters with pore sizes of 0.3 µm and 2.7 µm (Sterlitech, GF-75 and Grade D, respectively). Acetone (90%; 5 mL) was added to foil-wrapped borosilicate test tubes containing the filters that were then incubated at -20°C for 24 hours. Additionally, duplicate seawater samples (4 L) were gently vacuum-filtered through combusted 47 mm-diameter, 0.3 µm-pore size GF-75 filters for POC and PON concentrations and δ^{15}N-PON. Filters were stored in combusted foil envelopes at -80°C.

For microscopy, unfiltered seawater samples (250 mL) were collected along leg S in darkened glass bottles and immediately fixed by the addition of 2.5 mL of Lugol's iodine solution (2% final concentration), then stored at low room temperature away from direct sunlight until analysis. Surface seawater samples (~2 mL) were collected in triplicate microcentrifuge tubes for flow cytometry. These samples were fixed with glutaraldehyde (1% final concentration) and stored at -80°C until analysis (Marie et al., 2005; Vaulot et al., 1989).

Ten incubation experiments were conducted during leg S to measure the rate of net primary production (NPP). NH_4^+ and chlorophyll-a samples were collected at the beginning of each experiment as described above. In addition, four NPP experiments were conducted during leg N using seawater collected from Niskin bottles fired at 10 m. In all cases, pre-screened (using 200-µm mesh to remove large grazers) seawater was collected in three 2-L polycarbonate bottles to which $NaH^{13}CO_3$ was added at ~5% of the ambient DIC concentration. ^{13}C enrichment was re-calculated post-cruise using measured DIC concentrations, and these

enrichments were used in all NPP rate calculations. Bottles were incubated on the deck for 5 to 6.5 hours in custom-built incubators shaded with neutral-density screens to mimic the 55% light level (typically encountered between 5 and 10 m) and supplied with running surface seawater. Following incubation, each sample was divided (1 L per size fraction) and gently vacuum filtered through 0.3 μm, and 2.7 μm combusted glass fibre filters that were stored in combusted foil at -80°C until analysis.

N uptake (as NO_3^-, NH_4^+ and urea) and NH_4^+ oxidation experiments were conducted at five stations during leg S using seawater from the ship's underway system, with NH_4^+ oxidation measured at two additional stations at the ice edge (Fig. 2). On leg N, experiments were also conducted using seawater collected from 10 m at the same four CTD stations as the NPP experiments. In all cases, duplicate 1 L polycarbonate bottles were amended with ^{15}N-labeled NO_3^-, NH_4^+ or urea at ~10% of the ambient N concentration, estimated based on past wintertime measurements (Mdutyana et al., 2020) and, in the case of NH_4^+, coincident shipboard analyses. ^{15}N enrichment was re-calculated post-cruise using the measured nutrient concentrations, and these enrichments were used in all rate calculations. Incubations were carried out as described above for NPP. For NH_4^+ oxidation, duplicate black 250 mL HDPE bottles were amended with 0.1 μM $^{15}NH_4^+$ and 0.1 μM $^{14}NO_2^-$ (the latter as a "trap" for the $^{15}NO_2^-$ produced by NH_4^+ oxidation given the expected low ambient NO_2^- concentrations (<0.2 μM; Zakem et al., 2018; Fripiat et al., 2019; Mdutyana et al., 2020). NH_4^+ oxidation bottles were incubated for 24 hours under the same temperature conditions as the N uptake and NPP experiments. Subsamples (50 mL) were collected from each bottle immediately following the addition of $^{15}NH_4^+$+$^{14}NO_2^-$ (T_0) and at the end of the experiments (T_f), and frozen at -20°C until analysis.

3.2 SAMPLE PROCESSING

3.2.1 Ammonium concentrations

NH_4^+ concentrations were measured shipboard following the fluorometric method of Holmes et al. (1999) and using a Turner Designs Trilogy fluorometer 7500-000 equipped with a UV module. The detection limit, calculated as thrice the standard deviation of all blanks, was 0.06 μM. To prevent possible in/efflux of contaminant ammonia (NH_3) due to the temperature difference between winter surface waters and the shipboard laboratory, samples were frozen immediately upon collection and OPA working reagent was subsequently added (8 mL, i.e., ratio of OPA working reagent to sample of 1:5) to the frozen samples prior to defrosting them

for analysis. Samples were frozen for a maximum of 24 hours. Samples were slowly warmed to room temperature in a water bath after OPA addition, incubated in the dark for four hours once defrosted, then each replicate was analysed in triplicate. Standards and blanks were made daily using Type-1 ultrapure Milli-Q water (18 MΩ cm^{-1}; UHP water) from the Milli-Q system onboard the R/V *SA Agulhas II*. Precision was ± 0.03 µM for replicate samples and standards (i.e., the pooled standard error of all samples and standards).

During VOY040 onboard the R/V *SA Agulhas II* in spring (see methods at section 3.3), the possibility for the ship's underway system to have an effect on the NH_4^+ concentrations was examined. Surface samples were collected from the underway (~7 m) and Niskin bottles (~5 m) concurrently. The measured difference between them was 0.07 ± 0.15 µM with no noticeable trend of one collection consistently resulting in higher concentrations.

3.2.2 Macronutrient concentrations

Following the cruise, duplicate seawater samples were analysed manually for NO_2^- and PO_4^{3-} concentrations (Bendschneider & Robinson, 1952; Murphy & Riley, 1962) using a Thermo Scientific Genesys 30 Visible spectrophotometer. Standards and blanks were prepared in UHP water. Precision and detection limit was ± 0.05 µM and 0.05 µM, respectively, for NO_2^-. NO_3^- + NO_2^- concentrations were measured in duplicate using a Lachat QuickChem 8500 Series 2 flow injection autoanalyzer. Aliquots of a certified reference material (JAMSTEC) were measured during each run to ensure measurement accuracy (SD ≤ 2%). The precision of the NO_3^- + NO_2^- and $Si(OH)_4$ measurements was ± 0.4 µM and ± 0.2 µM, respectively, and the detection limit was 0.1 µM and 0.2 µM. The NO_3^- concentration was calculated by subtraction (i.e., $[NO_3^- + NO_2^-] - [NO_2^-]$), with error propagated according to standard statistical practices. Urea-N (hereafter, urea) concentrations were determined according to the room-temperature, single-reagent colorimetric method (Revilla et al., 2005) using a Thermo Scientific Genesys 30 Visible spectrophotometer; precision was ± 0.04 µM and the detection limit was 0.04 µM.

3.2.3 Chlorophyll-a concentrations

Chlorophyll-a concentrations ([chl-a]) were determined shipboard using the nonacidified fluorometric method (Welschmeyer, 1994). The fluorometer was calibrated with an analytical standard (*Anacystis nidulans*, Sigma-Aldrich®) prior to and following the cruise. The [chl-a] of the 0.3-2.7 µm size class (hereafter, "pico" size class) was calculated by subtracting the measured [chl-a] of the >2.7 µm size class (hereafter, "nano+" size class) from the >0.3 µm size class (hereafter, "bulk" size class). It was assumed based on previous work (e.g., Hewes

et al., 1985; 1990; Weber & El-Sayed, 1987) that the wintertime phytoplankton community would be composed primarily of small cells (i.e., typically <15 μm), such that microphytoplankton were not separated from nanophytoplankton.

3.2.4 Bulk POC, PON and δ^{15}N-PON

The NPP and N uptake filters were fumed with hydrochloric acid in a desiccator for 24 hours to remove inorganic C, then dried for 24 hours at 40°C and packaged in tin cups. Filters to be measured for δ^{15}N were dried in the same way as the NPP/N uptake filters, but not acidified. Samples were analysed using a Delta V Plus isotope ratio mass spectrometer (IRMS) coupled to a Flash 260 elemental analyser, with a detection limit of 0.17 μmol C and 0.07 μmol N and precision of ±0.005 At% for C and N. Unused pre-combusted filters (blanks) were prepared with each batch run. POC and PON content was determined from daily standard curves of IRMS area versus known C and N masses. For isotope ratios, sample measurements were standardised to Merck Gel (δ^{15}N = 7.5‰, δ^{13}C = -20.1‰; Merck), Valine (δ^{15}N = 12.1‰, δ^{13}C = -26.8‰; Sigma), Choc (δ^{15}N = 4.3‰, δ^{13}C = -17.8‰), and NH_4Cl (δ^{15}N = -0.6‰), internal laboratory standards calibrated against IAEA reference materials and measured after every 5-7 samples.

3.2.5 Size-fractionated rates of NPP and N uptake

Carbon and N uptake rates (NPP, ρNH_4^+, ρNO_3^-, ρUrea) were calculated according to the equations outlined in Dugdale & Wilkerson (1986) as:

$$\rho M = \frac{[PM]\ x\ (At\%_{meas} - At\%_{amb})}{T\ x\ (At\%_{init} - At\%_{amb})} \quad \text{(Eqn 1)}$$

$$\text{where, } At\%_{init} = \frac{([M]\ x\ At\%_{amb}) + ([M_{tracer}]\ x\ At\%_{tracer})}{[M] + [M_{tracer}]} \quad \text{(Eqn 2)}$$

Here, M is the species of interest (C, NH_4^+, NO_3^-, or urea); ρM is the uptake rate of that species (nM $hour^{-1}$, i.e., nmol N L^{-1} $hour^{-1}$); [PM] is the concentration of POC or PON (μM) on the filters; [M] is the ambient concentration of DIC, NH_4^+, NO_3^-, or urea at the time of sample collection; [M_{tracer}] is the concentration of $NaH^{13}CO_3$, $^{15}NH_4^+$, $^{15}NO_3^-$, or ^{15}N-urea added to the incubation bottles; and T is the incubation period (days). DIC concentrations were measured shipboard using a VINDTA 3C instrument (Bakker et al., 2016) and ranged from 2017 to 2130 μM. The PM and ρM of the pico size class was calculated by subtracting the >2.7 μm-filter measurements (i.e., nano+) from the >0.3 μm-filter (i.e., bulk) measurements. The ρM in nM

411 day^{-1} (i.e., nmol N L^{-1} day^{-1}) was calculated by multiplying the rate in nM hour^{-1} by the number
412 of daylight hours, which was calculated using the latitude and day of the year (Forsythe et al.,
413 1995).

414 The specific carbon fixation rate (V_C) was calculated as ρC/POC and the specific uptake rate
415 of total N (V_{Ntot}) was calculated as $\rho N_{tot}/PON$ (where $\rho N_{tot} = \rho NH_4^+ + \rho NO_3^- + \rho Urea$), to
416 assess the relationship between V_C and V_{Ntot}. The f-ratio (i.e., flux ratio; Eppley & Peterson,
417 1979), used to estimate the fraction of NPP potentially available for export, was then calculated
418 as:

419 $$\mathrm{f-ratio} = \frac{\rho NO_3^-}{\rho N_{tot}} \quad \text{(Eqn 3)}$$

420 No urea uptake experiments were conducted at the underway stations at 50.7ºS and 55.5ºS
421 (both AZ); here, the f-ratio was calculated omitting ρUrea. For the other two AZ stations at
422 which urea uptake was measured, including ρUrea decreased the fraction of new-to-total
423 production by 8-25% compared to f-ratio calculations based on ρNO_3^- and ρNH_4^+ alone.

424 #### 3.2.6 Ammonia oxidation rates

425 The azide method of McIlvin and Altabet (2005) was used to convert NO_2^- deriving from NH_4^+
426 oxidation to N_2O gas that was measured using a Delta V Plus IRMS with a custom-built purge-
427 and-trap front end (McIlvin & Casciotti, 2011). This configuration yields a detection limit of
428 0.2 nmol N with a $\delta^{15}N$ precision of ± 0.1‰. The $\delta^{15}N$ of NO_2^- was derived from $^{45}N_2O/^{44}N_2O$
429 and the rate of NH_4^+ oxidation ($NH_4^+{}_{ox}$; nM day^{-1}) was calculated following Peng et al. (2015)
430 as:

431 $$\mathrm{NH_4^+}_{\mathrm{ox}} = \frac{\Delta[^{15}NO_2^-]}{f_{NH_4^+}^{15} \times T} \quad \text{(Eqn 4)}$$

432 Here, $\Delta[^{15}NO_2^-]$ is the change in the concentration of $^{15}NO_2^-$ (nM) between the start and end of
433 the incubation, calculated as the difference in the measured $\delta^{15}N$ of NO_2^- between the T_f and
434 T_0 samples, $f_{NH_4}^{15}$ is the fraction of the NH_4^+ substrate labelled with ^{15}N at the start of the
435 incubation, and T is the incubation length (days). All $^{15}NO_2^-$ produced during the incubations
436 was assumed to derive from $^{15}NH_4^+$ oxidation. The detection limit ranged from 0.02 to 0.11
437 nM day^{-1}, calculated according to Santoro et al. (2013) and Mdutyana et al. (2020).

3.2.7 Plankton community composition

Microphytoplankton and microzooplankton groups (>15 µm) were identified and counted in a subsample (20 mL) from each 250 mL amber bottle using the Utermöhl technique (Utermöhl, 1958) and following the recommendations of Hasle (1978). Plankton groups and individual species were counted and identified using an inverted light microscope (Olympus CKX41) at 200x magnification.

Cells (<15 µm) were also enumerated using an LSR II flow cytometer (BD Biosciences) equipped with blue, red, violet, and green lasers. Flow cytometric analysis allows for differentiation between autotrophs and heterotrophs that size-fractionated POC/N and microscopy do not, due to overlapping sizes between the groups and to taxonomic complexity, respectively. Here, the focus was on enumerating pico- and nanoplankton. Prior to flow cytometric analysis, 1 mL of each sample was incubated with 10 µL of 1% (v/v) SYBR Green-I, which stains DNA, at room temperature in the dark for 10 minutes (Marie et al., 1997). Based on the detected autofluorescence, the isolated DNA-containing cells were grouped into the following populations: Nano- and picoeukaryotes, and *Synechococcus*. Additionally, small heterotrophic prokaryotes (i.e., bacteria and possibly archaea; hereafter "bacteria") were identified as DNA-containing particles with the lowest detected autofluorescence (Marie et al., 1997; Gasol & del Giorgio, 2000). All particles lacking DNA were considered detritus. The populations of interest were gated using FlowJo 10.3 software (TreeStar, Inc.; www.flowjo.com).

Autofluorescence was detected in the following bandpass filter sets, named for commonly-used fluorochromes: allophycocyanin (APC, 660/20), R-phycoerythrin (PE) (575/25), fluorescein isothiocyanate (FITC) (525/20), PE-cyanine 7 (PE-Cy7) (780/40), PE-Texas Red (610/20), and Pacific Blue (450/50). Background 'noise' was gated out based on the forward and side light scatter values (FSC = 800 and SSC = 200). DNA-containing cells were isolated in each sample based on their detected autofluorescence on the FITC bandpass filter (above a minimal fluorescence threshold of $x10^3$ RFU). Subsequently, based on their detected autofluorescence on the APC bandpass filter relative to the PE bandpass filter, the isolated DNA-containing cells were grouped into the following populations: Nano- and picoeukaryotes, and Synechococcus. Additionally, small heterotrophic cells were identified as containing DNA but with the lowest detected autofluorescence across all bandpass filters, except the FITC (Marie et al., 1997; Gasol & del Giorgio, 2000). For each sample, data acquisition was

terminated when a minimum of 5000 and maximum of 10000 events were recorded. Relative cell sizes were determined using 60 µL of SPHERO™ Blank Calibration Particles, 1.8 – 2.2 µm in diameter, added to 1 mL of selected samples to yield a final concentration of ~$6x10^5$ particles mL^{-1}. Relative to the 1.8 – 2.2 µm calibration beads, nanoeukaryotes were larger than 2.2 µm, picoeukaryotes and heterotrophic cells were smaller than 1.8 µm, and Synechococcus exhibited a range of sizes around 2 µm, with two distinct subgroups; one of ~2 µm in size and another slightly larger than 2.2 µm (Fig. 3). Synechococcus was isolated from the nanoeukaryotes by its pigment characteristics – both subgroups of Synechococcus had high PE relative to APC content (Barlow et al., 1985; Marie et al., 1997), whereas nanoeukaryotes had high APC and PE.

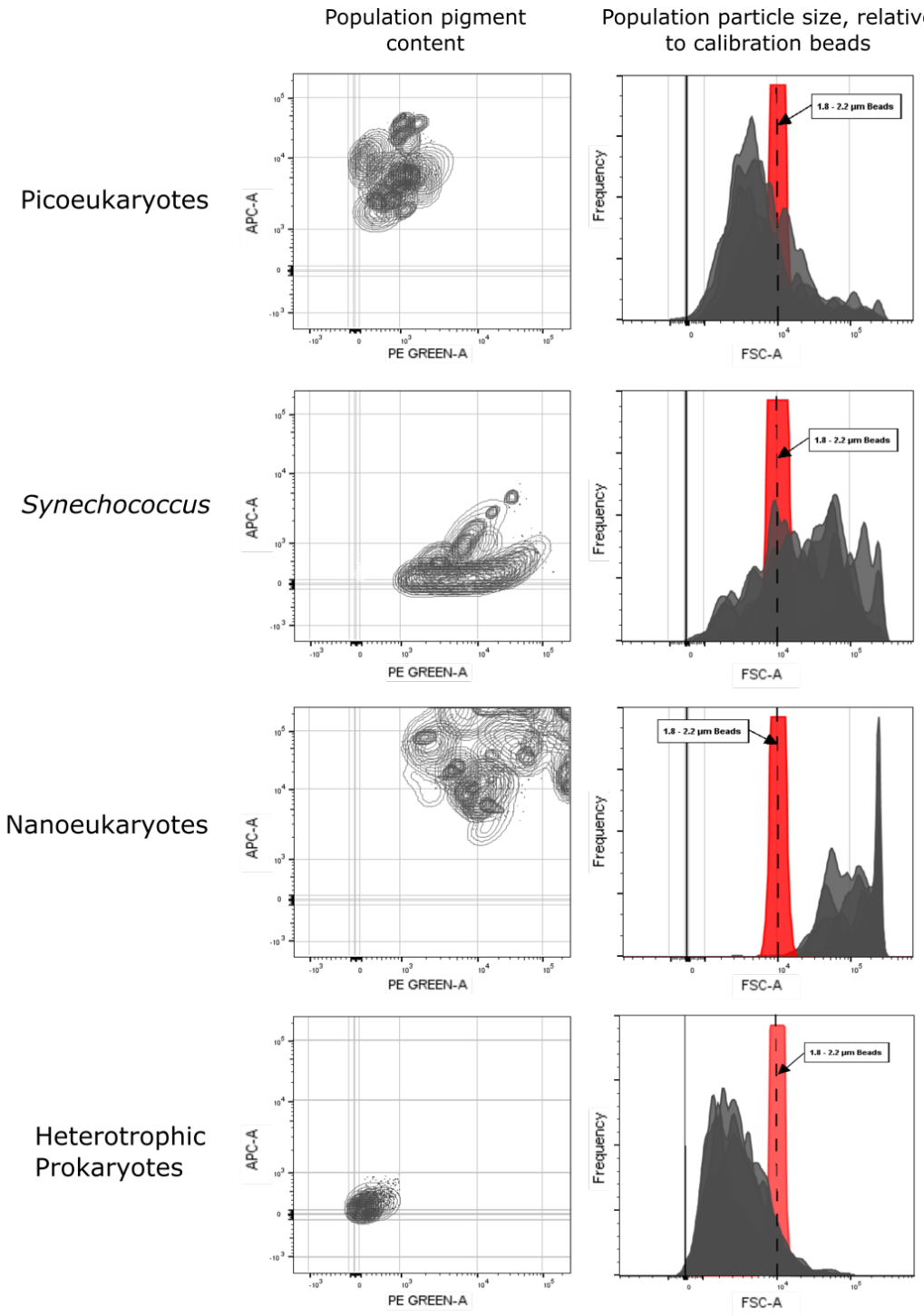

480

481 *Figure 3*: Size distributions (inferred from forward scatter area, FSC-A) of a) heterotrophs, c)
482 nanoeukaryotes, e) picoeukaryotes, and g) *Synechococcus* relative to SPHERO™ Blank Calibration
483 Particles (1.8 – 2.2 µm in diameter; indicated by the red band), and cytograms showing allophycocyanin
484 content (APC-A) relative to phycoerythrin content (PE-A) for the populations of b) heterotrophs, d)
485 nanoeukaryotes, f) picoeukaryotes, and h) *Synechococcus*.

486

In this study, NH_4^+ regeneration (i.e., heterotrophy) was not directly measured. Instead, the abundance of heterotrophic bacteria as a qualitative indicator of NH_4^+ regeneration potential was used, recognizing that cell abundance does not imply activity. The availability of organic matter to heterotrophs was inferred from the abundance of detritus.

3.3 2018/19 SEASONAL CYCLE

3.3.1 Surface ocean NH_4^+ concentrations

To contextualize the 2017 wintertime observations, the seasonality of the NH_4^+ pool in the surface Southern Ocean in 2018/19 was explored. Surface NH_4^+ concentrations were measured during three additional cruises in the Atlantic sector (December 2018-March 2019, early- and late summer; July-August 2019, winter; October-November 2019, spring; Fig. 4a-e). During these cruises, underway samples were collected for analysis of NH_4^+ concentrations every two hours between Cape Town and Antarctica (early- and late summer) or the MIZ (winter and spring) and were analysed as described in section 3.2.1 for winter 2017. However, in contrast to the method in 3.2.1, here the matrix effect was calculated using the standard addition method (Saxberg & Kowalski, 1979) and equations outlined in Taylor et al. (2007). One standard and one sample duplicate was used for the matrix effect calculation during each analysis of seawater samples. The matrix effect is created by the difference in fluorescence of seawater and UHP water of the samples and standards, respectively. The calculation corrects the concentration to account for salts in seawater, such that the final concentration is typically higher than what was measured, since the salts absorb and scatter some of the fluorescence and thus minimise the fluorescence received by the sensor. The matrix effect correction was not applied to the winter 2017 data.

In early (2018) and late (2019) summer, the NH_4^+ concentrations had a detection limit of 0.05 µM and precision of ±0.03 µM and the matrix effect was always <40% (average 4±24%). In winter 2019, NH_4^+ concentrations had a detection limit of 0.01 µM and precision of ±0.06 µM and the matrix effect was always <13% (average 11±2%). While in early and late spring of 2019, NH_4^+ concentrations had a detection limit of 0.04 µM and precision was ±0.07 µM and the matrix effect was always <21% (average 10±8%). The average matrix effect for all six

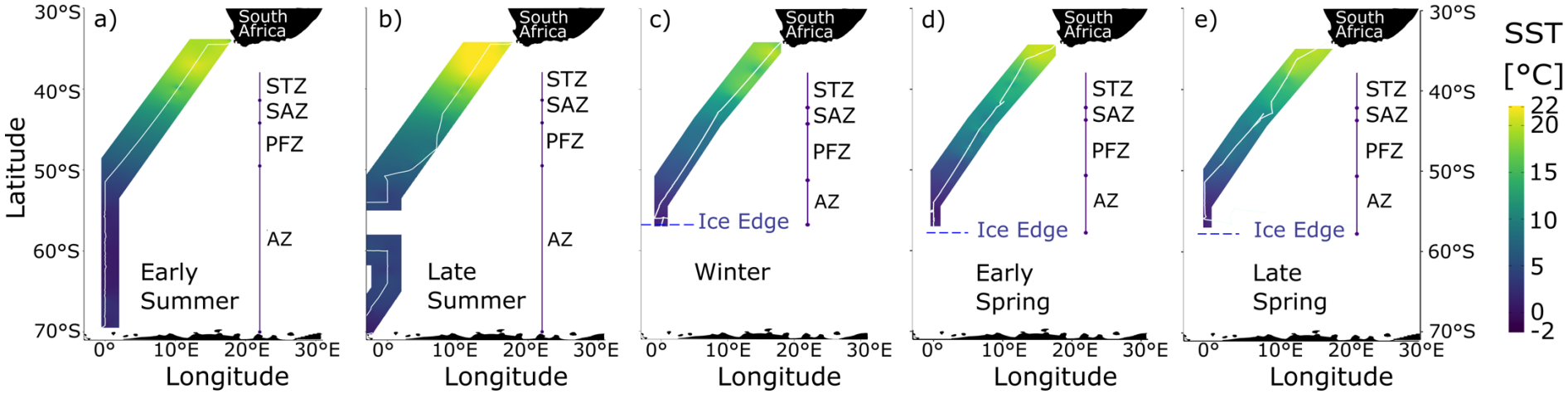

Figure 4: Cruise tracks for a) summer 2018-2019, b) winter 2019, and c) spring 2019 overlaid on sea surface temperature (SST) measured by the ship' s thermosalinograph. Solid lines indicate the positions of the fronts. Abbreviations as in Figure 2, with AZ referring to the combined OAZ and PAZ. Figure produced using the package ggplot2 (Wickham, 2016).

transects in 2018/19 was 8±15%. Six out of 34 matrix effect measurements resulted in a matrix effect less than zero (average of -19±15%), thereby decreasing the NH_4^+ concentration of related samples. Excluding these six experiments, yields an average matrix effect for all six transects of 14±7%.

3.3.2 Mixed-layer NH_4^+ residence time and NH_4^+ production rate estimates

The residence time of the NH_4^+ pool was determined using the measured ambient NH_4^+ concentrations and corresponding NH_4^+ consumption rates ($NH_4^+{}_{consumption\ rate} = \rho NH_4^+ + NH_4^+{}_{ox}$ in winter and $NH_4^+{}_{consumption\ rate} = \rho NH_4^+$ in late summer; ρNH_4^+ is the rate of ammonium uptake and $NH_4^+{}_{ox}$ is the rate of ammonium oxidation – see Eqn 1, 2, and 3):

$$NH_4^+{}_{residence\ time} = \frac{[NH_4^+]}{NH_4^+{}_{consumption\ rate}} \quad \text{(Eqn 5)}$$

Where $NH_4^+{}_{residence\ time}$ is the number of days over which a given NH_4^+ concentration, $[NH_4^+]$ in nM, would be depleted assuming a constant $NH_4^+{}_{consumption\ rate}$, in nM day^{-1}.

To determine the contribution of late summer to the wintertime NH_4^+ pool, a rate of decline is defined as $NH_4^+{}_{rate\ of\ decline} = NH_4^+{}_{production\ rate} - NH_4^+{}_{consumption\ rate}$. The $NH_4^+{}_{production\ rate}$ is estimated as the flux required to compensate for NH_4^+ consumption over the late-summer-to-winter period, to yield the observed seasonal change in the ambient NH_4^+ concentration. The equations below assume that the elevated wintertime NH_4^+ concentrations result from continuous NH_4^+ production and consumption rather than from sporadic events of consumption and/or production occurring between late summer and winter.

Since $$NH_4^+{}_{rate\ of\ decline} = NH_4^+{}_{production\ rate} - NH_4^+{}_{consumption\ rate} \quad \text{(Eqn 6)}$$

And $$t = \frac{[NH_4^+]_{decline}}{NH_4^+{}_{rate\ of\ decline}} \quad \text{(Eqn 7)}$$

Then,

$$NH_4^+{}_{production\ rate} = \frac{[NH_4^+]_{decline}}{t} + NH_4^+{}_{removal\ rate} \quad \text{(Eqn 8)}$$

$[NH_4^+]_{decline}$ is the difference between the late summer and winter 2019 NH_4^+ concentrations in nM, *t* is the time period in days between late summer and winter.

3.4 STATISTICS AND FIGURES

The correlations among latitude, N concentrations, inorganic carbon and N uptake rates, and NH_4^+ oxidation rates were investigated at the 5% significance level using the Pearson

correlation coefficient and the R packages, stats (R Core Team, 2020) and corrplot (Wei & Simko, 2017). Standard deviations were propagated using standard practices.

Figures were produced in R (R Core Team, 2017) using the ggplot2 (Wickham, 2016), abind (Plate & Heiberger, 2016), ggpubr (Kassambara, 2019), lubridate (Grolemund & Wickham, 2011), metR (Campitelli, 2019), mgcv (Wood, 2017), and scales (Wickham & Seidel, 2020) R packages. Seabird CTD and SDS data was processed using the oce package (Kelley & Richards, 2018). Interpolation of the data using multilevel B-splines, which was required for surface maps, was produced using the mba.surf function (MBA package; Finley et al., 2017). Figures were made using the.

4 RESULTS

4.1 HYDROGRAPHY

Sea surface temperature (SST) decreased from Cape Town (~34°S) to the edge of the MIZ (61.7°S) by ~17°C with similar gradients for leg S and N (Fig. 2). During leg N, fairly deep MLDs were observed (124-212 m), similar to June and July climatological MLDs compiled from Argo float data for this region (Dong et al., 2008). While the focus of this study is the surface (i.e., upper ~10 m), the hydrography of the mixed layer is described to demonstrate that sampling took place under conditions typical of winter, with the deep MLDs evincing ongoing wintertime mixing and associated nutrient recharge. Where not specified, the trends discussed below refer to the surface data only. For each parameter, the average ± 1 standard deviation (SD) calculated for each Southern Ocean zone is reported in Table 1.

Table 1: Mean (± 1 SD) of surface ocean POC, PON, chl-a, and nutrient concentrations, cell abundances, and nutrient uptake rates measured in each zone of the Southern Ocean in winter 2017. Where no SD is given, only one sample was measured. The >0.3 µm and >2.7 µm size fractions are referred to as "bulk" and as "nano+", respectively, as defined in section 3.2.3. The percentage of the total by the >2.7 µm (nano+) size fraction shown for chl-a, POC, and PON, is the average of the percentage contribution calculated for each station within a zone. ND – no data available. Abbreviations as in Figure 2.

	STZ	SAZ	PFZ	OAZ	PAZ
NH_4^+ (µM)	0.08±0.03	0.06±0.01	0.42±0.01	0.52±0.01	0.58±0.01
PO_4^{3-} (µM)	0.44±0.07	0.90±0.06	1.59±0.1	2.00±0.13	1.99±0.09
NO_3^- (µM)	3.6±0.2	10.5±0.5	21.5±0.2	26.7±0.4	27.5±0.4
$Si(OH)_4$ (µM)	2.6±0.1	2.5±1.8	6.6±0.1	40.3±0.5	45.0±0.8
NO_2^- (µM)	0.15±0.02	0.13±0.02	0.17±0.02	0.19±0.01	0.21±0.02
Urea (µM)	0.23±0.04	0.11±0.04	0.26±0.08	0.24	0.21±0.03
chl-a (bulk) (µg L^{-1})	0.65±0.08	0.43±0.05	0.35±0.03	0.25±0.02	0.21±0.00
chl-a (nano+) (µg L^{-1})	0.50±0.05	0.30±0.04	0.24±0.02	0.18±0.02	0.17±0.02
chl-a (pico) (µg L^{-1})	0.15±0.1	0.13±0.07	0.11±0.04	0.06±0.03	0.04±0.02
chl-a (% of nano+)	77.5±13.9	73.1±10.9	69.8±8.7	76.7±11.3	80.1±8.5
POC (bulk) (µM)	4.4±6.7	3.4±0.4	3.2±0.3	3.4±0.5	3.5+0.2
POC (nano+) (µM)	2.6±0.5	2.6±0.4	1.9±1.2	1.9±0.4	4.6
PON (bulk) (µM)	0.6±0.2	0.5±0.1	0.4±0.1	0.5±0.1	0.5±0.1
PON (nano+) (µM)	0.3±0.1	0.3±0.1	0.2±0.3	0.2±0.1	0.4±0.0
POC (% of nano+)	79.7±24.6	79.6±19.0	50.9±33.2	77.2±21.8	ND
PON (% of nano+)	69.0±31.9	67.1±17.2	53.8±24.1	67.0±21.9	51.1±24.7
POC:chl-a (g g^{-1})	103.0±22.1	102.5±14.4	122.5±11	234.1±29.2	219.3±1.0
POC:PON (M/M)	7.81±6.49	6.90±1.25	7.13±0.71	6.72±1.62	5.80±3.75
δ^{15}N-PON	1.4±0.9	1.2±1.0	0.3±0.5	-1.3±0.5	-1.3±0.4

Table 2: continued

	STZ	SAZ	PFZ	OAZ	PAZ
NPP (bulk) (nM day^{-1})	497.1±42.4	277.5±21.3	289.7±19.2	85.3±26.1	27.7±0.2
NPP (nano+) (nM day^{-1})	384.7±29.7	178.2±23.4	193.5	49.6±5.0	ND
ρNH$_4^+$ (bulk) (nM day^{-1})	5.7±0.8	8.9±1.1	12.9±0.4	4.8±0.1	3.0±0.8
ρNH$_4^+$ (nano+) (nM day^{-1})	4.0±1.1	4.1±1.2	4.2±4.7	3.1±0.4	ND
ρNO$_3^-$ (bulk) (nM day^{-1})	4.1±0.4	11.5±1.4	5.9±1	3.6±0.4	3.7±1.8
ρNO$_3^-$ (nano+) (nM day^{-1})	3.4±0.3	6.6±0.4	4.3±0.4	2.6±0.8	2.7±1.2
ρUrea (bulk) (nM day^{-1})	7.5±0.6	6.9±0.3	6.5±1.0	2.1±0.3	0.6±0.01
ρUrea (nano+) (nM day^{-1})	4.9±0.3	3.8±0.2	4.0±0.6	1.3±0.2	0.7±0.4
f-ratio (bulk) (including ρUrea)	0.21±0.31	0.43±0.11	0.23±0.18	ND	0.51±0.53
f-ratio (bulk) (excluding ρUrea)	0.43±0.32	0.57±0.12	0.31±0.18	0.43±0.16	0.55±0.54
NH$_4^+$ox (nM day^{-1})	9.3±0.5	12.9±0.6	11.1	17.7±0.6	14.3±1.0
Total microplankton (cells mL^{-1})	13±11	5±3	9±3	6±6	4±2
Centric diatoms (cells mL^{-1})	<1	<1	<1	<1	1±2
Pennate diatoms (cells mL^{-1})	2±4	<1	2±1	2±3	<1
Dinoflagellates (cells mL^{-1})	7±6	4±0	6±2	3±2	2±0
Micro-zooplankton (cells mL^{-1})	4±3	<1	2±2	1±2	<1
Nanoeukaryotes (cells mL^{-1})	ND	2.2±1.4 E+03	1.5±0.7 E+03	1.6±0.7 E+03	1.4E+03
Picoeukaryotes (cells mL^{-1})	ND	4.5±2.9 E+03	4.9±3.7 E+03	1.5±0.5 E+03	8E+02
***Synechococcus* (cells mL^{-1})**	ND	3.8±1.8 E+03	2.3±1.1 E+03	1.4±0.2 E+03	1E+03
Heterotrophic prokaryotes (cells mL^{-1})	ND	4.5±3.2 E+03	2.3±1.2 E+03	2.1±2.3 E+03	3.2E+03
Detritus (particles mL^{-1})	ND	38.2±14.9 E+03	63.8±42.9 E+03	25.7±18.6 E+03	2.57E+04

4.2 MACRONUTRIENT CONCENTRATIONS

The surface and mixed-layer concentrations of NH_4^+ ranged from below detection to 0.70 µM along legs S and N (Fig. 5a and b). The surface concentrations were higher in the PFZ, OAZ, and PAZ (0.42 ± 0.01 µM, 0.52 ± 0.01 µM, and 0.58 ± 0.01 µM, respectively) than in the Subtropical Zone (STZ) and SAZ (0.08 ± 0.03 µM and 0.06 ± 0.01 µM, respectively), with a sharp gradient observed in the PFZ, just south of the SAF. South of the SAF, high NH_4^+ concentrations persisted near-homogeneously throughout the mixed layer, ranging from 0.65 ± 0.01 µM at station 58.5°S to 0.27 ± 0.01 µM at station 48.0°S, with concentrations that were below detection north of the SAF (Fig. 5b). Beneath the mixed layer, the NH_4^+ concentration decreased rapidly at all stations to values below detection by 200 m.

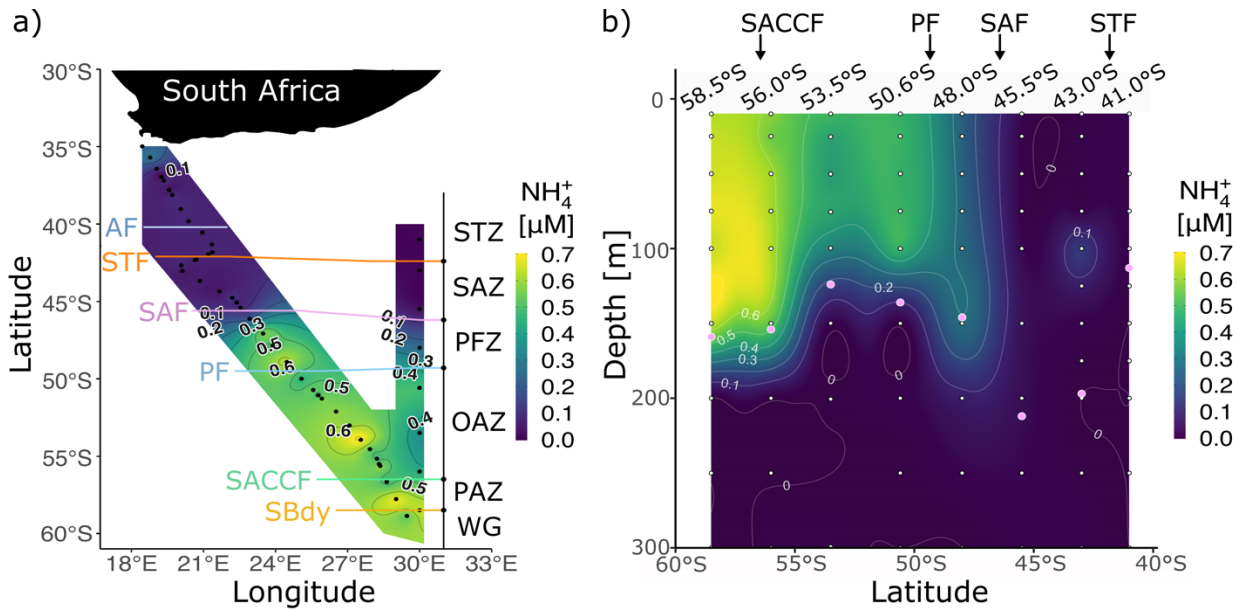

Figure 5: Concentrations of dissolved ammonium (NH_4^+) a) at the surface for Legs S and N and b) with depth for Leg N. Pink circles in panel b show the mixed layer depth at each CTD station. Abbreviations as in Figure 2. Figure produced using the package ggplot2 (Wickham, 2016).

The concentrations of NO_3^- and PO_4^{3-} increased southwards from <10 µM and <1 µM, respectively, in the STZ to >20 µM and >1.5 µM, respectively, in the PFZ, OAZ, and PAZ (Fig. 6a and b), with the sharpest gradients occurring near the SAF. The concentrations of $Si(OH)_4$ increased rapidly across the PF, from an average of 3.2 ± 1.1 µM between 35.0°S and 48.0°S to 45.6 ± 0.6 µM between 52.1°S and 58.9°S (Fig. 6c). The NO_2^- concentrations were consistently low across the transect (0.16 ± 0.02 µM; Fig. 6d), as were the concentrations of urea (0.20 ± 0.04 µM, Table 1), although slightly lower urea concentrations were observed in the SAZ than in the other zones.

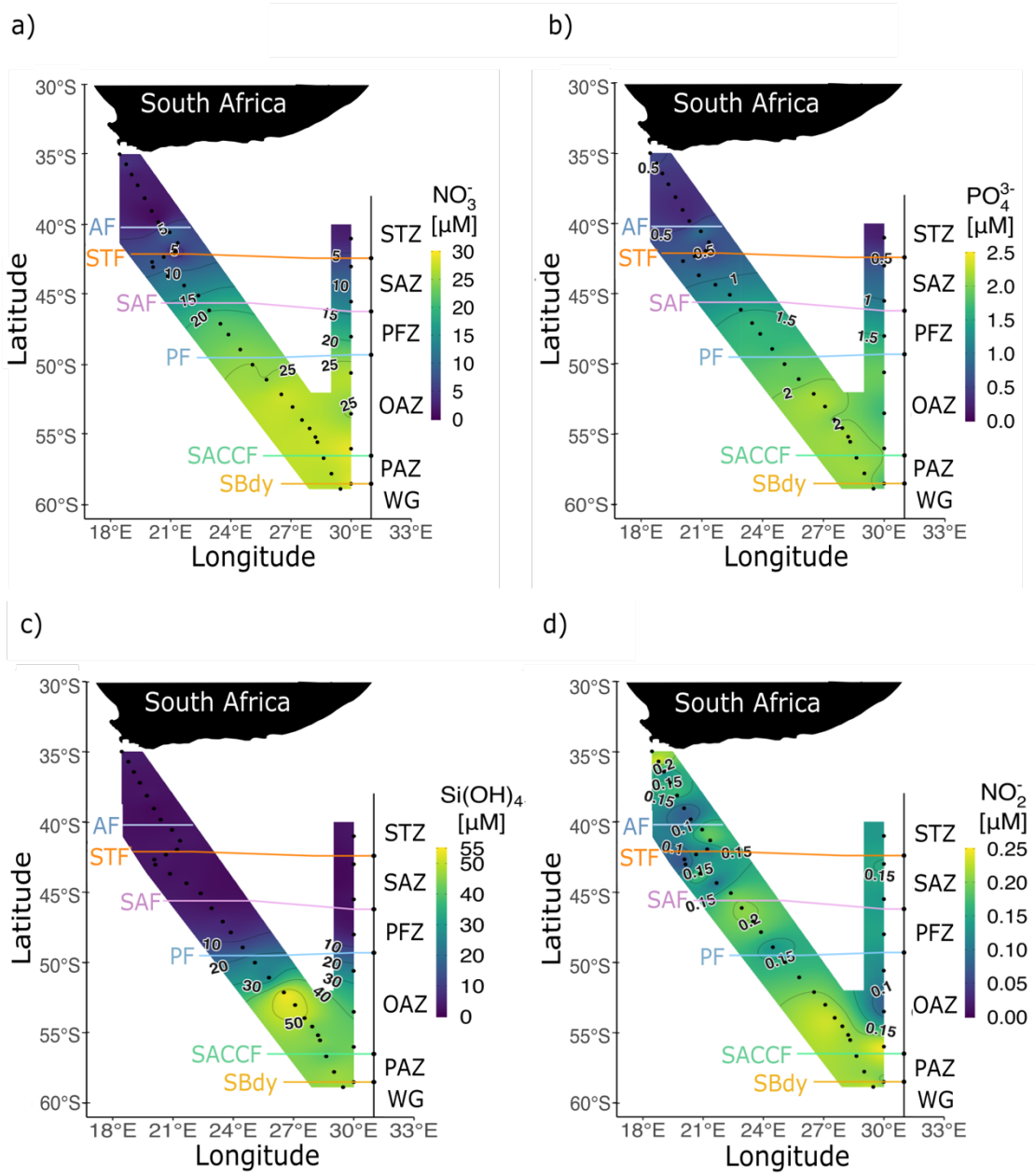

Figure 6: Surface concentrations of dissolved a) nitrate (NO_3^-), b) phosphate (PO_4^{3-}), c) silicic acid ($Si(OH)_4$), and d) nitrite (NO_2^-) during Legs S and N. Abbreviations are as in Figure 2. Figure produced using the package ggplot2 (Wickham, 2016).

4.3 CHLOROPHYLL-A, POC AND PON

The highest bulk (i.e., >0.3 µm) [chl-a] was observed near the South African continental shelf, decreasing across the STF and remaining low thereafter (Fig. 7a), consistent with previous autumn and winter studies (Froneman et al., 1999; Philibert et al., 2015; Scharek et al., 1994). The proportion of chl-a in the nano+ size class varied across the region but was >50% at all stations, with higher (>80%) contributions near the fronts and at many OAZ and PAZ stations

609 (Fig. 7b). The nano+ contribution was ≤60% at only five stations (three in the SAZ, two in the
610 OAZ).

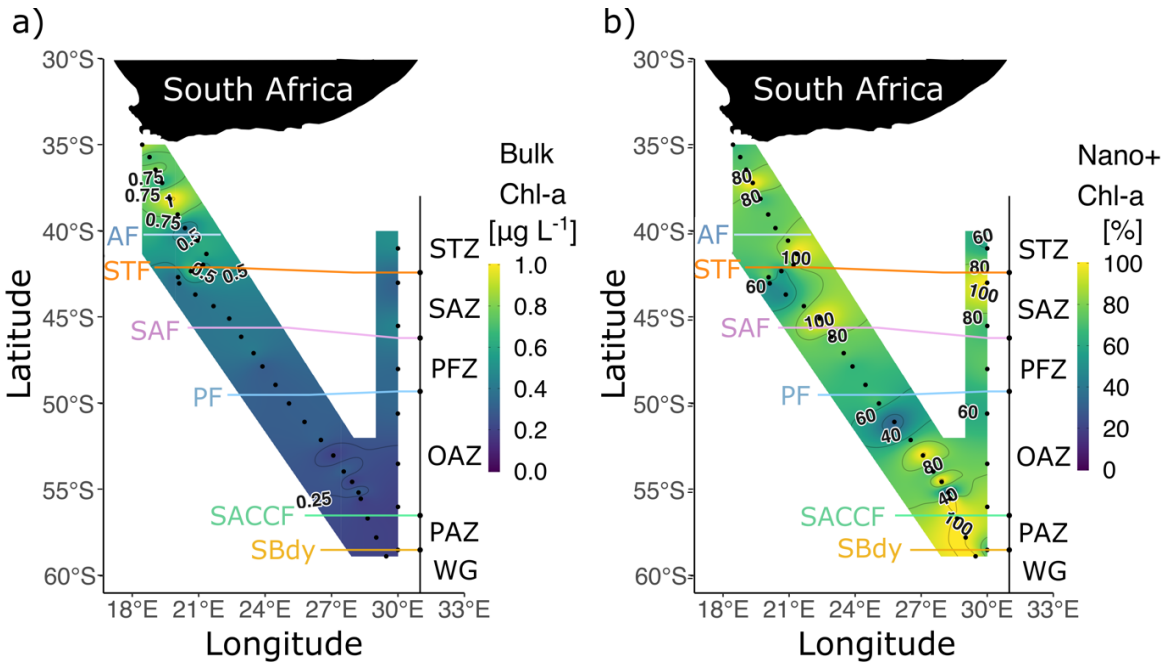

611

612 *Figure 7*: a) Bulk (>0.3 µm) chlorophyll-a (chl-a) concentrations and b) proportion of chlorophyll-a in
613 the >2.7 µm size fraction (i.e., nanophytoplankton; % of total bulk chl-a) at the surface for Legs S and
614 N. Abbreviations as in Figure 2. Figure produced using the package ggplot2 (Wickham, 2016).

615 The concentrations of bulk POC and PON were highest north of the STF and slightly higher in
616 the OAZ than in the SAZ and PFZ (Fig. 8a and b). The contribution of the nano+ size fraction
617 to POC and PON across the transect was 77.1 ± 22.6% and 66.9 ± 24.2%, respectively (Fig. 8c
618 and d). The δ^{15}N-PON also decreased southwards from the STZ and SAZ to the PFZ and OAZ
619 (Fig. 9). Despite considerable differences among zones, the δ^{15}N-PON was relatively
620 homogenous within each zone.

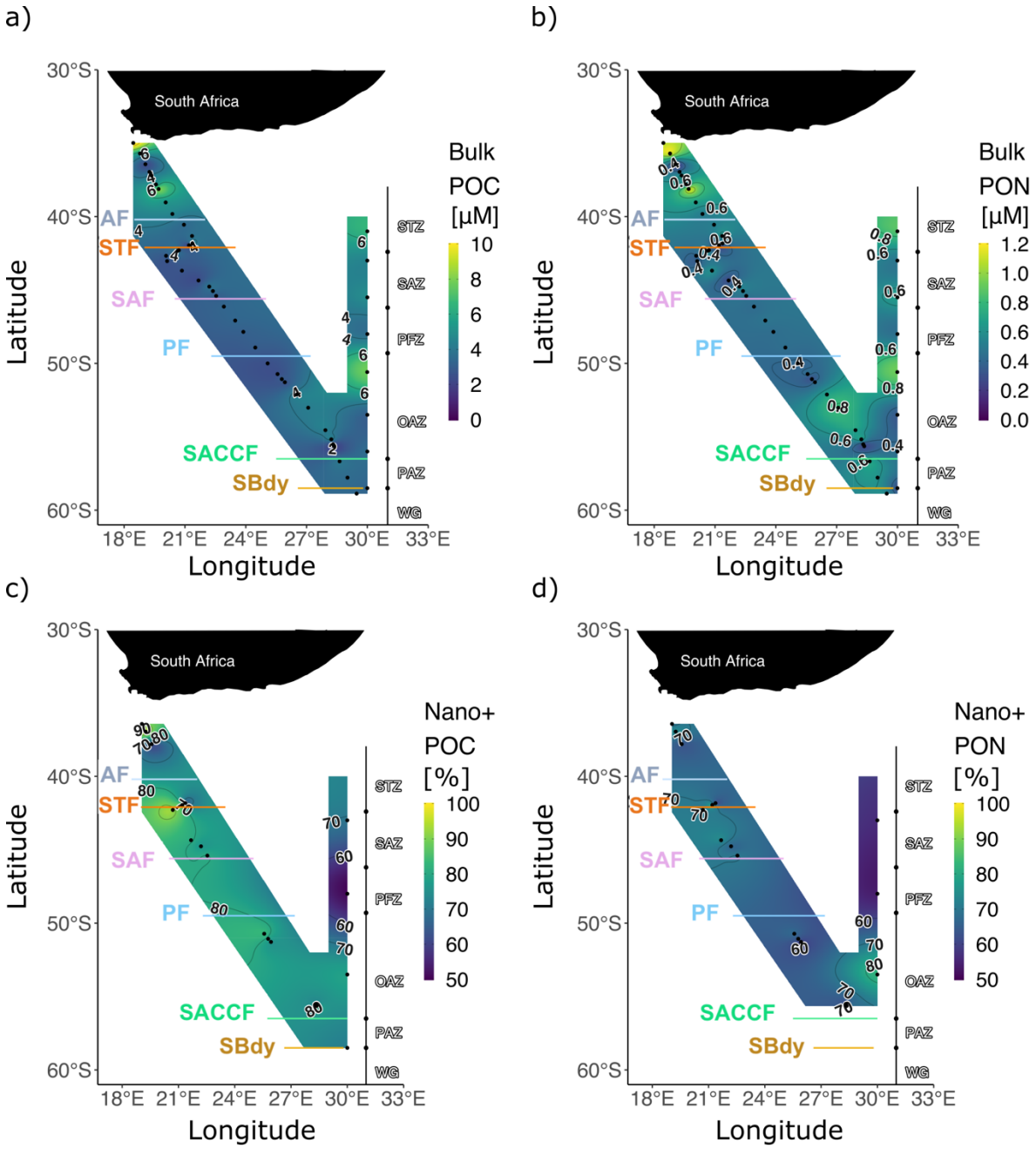

Figure 8: Leg S and N surface ocean concentrations of bulk (>0.3 µm) a) POC and b) PON, and nano+ (>2.7 µm) plankton contributions (%) to bulk c) POC and d) PON. Note that the colour scales in panels c and d have been skewed to show 50 to 100%. Only stations where PON and POC concentrations for the nano+ size class were measured are shown in panels c and d (black circles). Station 58.5°S, where the nano+ contribution was >100% of the corresponding bulk PON concentration, was excluded from panel d. Abbreviations are as in Figure 2. Figure produced using the package ggplot2 (Wickham, 2016).

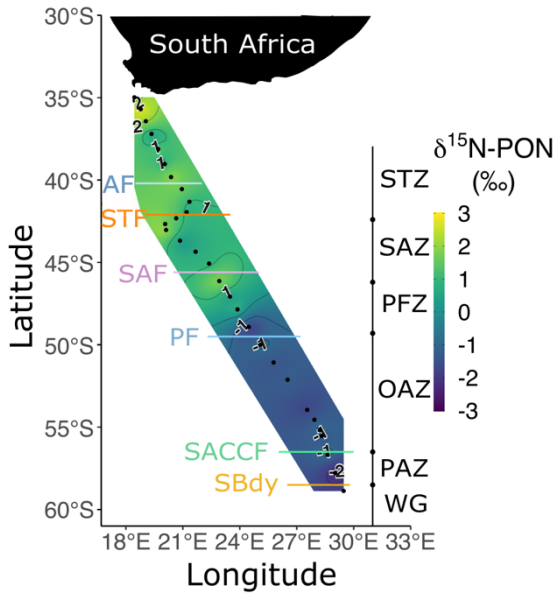

Figure 9: Bulk (>0.3 µm) δ^{15}N-PON at the surface for Leg S. The stations nearest South Africa at which biomass concentrations were extremely high have been excluded. Abbreviations as in Figure 2. Figure produced using the package ggplot2 (Wickham, 2016).

4.4 RATES OF NET PRIMARY PRODUCTION, NITROGEN UPTAKE, AND AMMONIUM OXIDATION

The surface rates of bulk NPP were high in the STZ, and two- to six-fold higher in the SAZ and PFZ than has been reported previously for the Atlantic sector in winter (Mdutyana et al., 2020; Froneman et al., 1999) (Fig. 10a). By contrast, NPP was low in the OAZ, consistent with previous measurements (Kottmeier & Sullivan, 1987; Mdutyana et al., 2020). The relative contribution of the pico size class generally increased southwards, from 14.6% at 37.0°S to 75.6% at 53.5°S, before decreasing to <20.0% at ~55.5°S near the SACCF.

The bulk NH_4^+ uptake rates (ρNH_4^+) generally increased southwards from the STZ to the SAZ and PFZ, and then decreased across the OAZ to reach a minimum at the southernmost station (58.5°S; 3.0 ± 0.8 nM day^{-1}) (Fig. 10b). In the nano+ size fraction, ρNH_4^+ changed little latitudinally, although it was slightly lower in the PFZ than in the other zones. The contribution of nanoplankton to ρNH_4^+ ranged from 32.8% in the PFZ to 71.9% in the STZ. The bulk NO_3^- uptake rates (ρNO_3^-, Fig. 10c) were also low in the STZ, while the highest ρNO_3^- was measured in the SAZ before decreasing southwards. ρNO_3^- in the nano+ size class followed the same trend as total community ρNO_3^-, with the nanoplankton accounting for 71.5 ± 0.3% of bulk ρNO_3^- on average. The rates of bulk urea uptake (ρUrea) were highest in the STZ, with the

SAZ and the PFZ hosting similar rates, and the lowest rates were measured in the OAZ. ρUrea for the nano+ size class followed a similar trend to bulk ρUrea, and nanoplankton accounted for 51.8% of ρUrea in the SAZ to 100% in the PAZ (Fig. 10d). The uptake rates of the different N forms were not significantly correlated with one another or with the ambient N concentrations (Table 2).

Surface ammonium oxidation rates ($NH_4^+{}_{ox}$) increased southwards, with higher $NH_4^+{}_{ox}$ in the OAZ and PAZ than in the STZ, SAZ, and PFZ (Fig. 10e). Generally, $NH_4^+{}_{ox}$ was comparable to previous wintertime measurements from the surface of the open Southern Ocean (Bianchi et al., 1997; Mdutyana et al., 2020), and also similar to summertime rates measured deeper in the mixed layer in the Ross and Scotia Seas (Tolar et al., 2016). $NH_4^+{}_{ox}$ was not correlated with the ambient NH_4^+ concentration (Table 2).

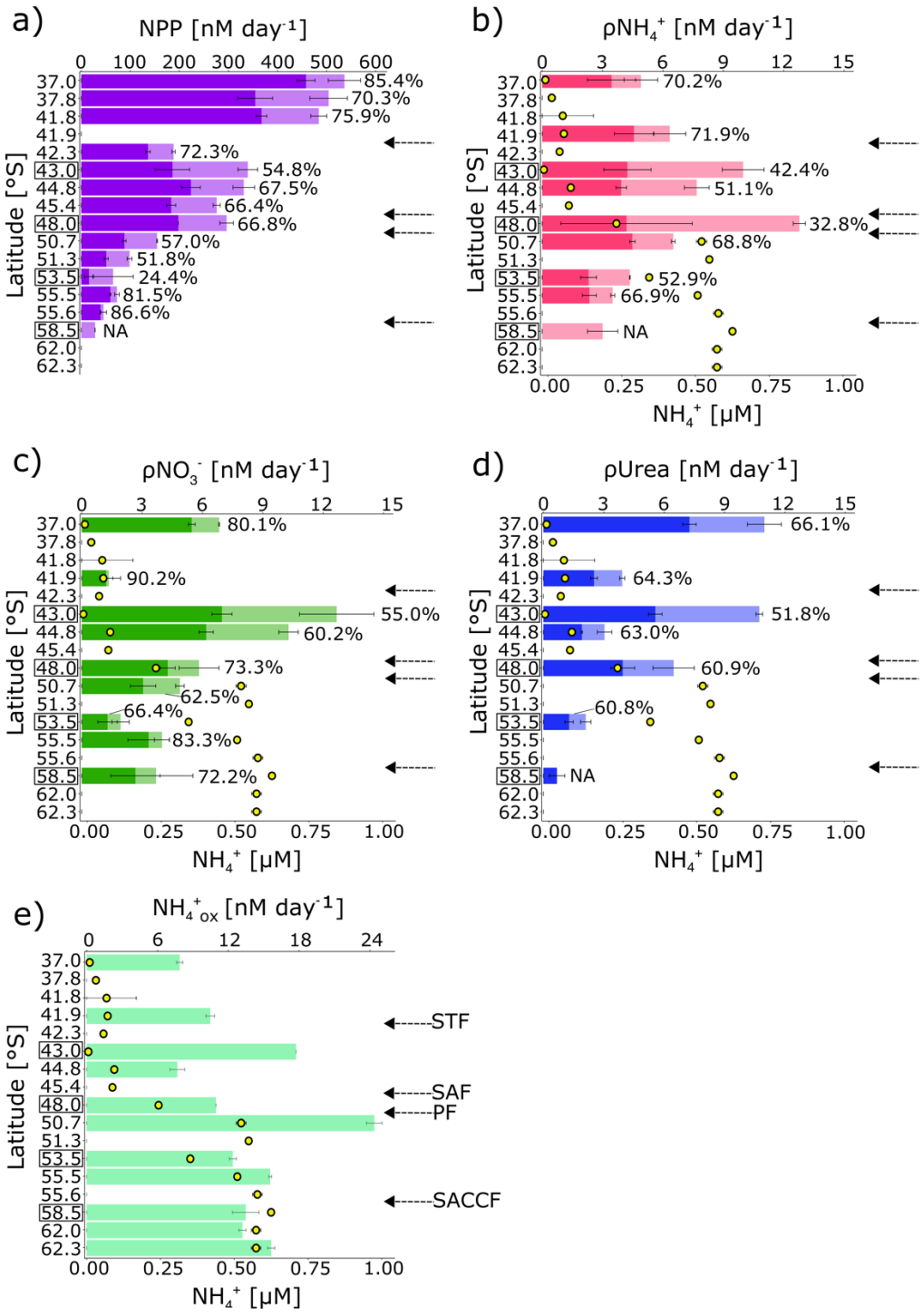

Figure 10: Surface rates of a) net primary production (NPP; ρC) for two plankton size fractions (>0.3 and >2.7 µm); b) ammonium (NH_4^+), c) nitrate (NO_3^-), and d) urea uptake for two plankton size fractions (>2.7 µm overlaid on >0.3 µm), and e) NH_4^+ oxidation. Error bars indicate ±1 standard deviation of duplicate experiments. The percentage of total NPP attributable to the 0.3-2.7 µm size fraction is written next to each bar in panel a. NPP and NH_4^+ uptake were not measured for the >2.7 µm size fraction at 58.5°S, and urea uptake was not measured at 50.7°S and 55.5°S. On panels b-e, the surface NH_4^+ concentration at each station is shown by the yellow circles. Leg N stations (i.e., at which samples were collected from Niskin bottles fired at 10 m) are indicated by the open square around the station latitude. Abbreviations are as in Figure 2. Figure produced using the package ggplot2 (Wickham, 2016).

Table 2: Correlation matrix of leg S and N surface ocean concentrations of bulk PON, bulk POC, bulk chl-a, NH_4^+, NO_3^-, and urea, and rates of net primary production (NPP), N uptake (as NH_4^+, NO_3^-, and urea), f-ratio (excluding ρUrea), and NH_4^+ oxidation. * (blue), ** (green), *** (orange), and **** (pink) indicate levels of significance of the Pearson correlation coefficients of 0.05, 0.01, 0.001, and 0.0001, respectively.

	Latitude (°N)	PON (bulk) (µM)	POC (bulk) (µM)	chl-a (bulk) (µg L^{-1})	NH_4^+ (µM)	NO_3^- (µM)	ρNH_4^+ (bulk) (nM day^{-1})	ρNH_4^+ (nano+) (nM day^{-1})	ρNO_3^- (bulk) (nM day^{-1})	ρNO_3^- (nano+) (nM day^{-1})	f-ratio (bulk) (excl. ρUrea)	ρUrea (bulk) (nM day^{-1})	ρUrea (nano+) (nM day^{-1})	NPP (bulk) (nM day^{-1})	NPP (nano+) (nM day^{-1})
PON (bulk) (µM)	0.28														
POC (bulk) (µM)	0.38**	0.85****													
chl-a (bulk) (µg L^{-1})	0.86****	0.44**	0.51***												
NH_4^+ (µM)	-0.84****	-0.08	-0.19	-0.63****											
NO_3^- (µM)	-0.94****	-0.22	-0.31	-0.82****	0.88****										
ρNH_4^+ (bulk) (nM day^{-1})	0.38	0.65	0.63	0.92**	-0.5	-0.79									
ρNH_4^+ (nano+) (nM day^{-1})	0.5	0.56	0.79*	0.94*	-0.48	-0.68	0.67								
ρNO_3^- (bulk) (nM day^{-1})	0.44	0.57	0.5	0.16	-0.55	-0.38	0.63	0.67							
ρNO_3^- (nano+) (nM day^{-1})	-0.26	0.6	0.76*	-0.45	0.06	0.11	0.23	0.56	0.32						
f-ratio (bulk) (excluding ρUrea)	-0.13	-0.18	0	-0.3	0.19	-0.06	-0.36	0.04	0.4	0.48					
ρUrea (bulk) (nM day^{-1})	0.83*	0.19	0.18	0.72	-0.66	-0.80*	0.87	0.97	0.41	-0.18	0.13				
ρUrea (nano+) (nM day^{-1})	0.85*	0.04	0.03	0.82*	-0.6	-0.80*	0.92	1	0.3	-0.29	0.1	0.98****			
NPP (bulk) (nM day^{-1})	0.93****	0.79***	0.75**	0.96*	-0.85***	-0.91	0.23	0.43	0.83	0.22	0.06	0.98*	0.99**		
NPP (nano+) (nM day^{-1})	0.90****	0.66**	0.61*	0.8	-0.79***	-0.99**	-0.07	0.17	0.96*	0.37	0.26	0.99*	0.97*	0.96****	
NH_4^+ox (nM day^{-1})	-0.35	0.08	0.02	-0.5	0.51	0.44	-0.12	0.26	0.01	0.14	0.35	0.03	-0.11	-0.19	-0.14

$p < .0001$ '****'; $p < .001$ '***', $p < .01$ '**', $p < .05$ '*'

4.5 PLANKTON COMMUNITY COMPOSITION

The abundance of microplankton, analysed at 16 stations on leg S, was generally low, with the highest cell counts at stations 37.2°S and 41.3°S in the STZ and no cells counted at 38.1°S (STZ) and 55.5°S (OAZ) (Fig. 11a). Total microplankton abundance was on average higher in the STZ than in the SAZ, PFZ, and OAZ. The greatest diversity of microplankton groups was observed at 41.3°S near the AF and at 50.0°S near the PF.

Centric diatoms (including *Planktoniella*, *Coscinodiscus*, and *Thalassiosira* species) were detected only at 58.9°S (3 cells mL^{-1}), the southernmost station. Pennate diatoms (including *Pseudo-nitzschia*, *Pleurosigma*, and *Navicula* species) were more abundant in the STZ, PFZ, and OAZ, with negligible abundances observed in the SAZ. Higher pennate diatom abundances occurred near the PF (7 cells mL^{-1}), as has been observed in summer (e.g., Bracher et al., 1999). Dinoflagellates were identified at every station except 38.1°S and were most abundant in the STZ and PFZ. At all but three stations, small (<15 µm) dinoflagellates were the most abundant group, although the larger *Protoperidinium* dinoflagellate species (mainly heterotrophic; Jeong & Latz, 1994) were almost as abundant in the PFZ and at 54.0°S. The abundance of microzooplankton (ciliates only, 20-200 µm) was highest across the STZ, and microzooplankton were also identified in the PFZ at 46.1°S (3 individuals mL^{-1}) and 48.9°S (3 individuals mL^{-1}) and in the OAZ at 50.0°S (1 individuals mL^{-1}) and 54.0°S (4 individuals mL^{-1}). All other stations were characterized by negligible (<1 individuals mL^{-1}) microzooplankton abundances.

Nano- and picoeukaryotes, *Synechococcus*, and small heterotrophs (collectively, "small cells") sampled at 13 stations along leg S were roughly 10^3-times more abundant than the microplankton (Fig. 11b). Notwithstanding a lack of data from the STZ, the highest small cell abundances occurred in the SAZ near the SAF. Across the transect, picoeukaryotes were generally more abundant than all other phytoplankton groups (average picoeukaryote contribution to total small cells of 12-54%; nanoeukaryotes of 7-39%; *Synechococcus* of 15-42%). A similar trend was observed previously for the Southern Ocean in spring (Detmer & Bathmann, 1997) and late summer (Fiala et al., 1998), in contrast to mid-summer observations showing nanoplankton dominance (e.g., Ishikawa et al., 2002; Weber & El-Sayed, 1987). Additionally, picoeukaryotes were two- to three orders of magnitude more abundant in the SAZ and PFZ than in the OAZ. Nanoeukaryotes dominated small cell abundances near the PF at 50.0°S (39%) and in the southern OAZ at 55.5°S (36%), while *Synechococcus* dominated at

42.7°S and 54.0°S (42% and 33%, respectively). Nanoeukaryote abundance was higher in the SAZ than in the PFZ and OAZ, as was the abundance of *Synechococcus*.

The contribution of small photosynthetic cells to total small particle abundance decreased southwards, while detritus contributed >70% at all stations (Fig. 12a). The contribution of heterotrophic bacteria to total small cells varied considerably (10-62%), reaching a maximum south of the PF at 53.0°S and 57.8°S (62% and 50%), and with higher abundances in the SAZ than in the PFZ and OAZ (Fig. 12b). Additionally, heterotrophic bacterial abundances were ten-fold lower to two-fold higher than the total pico- and nanophytoplankton cell counts. Detrital particles were most abundant near the southern edge of the SAF and were generally more abundant in the PFZ than in the SAZ and OAZ (Fig. 12c).

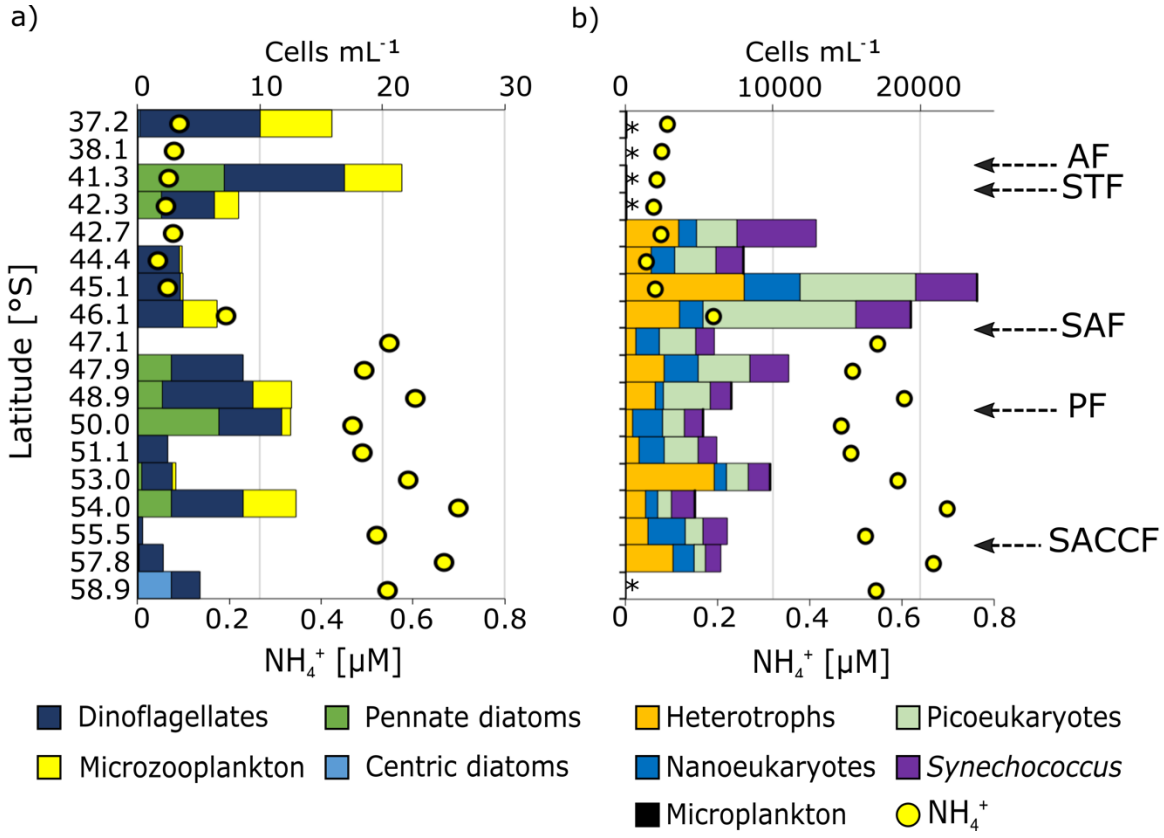

Figure 11: Surface community composition for a) plankton >5-10 µm (enumerated by microscopy) and b) the total community <15 µm (enumerated by flow cytometry). The surface NH_4^+ concentration at each station is shown by the yellow circles for context. * indicates stations at which no measurements were made. The abundance axis in panel b is 10^3-times greater than the abundances shown in panel a. "Microplankton" are shown on panel b to provide context as to the magnitude of the difference in abundance between the cells >15 µm and those <15 µm. The fronts are indicated on panel a with abbreviations as in Figure 2.

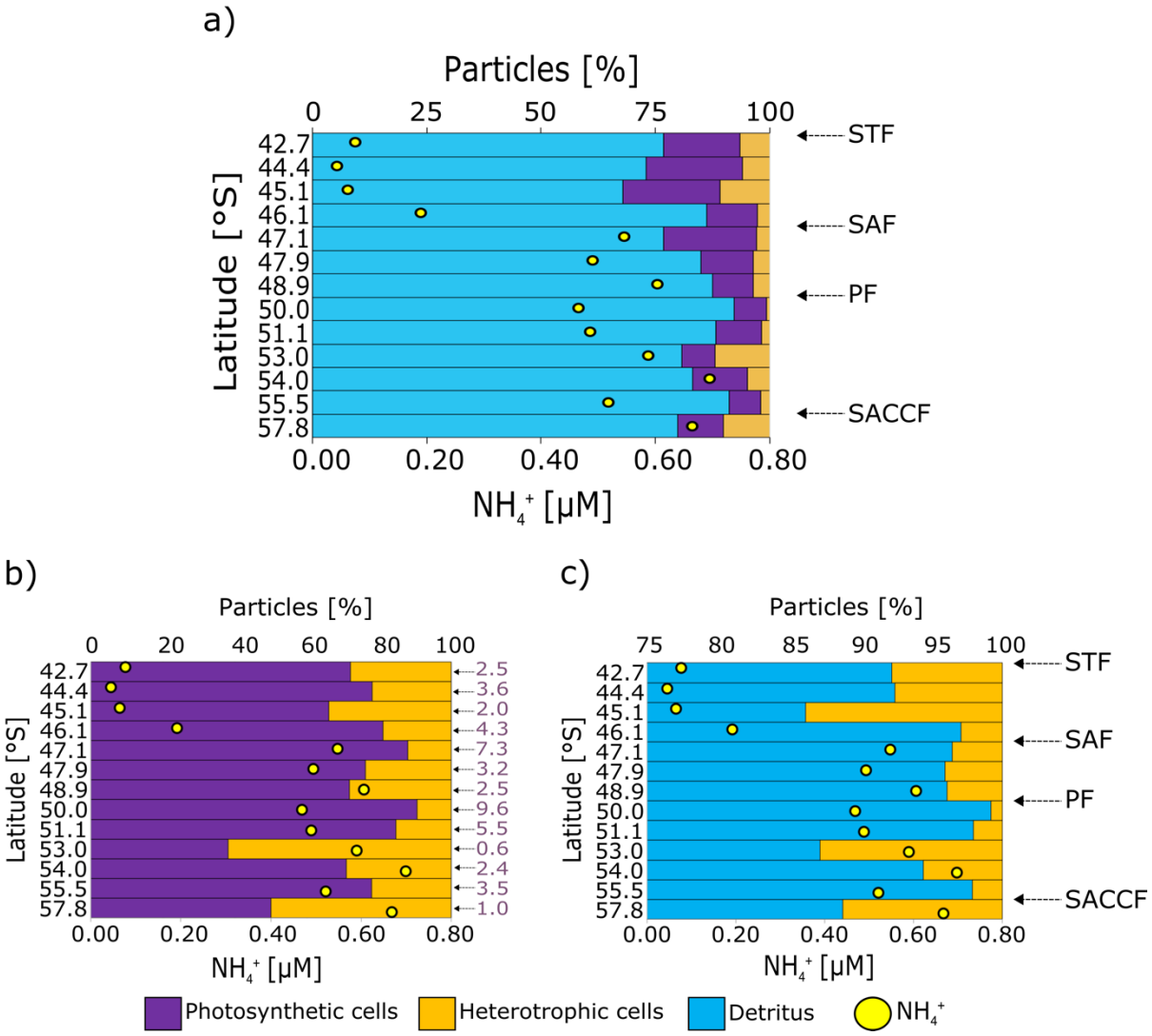

Figure 12: Relative abundances of a) photosynthetic, heterotrophic bacterial, and detrital particles, b) total photosynthetic versus heterotrophic cells, and c) detritus (DNA-negative) versus heterotrophic cells at the surface for Leg S. The coincident surface NH_4^+ concentration is indicated by the yellow dots. The values shown on the right side of panel b are the photosynthetic-to-heterotrophic cell ratios. The upper x-axis in panel c begins at 75% in order to highlight the (much smaller) heterotrophic contribution to the summed detrital + heterotrophic particles. Abbreviations are as in Figure 2.

4.6 2018/19 SEASONAL CYCLE – AMMONIUM CONCENTRATIONS

4.6.1 Surface ocean NH_4^+

In early summer, the surface NH_4^+ concentrations were uniformly low across the transect (average of 0.11 ± 0.09 µM; Fig. 13a). South of the SAF, NH_4^+ concentrations increased significantly as the growing season progressed, reaching an average concentration of 0.81 ± 0.92 µM by late summer (Fig. 13b). In winter 2019, the NH_4^+ concentrations measured south of the SAF were ~40% lower than in late summer (Fig. 13c) and were similar to those observed in winter 2017 (0.50 ± 0.30 µM and 0.52 ± 0.11 µM, respectively), confirming that the 2017

observations are generally representative of the wintertime Southern Ocean. By the early spring, the NH_4^+ concentrations south of the SAF had declined to near or below the methodological detection limit (0.09 ± 0.08 µM; Fig. 13d). NH_4^+ concentrations south of the SAF rose again by the late spring to an average value only slightly lower than that measured in winter (0.40 ± 0.74 µM; Fig. 13e). However, late-spring NH_4^+ concentrations were only elevated in the PFZ (range of 0.11 ± 0.01 to 4.39 ± 0.03 µM, average of 0.77 ± 1.11 µM), as has been observed previously (Bathmann et al., 1997). Excluding the PFZ data yields a far lower late-spring average NH_4^+ concentration of 0.17 ± 0.11 µM south of the SAF, which is taken as broadly representative of this season.

4.6.2 Mixed-layer NH_4^+ residence time and NH_4^+ production rate estimates

The $NH_4^+{}_{\text{residence time}}$ in winter 2017, computed using equation 5, yields a range of 10 to 38 days (median of 21 days). However, these estimates, calculated using wintertime measurements, may not be representative of the transition from summer to winter; thus data from summer 2019 were used to refine the estimates. For late summer 2019, ρNH_4^+ alone was taken as representative of the $NH_4^+{}_{\text{consumption rate}}$, which is reasonable given the evidence for negligible surface NH_4^+ oxidation rates in this season (Bianchi et al., 1997; Mdutyana et al., 2020). Using the average ρNH_4^+ and NH_4^+ concentration measured south of the SAF in late summer (50.6 ± 24.0 nM day^{-1} and 0.81 ± 0.92 µM, respectively; Deary, 2020), an $NH_4^+{}_{\text{residence time}}$ of 2 to 27 days (median of 5 days) was estimated, consistent with the scenario of net NH_4^+ production over this period.

The $NH_4^+{}_{\text{production rate}}$, calculated using equation 8 and an $[NH_4^+]_{\text{decline}}$ of 330 nM (i.e., 810 nM – 480 nM), t of 141 days, and $NH_4^+{}_{\text{consumption rate}}$ of 50.6 ± 24.0 nM day^{-1} (here, the average late-summer ρNH_4^+ south of the SAF is used as representative of $NH_4^+{}_{\text{consumption rate}}$), was 52.9 ± 25.0 nM day^{-1}. This estimate is consistent with the only existing remineralisation rates measured previously in the Southern Ocean in summer (average of 55.2 nM day^{-1}; Goeyens et al., 1991). However, if the average wintertime $NH_4^+{}_{\text{consumption rate}}$ and NH_4^+ concentration from 2017 is used instead (21.4 ± 0.6 nM day^{-1} and 520 ± 110 nM), the $NH_4^+{}_{\text{production rate}}$ is 23.4 ± 6.6 nM day^{-1}. Additionally, the $NH_4^+{}_{\text{production rate}}$ ranges from 18.8 to 100.9 nM day^{-1} over the late-summer-to-winter transition period (using the range of $NH_4^+{}_{\text{consumption rate}}$ and average ambient NH_4^+ concentration south of the SAF for winter 2017, 16.7 to 31.2 nM day^{-1} and 520 nM, and late summer 2019, 22.6 to 98.6 nM day^{-1} and 810 nM).

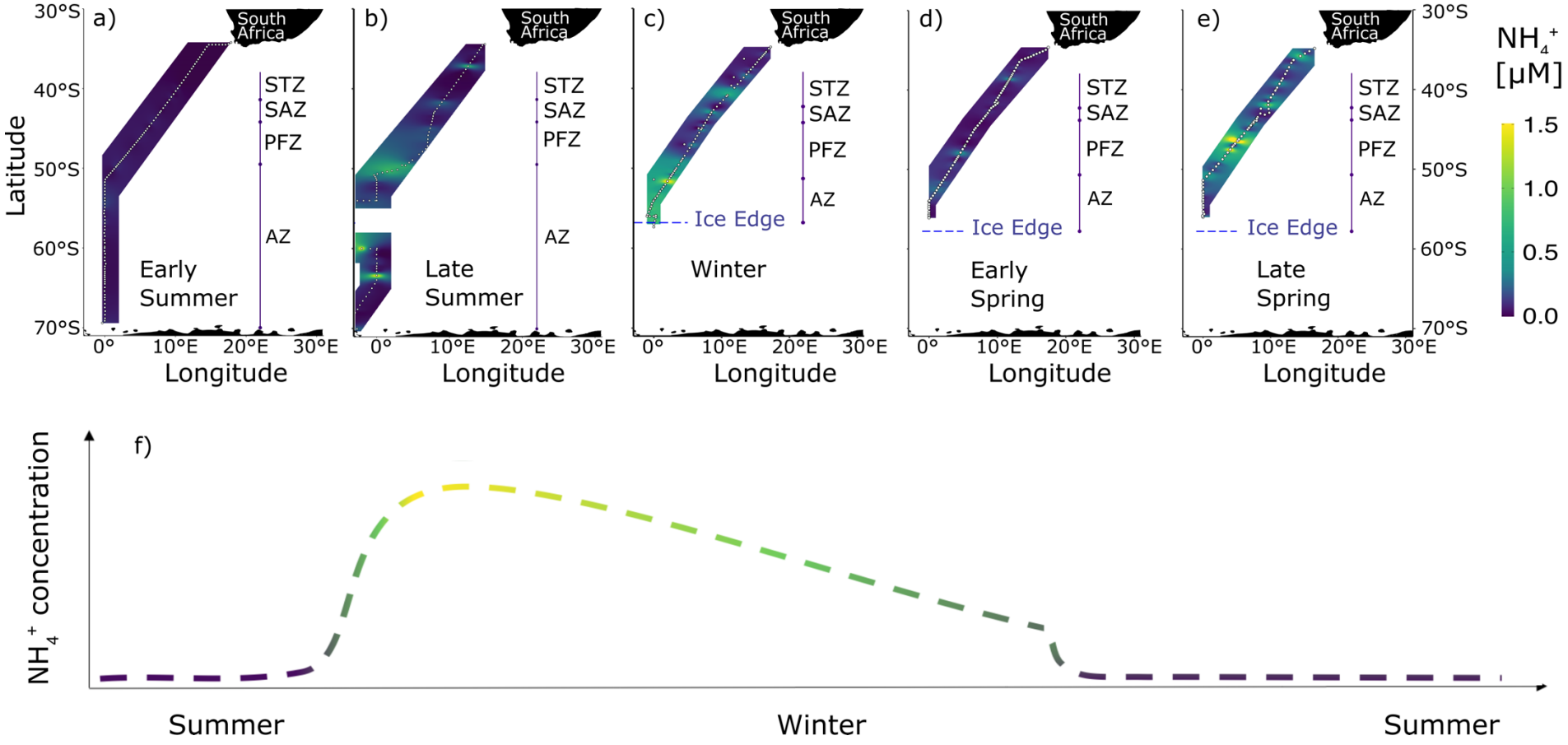

Figure 13: Surface concentrations of NH_4^+ across the Atlantic sector of the Southern Ocean measured between December 2018 and November 2019. Five unique transects additional to the winter 2017 dataset are shown: a) early summer 2018, b) late summer 2019, c) winter 2019, d) early spring 2019, and e) late spring 2019. f) Proposed seasonal cycle of NH_4^+ concentrations in the mixed layer for the waters south of the Subantarctic Front. The colour gradient in panel f indicates the transition period between winter and summer. Panels a and b cover a latitudinal extent of 30-70°S, while panels c-e cover 30-60°S due to the presence of sea-ice. Early- and late summer data were collected during the SANAE 58 Relief Voyage (6 December 2018 to 15 March 2019; VOY035); winter data were collected during the SCALE 2019 (www.scale.org.za) winter cruise to the MIZ (18 July to 12 August 2019; VOY039); and spring data were collected during the SCALE 2019 spring cruise to the MIZ (12 October to 20 November 2019; VOY040). All sampling was conducted onboard the R/V *SA Agulhas II*. Abbreviations as in Figure 1, with AZ referring to the combined OAZ and PAZ. Figure produced using the package ggplot2 (Wickham, 2016).

5 DISCUSSION

5.1 DRIVERS OF NH_4^+ CYCLING IN THE SURFACE LAYER OF THE SOUTHERN OCEAN

Previous work has suggested that NH_4^+ accumulates in the Southern Ocean mixed layer following the late summer increase in zooplankton abundance and heterotrophic activity, then decreases into autumn as heterotrophic activity subsides, to be depleted by winter due to advective processes and assimilation (Koike et al., 1986; Serebrennikova & Fanning, 2004). However, the data in this study show that NH_4^+ concentrations are elevated in the Southern Ocean mixed layer in winter, particularly south of the SAF (Fig. 5). Similarly elevated winter surface-layer NH_4^+ has been observed previously in both the Atlantic and Indian sectors, with concentrations typically increasing towards the south (Bianchi et al., 1997; Philibert et al., 2015; Mdutyana et al., 2020). Numerous overlapping processes are likely involved in setting the ambient NH_4^+ concentrations, as summarized in Figure 14. This study determined the rates of NH_4^+ uptake by different size fractions of the winter plankton community, as well as the rates of NH_4^+ oxidation. The contribution of heterotrophic bacteria and microzooplankton to NH_4^+ production was inferred from cell count data and the abundance of small heterotrophs relative to phytoplankton and detritus. For the NH_4^+ cycle processes in Figure 14 that are not quantified or inferred here – microzooplankton grazing, atmospheric NH_4^+ deposition, NH_3 air-sea exchange, sea-ice melt, and dissolved organic nitrogen (DON) conversion to NH_4^+ –, their potential role in Southern Ocean NH_4^+ cycling, based on findings reported in the literature, is considered.

The high NH_4^+ concentrations observed in the winter PFZ and AZ (OAZ + PAZ) may result from net NH_4^+ accumulation during late summer, autumn and/or winter. The persistence of high NH_4^+ concentrations that are near-homogeneously distributed throughout the mixed layer suggests a residence time for the winter NH_4^+ reservoir in excess of the time-scale for upper-ocean mixing. One implication of this suggestion is that the wintertime NH_4^+ pool likely reflects processes that occurred earlier in the season, as well as those that are ongoing. This study posits that the elevated NH_4^+ concentrations in the PFZ and AZ may result from higher wintertime rates of NH_4^+ production than assimilation and/or from the gradual but incomplete depletion in winter of NH_4^+ produced mainly in late summer and autumn. Both possibilities are evaluated throughout the discussion below.

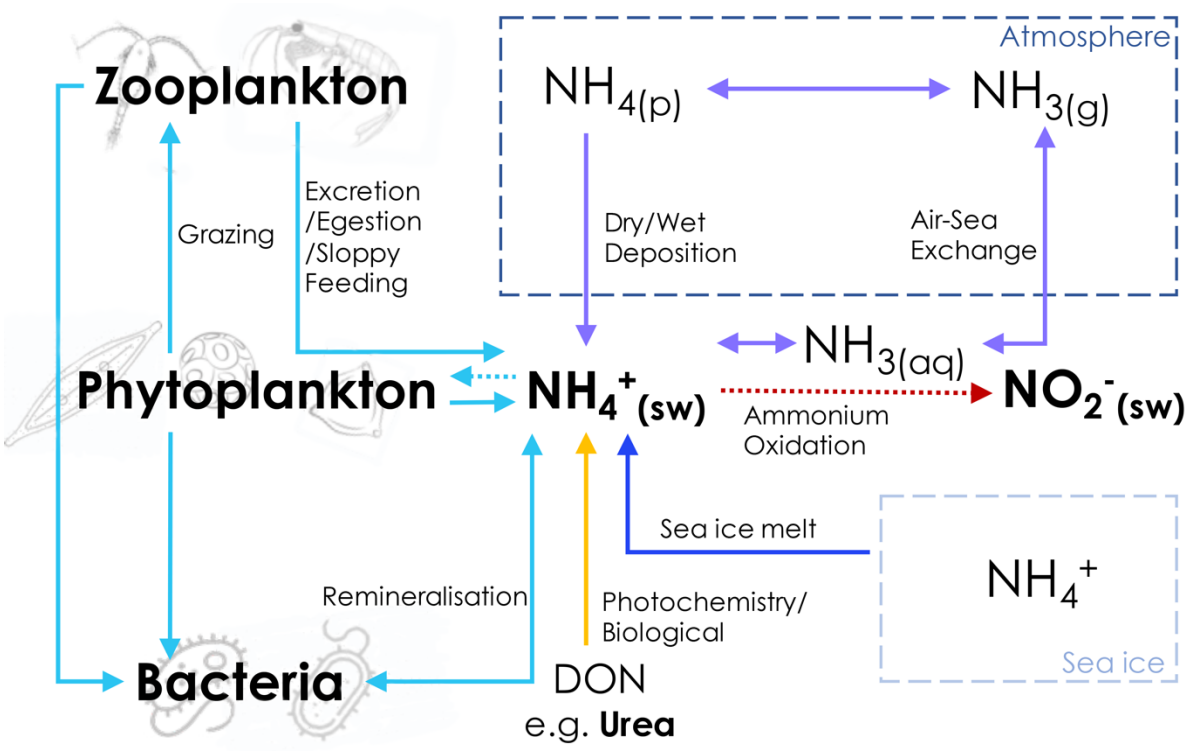

Figure 14: Schematic of the possible mixed-layer NH_4^+ assimilation and production pathways. Bold text indicates components of the NH_4^+ cycle that were directly measured (seawater concentrations of NH_4^+, NO_2^-, and urea; phytoplankton and microzooplankton cell abundances) or inferred (bacterial NH_4^+ remineralization) in this study. Dotted lines indicate processes for which rate measurements are given in this study (phytoplankton uptake of NH_4^+; oxidation of NH_4^+ to NO_2^-). Dashed-line boxes represent the atmosphere and sea-ice, with all other processes occurring in the ocean. DON – dissolved organic nitrogen; $NH_{3(aq)}$ – aqueous (seawater) ammonia; $NH_{4(p)}$ – ammonium aerosols (including ammonium sulphate, ammonium bisulphate, and ammonium nitrate); $NH_{3(g)}$ – ammonia gas.

5.1.1 Ammonium assimilation

5.1.1.1 Ammonium uptake

Microbial growth is limited in the winter Southern Ocean (Arrigo et al., 2008; Smith Jr et al., 2000, Takao et al., 2012), resulting in low cell abundances and nutrient uptake rates (Church et al., 2003; Iida & Odate, 2014; Mdutyana et al., 2020). While the concentrations of chl-a and rates of NPP were low across the transect, they were not negligible (Fig. 7a and 10a), consistent with previous reports for this season (Mordy et al., 1995; Pomeroy & Wiebe, 2001). Southern Ocean phytoplankton are adapted to survive suboptimal conditions; for example, numerous species achieve their maximum growth rates at temperatures that are considerably lower than the optimal growth temperatures of temperate and tropical species (2-9°C versus 10-30°C and 15-35°C, respectively), with sharp declines in growth rates observed for temperatures outside this range (Boyd et al., 2013; Coello-Camba & Agustí, 2017; Fiala & Oriol, 1990). In addition, ice-free Southern Ocean waters typically extend to <60°S in the eastern Atlantic and western

824 Indian sectors in winter, so that although irradiance levels may not be optimal for
825 phytoplankton growth, there is always some light available for photosynthesis. The hostile
826 conditions of the open winter Southern Ocean do not, therefore, prevent ecosystem functioning
827 (Moreau et al., 2020; Pomeroy & Wiebe, 2001), although the microbial dynamics and
828 associated biogeochemical processes differ from those occurring in summer (Behrenfeld et al.,
829 2017; Moreau et al., 2020; Mdutyana et al., 2020; Smart et al., 2015).

830 Fairly low NH_4^+ uptake rates were measured in surface waters (3.0-13.2 nM day^{-1}; Fig. 10b)
831 compared to previous wintertime observations (ranging from 32-66 nM day^{-1}; Cota et al., 1992;
832 Mdutyana et al., 2020; Philibert et al., 2015). Such low rates, if generally representative of
833 winter, would limit mixed-layer NH_4^+ drawdown, especially south of the PF where ρNH_4^+ was
834 particularly low. Recycled N (NH_4^+ + urea) nonetheless accounted for most of the N consumed,
835 including in the AZ (Fig. 10b).

836 The available δ^{15}N-PON data (Fig. 9) suggest that this elevated reliance on recycled N may
837 have persisted from the late summer. In theory, PON generated in early- through mid-summer
838 from the assimilation of upwelled NO_3^- (δ^{15}N-NO_3^- of 5.2‰ in the AZ and 6.2‰ in the SAZ;
839 Smart et al., 2015; Fripiat et al., 2019) will have a δ^{15}N of ~0‰ in the AZ and 1-2‰ in the
840 SAZ given the isotope effect of NO_3^- assimilation and the degree of seasonal NO_3^- drawdown
841 (Sigman et al., 1999; Granger et al., 2004; 2010). Such δ^{15}N-PON values have indeed been
842 observed in early- and mid-summer (Lourey et al., 2003; Smart et al., 2020; Soares et al., 2015).
843 By late summer, δ^{15}N-PON declines to -5 to -1‰, with the lowest values occurring in the AZ
844 (Lourey et al., 2003; Smart et al., 2020; Trull et al., 2008). Since the δ^{15}N of recycled N is
845 expected to be low (<0‰; Checkley & Miller, 1989, Macko et al., 1986), the early-to-late
846 summer decline in δ^{15}N-PON implicates a switch from dominantly NO_3^-- to dominantly
847 recycled N-supported phytoplankton growth (Lourey et al., 2003). For the SAZ, the subsequent
848 late summer-to-winter rise in δ^{15}N-PON (i.e., from ~ -1‰ to 1-2.5‰; Fig. 9) has previously
849 been attributed to PON decomposition by heterotrophic bacteria (Smart et al., 2020), during
850 which ^{14}N-NH_4^+ is preferentially remineralized, leaving the remaining PON enriched in ^{15}N
851 (Möbius, 2013). That NH_4^+ concentrations are not elevated in the SAZ mixed layer in winter
852 (Fig. 5b) indicates that the remineralized NH_4^+ is rapidly re-assimilated by phytoplankton
853 and/or oxidized to NO_2^- in this zone. In the AZ, the δ^{15}N-PON of -3 to -1‰ that was observed
854 in this study in winter surface waters requires the sustained assimilation of low-δ^{15}N N (i.e.,
855 recycled NH_4^+ and urea) to offset a remineralization-driven δ^{15}N rise similar to that of the SAZ.

In conclusion, Southern Ocean phytoplankton dominantly consume regenerated N from late summer until at least July (albeit at low rates in winter), particularly south of the PF.

The fact that NH_4^+ accumulated in the winter mixed layer despite being the preferred phytoplankton N source in late summer through winter implies that low rates of NH_4^+ uptake contributed to its accumulation. Multiple factors may cause low rates of photoautotrophic NH_4^+ assimilation, including deplete NH_4^+ and micronutrient concentrations, light limitation, and low temperatures. North of the SAF, NH_4^+ concentrations below detection likely limited ρNH_4^+, as evidenced by the fact that in a series of experiments conducted on the same cruise, ρNH_4^+ increased with the addition of NH_4^+ at these stations (Mdutyana, 2021). By contrast, south of the SAF, NH_4^+ concentrations were similar to or higher than the half-saturation constant (K_m) derived for NH_4^+ uptake in the winter Southern Ocean (0.2 to 0.4 μM; Mdutyana, 2021), suggesting that something other than NH_4^+ availability was limiting to phytoplankton at these latitudes.

Iron is not directly involved in NH_4^+ assimilation but is required for electron transport during photosynthesis and respiration (Raven, 1988). While iron limitation is widespread across the Southern Ocean (Janssen et al., 2020; Pausch et al., 2019; Viljoen et al., 2019), iron availability appears to be higher in winter than during other seasons (Mtshali et al., 2019; Tagliabue et al., 2014) due to enhanced mixing, storms, and increased aeolian deposition (Coale et al., 2005; Honjo et al., 2000; Sedwick et al., 2008). The fact that ρNO_3^- and ρNH_4^+ were generally similar across the transect (Fig. 10b) argues against a dominant role for iron in controlling ρNH_4^+ since NO_3^- assimilation has a far higher iron requirement than NH_4^+ assimilation (Morel et al., 1991).

In contrast to NH_4^+ and iron availability, light limitation is exacerbated in winter due to low insolation, increased cloud-cover, and mixed layers that can be hundreds of meters deeper than the euphotic zone (Brightman & Smith Jr., 1989; Buongiorno Nardelli et al., 2017; Sallée et al., 2010). Light is thus often considered the dominant constraint on Southern Ocean primary productivity in this season (Thomalla et al., 2011; Llort et al., 2019; Wadley et al., 2014). However, since NH_4^+ assimilation by phytoplankton is fairly energetically inexpensive (Dortch, 1990), it should occur even under low light (recognizing that light remains critical for coincident CO_2 fixation). Heterotrophic bacteria can also consume NH_4^+ (Kirchman, 1994), including in the dark since they derive energy from organic carbon oxidation rather than light. At an ecosystem level, therefore, NH_4^+ assimilation may not be primarily limited by light, although this parameter clearly strongly controls the rate of NPP (Fig. 10a).

Previous observations suggest that temperature influences NH_4^+ uptake, especially in winter (Glibert, 1982; Reay et al., 2001). The negative effect of temperature appears to be enhanced under high-nutrient and low-light conditions, at least in the case of phytoplankton growth rates (Baird et al., 2001). Additionally, Southern Ocean phytoplankton may be psychrotolerant and not psychrophilic, which means that while they can function at *in situ* wintertime temperatures, their optimal temperatures for growth and photosynthesis are higher (Reay et al., 2001; Smith Jr & Harrison, 1991; Tilzer & Dubinsky, 1987). Experiments conducted coincident with the sampling in this study showed that the maximum rate of NH_4^+ uptake (V_{max}) achievable by the *in situ* community was strongly negatively correlated with temperature and latitude (Mdutyana, 2021), with the latter parameter indicative of the combined role of light, temperature, and possibly iron, the average concentration of which appears to increase from the SAZ to the AZ (Tagliabue et al., 2012). Thus, these three drivers, along with NH_4^+ availability north of the SAF, all play a role in controlling photoautotrophic NH_4^+ uptake in the winter Southern Ocean, with complex interactions among them that are difficult to disentangle.

In addition to physical and chemical limitations, microbial preference for other N species may impact the depletion of the NH_4^+ pool. For example, the preferential uptake of urea and other dissolved organic N (DON) species by some organisms (e.g., cyano- or heterotrophic bacteria) could result in a net decrease in the total NH_4^+ uptake rates. While large contributions of urea to total N uptake have previously been observed in the Southern Ocean in summer and autumn (albeit mainly in the SAZ; Joubert et al., 2011; Thomalla et al., 2011), ρUrea measured here were fairly low (Fig. 10b), which is perhaps unsurprising given the low ambient urea concentrations (Table 1). The exceptions were stations 37°S and 43.0°S where ρUrea was higher than ρNH_4^+, coincident with very low ambient NH_4^+ (0.10 µM and below detection) and relatively high urea concentrations (0.36 µM and 0.15 µM).

Community composition can also alter the N uptake regime. Smaller phytoplankton, such as the numerically-dominant nano- and picoeukaryotes, are more likely to consume NH_4^+ and urea than NO_3^- (Koike et al., 1986; Lee et al., 2012; 2013), especially in the Southern Ocean where NO_3^- assimilation is severely limited by iron and light availability (Sunda & Huntsman, 1997). Across this transect, the sum of NH_4^+ and urea uptake (i.e., reduced N uptake) exceeded NO_3^- uptake for both the total phytoplankton community (transect average of 12.0 ± 0.9 nM day^{-1} for reduced N versus 5.8 ± 1.0 nM day^{-1} for NO_3^-; f-ratio of 0.36) and the pico size fraction (5.0 ± 1.2 nM day^{-1} versus 1.9 ± 1.2 nM day^{-1}; f-ratio of 0.27 (Fig. 10b). That said, the NO_3^- uptake rates were not negligible, including in the pico size fraction. In the PFZ and AZ, NO_3^-

uptake by the pico size fraction was more strongly correlated with the abundance of picoeukaryotes than *Synechococcus* (r = 0.75 and 0.03, respectively), consistent with observations of dominant reliance on NO_3^- by picoeukaryotes and NH_4^+ by *Synechococcus* in other ocean regions (Fawcett et al., 2011; 2014; Painter et al., 2014). Nonetheless, *Synechococcus* can consume all N forms (Capone et al., 2008 and references therein) and has evolved strategies to conserve iron by using other trace metals in some enzymes (Palenik et al., 2003). Thus, *Synechococcus* may be adapted to consume NO_3^- in the Southern Ocean when reduced N concentrations are near depletion (e.g., north of the SAF in winter), but are likely to consume NH_4^+ as long as it is available, as implied by their strong correlation with NH_4^+ concentration south of the SAF (r = 0.65). In the nano+ size class, NO_3^- uptake was likely driven in the SAZ by dinoflagellates and some nanoeukaryotes, and in the PFZ and AZ by diatoms, which remain active in these zones in winter (Weir et al., 2020). By contrast, nanoeukaryotes, which have a higher per-cell nutrient requirement than the equally-abundant picoeukaryotes, may have dominated NH_4^+ uptake in the PFZ and AZ given that higher nanoeukaryote abundances corresponded with lower NH_4^+ concentrations at a number of stations (e.g., stations 50.0°S, 51.1°S, and 55.5°S; Fig. 11b).

The low abundances of diatoms and dinoflagellates and absence of coccolithophores (Fig. 11a) across the transect in this study are expected given the limitations imposed on nutrient uptake and CO_2 fixation by winter Southern Ocean conditions. The lower surface area-to-volume ratio of larger cells means that they rapidly experience diffusion-limitation of NH_4^+ and micronutrient uptake and are more susceptible to light limitation (Finkel et al., 2004), resulting in their being outcompeted by smaller species for essential resources (Franck et al., 2005; Cavender-Bares et al., 1999). The near-absence of centric diatoms is also best explained thus, particularly given their low surface area-to-volume ratio compared to pennate species (Kobayashi & Takahashi, 2002) that are more likely to consume NH_4^+ (Semeneh et al., 1998) and were more abundant. Diatom success in winter may also be limited by enhanced mixing, as this group is generally adapted for stratified waters (Kopczynska et al., 2007).

In sum, NH_4^+ uptake rates were low across the transect but not negligible, indicating that phytoplankton activity in winter, which is dominated by smaller species, represents a sink for NH_4^+. Hostile Southern Ocean conditions imposed limitations on NH_4^+ uptake that varied with latitude, with NH_4^+ concentrations controlling ρNH_4^+ north of the SAF, while light and temperature were important south of the SAF, with a possible supporting role for iron. Additionally, *Synechococcus*, nanoeukaryotes, and pennate diatoms likely dominated NH_4^+

assimilation, consistent with previous observations from the Southern Ocean and elsewhere (Klawonn et al., 2019; Semeneh et al., 1998).

5.1.1.2 Ammonium oxidation

Nitrification removes more mixed-layer NH_4^+ than phytoplankton assimilation south of the PF, with NH_4^+ oxidation rates that were two- to five-times the co-occurring NH_4^+ uptake rates (Fig. 10e and c). The comparative success of NH_4^+ oxidisers may be due to decreased competition with phytoplankton for NH_4^+ in winter, augmented by decreased photoinhibition (Wan et al., 2018; Lu et al., 2020), elevated NH_4^+ availability (Baer et al., 2014; Mdutyana et al., 2020; Mdutyana, 2021), and a minimal effect of temperature on NH_4^+ oxidation (Bianchi et al., 1997; Baer et al., 2014; Horak et al., 2013; Mdutyana, 2021). One implication of the dominance of NH_4^+ oxidation is that in addition to the limitations on phytoplankton NH_4^+ uptake discussed above, low phytoplankton success in the AZ may also result from nitrifiers outcompeting phytoplankton under conditions of low incident light and enhanced mixing for scarce resources (e.g., trace elements required for enzyme functioning, such as iron and copper; Amin et al., 2013; Maldonado et al., 2006; Shafiee et al., 2019).

The K_m derived for NH_4^+ oxidation in the winter Southern Ocean has recently been reported to be low (0.03 to 0.14 µM), with ammonia oxidizers observed to become saturated at ambient NH_4^+ concentrations of ~0.1-0.2 µM (Mdutyana, 2021). This means that south of the SAF in winter 2017, ammonia oxidizers were not substrate limited (as implied by the lack of correlation between $NH_4^+{}_{ox}$ and NH_4^+ concentration; Table 2), which raises the question of why NH_4^+ oxidation did not occur at higher rates. The answer may indirectly involve temperature, in that psychrophilic organisms can be less responsive to high substrate concentrations at low temperatures (Baer et al., 2014). Another possibility is that NH_4^+ oxidation was iron-limited (Shiozaki et al., 2018; Mdutyana, 2021), with a recent culture study revealing the surprisingly low affinity for iron of the globally-abundant ammonia oxidiser, *Nitrosopumilus maritimus* (Shafiee et al., 2019). In any case, NH_4^+ oxidisers were moderately successful across the surface Southern Ocean in winter, with low light, reduced competition with phytoplankton, and substrate repletion likely explaining the elevated NH_4^+ oxidation rates south of the PF compared to the stations to the north.

5.1.2 Ammonium production and other inputs

Although not measured directly, NH_4^+ production must have been sustained during the winter to retain an NH_4^+ pool that was high in concentration relative to the early summer. Additionally,

the residence times calculated for both winter and late summer ρNH_4^+ (10 to 38 days and 2 to 27 days, respectively) are shorter than the transition from late summer to winter (141 days; from the beginning of the late summer cruise, 28 February 2019, to the beginning of the winter cruise, 18 July 2019), so NH_4^+ production in autumn and winter, which would have occurred coincident with NH_4^+ consumption but was not measured here, cannot be ignored. Heterotrophic NH_4^+ production must, therefore, be ongoing in winter, albeit at a lower rate than in late summer due to the lower substrate (i.e., PON) concentrations and lower surface temperatures.

Heterotrophic bacteria contribute significantly to NH_4^+ production in the Southern Ocean (Hewes et al., 1985; Koike et al., 1986; Tréguer & Jacques, 1992), including in winter (Rembauville et al., 2017). In this dataset, lower ratios of photosynthetic-to-heterotrophic cells were observed at stations with higher NH_4^+ concentrations (e.g., stations 48.9°S, 53.0°S, 54.0°S, and 57.8°S; Fig. 12b), consistent with a role for heterotrophic bacteria present at the time of sampling in generating the ambient NH_4^+ pool. The potential for heterotrophic activity can also be inferred from the high detrital particle counts along the transect (Fig. 12c). However, since heterotrophic bacteria are likely more active in late summer and autumn when the temperature and the supply of labile PON are higher (Becquevort et al., 2000; Dennett et al., 2001; Pomeroy & Wiebe, 2001; Smart et al., 2020), it is expected that the winter NH_4^+ pool also includes residual NH_4^+ produced in late summer and autumn. A further potential complication is assimilation of NH_4^+ by heterotrophic bacteria. This can be seen at some AZ stations (53.5°S and 58.5°S) where the specific uptake rates of $NO_3^- + NH_4^+ +$ urea (i.e., V_{Ntot}) exceeded that of CO_2 fixation (V_C) (Fig. 15), an observation also found by Mdutyana et al. (2020) and interpreted as elevated wintertime assimilation of reduced N by heterotrophic bacteria (thus evincing their activity), which occurs in the absence of CO_2 fixation, thereby decoupling V_C and V_{Ntot} (Appendix 1). If this process is a persistent feature of the winter Southern Ocean, it will decrease the net contribution of heterotrophic bacteria to NH_4^+ accumulation. Thus, it is unlikely that the surface NH_4^+ pool measured in winter derived solely from wintertime bacterial NH_4^+ production given that yet higher NH_4^+ concentrations have been observed in late summer and autumn (Becquevort et al., 2000; Dennett et al., 2001), including in the present study (see section 5.2 below).

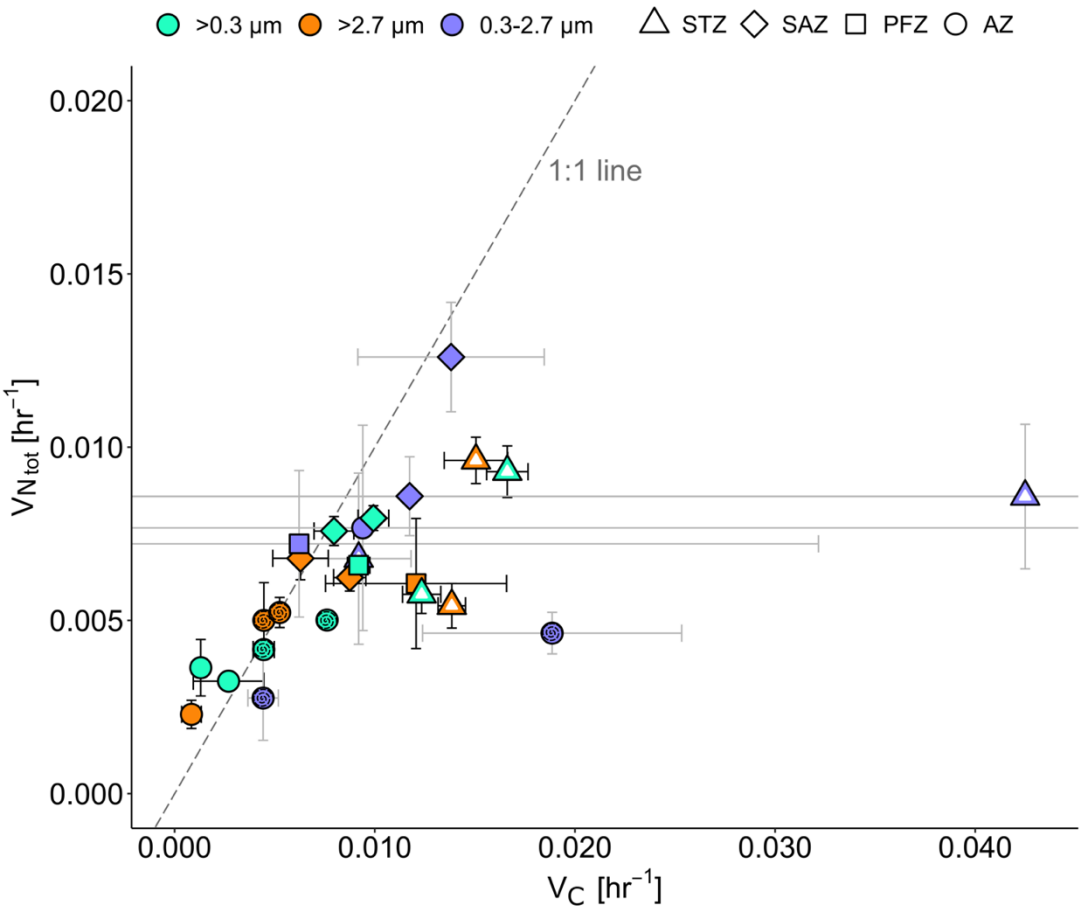

Figure 15: Specific rates of total nitrogen uptake (V_{Ntot}, = ρN_{tot} / [PON]) relative to carbon fixation (V_C). Error bars represent ± 1 standard error for duplicate experiments, with error propagated according to standard statistical practices. Light grey error bars indicate values calculated by subtraction (0.3-2.7 µm size class) and black error bars show the error for experimental duplicates. The specific rates are shown in relation to a 1:1 line, on which the data points are expected to fall if NPP is supported by the sum of NO_3^-, NH_4^+, and urea uptake. Circles indicate AZ stations (OAZ and PAZ), squares indicate PFZ stations, diamonds indicate SAZ stations, and open triangles indicate STZ stations. Open symbols are used for the STZ to differentiate them from 'true' Southern Ocean samples. Dotted circles indicate samples where no V_{urea} was measured. Abbreviations are as in Figure 2. Figure produced using the package ggplot2 (Wickham, 2016).

The microzooplankton enumerated in this study may also contribute to NH_4^+ accumulation. While the microzooplankton enumerated in this study occurred at very low abundances, those that were present likely contributed to the NH_4^+ flux. For example, at stations 48.9°S and 54.0°S in the PFZ and AZ, respectively, both the ratios of photosynthetic-to-heterotrophic cells and the absolute abundances of heterotrophic bacteria were low, while the microzooplankton abundances and NH_4^+ concentrations were elevated compared to nearby stations. In other words, elevated microzooplankton abundances may help to explain the high NH_4^+ concentrations in waters with low heterotrophic bacterial abundances, although it should be noted that this scenario only occurred at two stations. On balance, microzooplankton are likely

1037 less important for wintertime NH_4^+ production than heterotrophic bacteria given their low
1038 abundances in the surface layer (Fig. 11a; Atkinson et al., 2012).

1039 Above, it is assumed that the pathways leading to NH_4^+ production are associated with
1040 heterotrophy. However, there are other possible mechanisms of NH_4^+ generation that should
1041 be considered. Below these are addressed, noting that for most of the processes, there are no or
1042 very few observations from the Southern Ocean.

1043 NH_4^+ can be released by heterotrophic bacteria that directly consume DON (e.g., urea) (Billen,
1044 1984; Tupas & Koike, 1990), and possibly also by ammonia oxidisers that convert DON to
1045 NH_4^+ intracellularly, through the equilibration between intra- and extracellular NH_4^+ pools
1046 (Kitzinger et al., 2019). DON can also be converted to NH_4^+ through photodegradation by UV
1047 radiation (e.g., Aarnos et al., 2012). Bacterial decomposition of DON (rather than PON) to
1048 NH_4^+ is implicit in most estimates of ammonification, however, and cellular NH_4^+ efflux by
1049 ammonia oxidisers is likely extremely low given that they require NH_4^+ to fix CO_2. Finally,
1050 the low light levels of the wintertime Southern Ocean mean that photodegradation is unlikely
1051 to yield a significant NH_4^+ supply. Thus, DON conversion to NH_4^+, through any mechanism, is
1052 probably negligible.

1053 High surface ocean NH_4^+ concentrations may theoretically derive from external inputs of NH_4^+,
1054 such as from nitrogen fixation, NH_4^+ aerosol deposition, or sea-ice melt. Nitrogen fixation
1055 should be negligible in the winter Southern Ocean due to the extremely cold temperatures, low
1056 light and iron availability, and high NO_3^- concentrations (Jiang et al., 2018; Knapp et al., 2012;
1057 Kustka et al., 2003). Additionally, NH_4^+ aerosols are unlikely to be abundant over regions of
1058 the Southern Ocean remote from islands and coastal Antarctica, particularly in winter when
1059 NH_4^+ aerosol concentrations have been shown to reach a minimum (Legrand et al., 1998; Xu
1060 et al., 2019). Moreover, those that are present mainly originate from surface ocean NH_3 efflux;
1061 once re-deposited, this NH_4^+ does not constitute a new input term to surface waters (Altieri et
1062 al., 2021). NH_4^+ deposition to the surface Southern Ocean is thus likely minimal. Finally, since
1063 this sampling took place before the sea-ice reached its northernmost extent (Cavalieri &
1064 Parkinson, 2008), the dominant process would have been sea-ice formation rather than sea-ice
1065 melt, the latter an occasional source of NH_4^+ (Kattner et al., 2004; Zhou et al., 2014), although
1066 probably not during this study. In any case, elevated NH_4^+ was observed as far north as 46ºS in
1067 winter 2017, which is ~1700 km beyond the influence of sea-ice melt.

5.2 SEASONAL CYCLING OF NH_4^+ IN THE SOUTHERN OCEAN MIXED LAYER SOUTH OF THE SAF

To supplement the investigation above of the drivers of the wintertime NH_4^+ pool, NH_4^+ concentration data collected in 2018/19 over a single seasonal cycle is included. This will provide context to the 2017 dataset and assist in addressing the hypothesis presented here that NH_4^+ production in late summer and autumn contributes to the elevated NH_4^+ concentrations measured in winter.

A period of very low NH_4^+ concentrations occurred in the early summer in 2019 (Fig. 13a), resulting from rapid assimilation during the spring/summer phytoplankton bloom (Mdutyana et al., 2020; Savoye et al., 2004; Daly et al., 2001). This was followed by an increase in NH_4^+ concentrations in late summer due to elevated heterotrophic activity (i.e., bacterial decomposition and zooplankton grazing) following the accumulation of algal biomass (Mengesha et al., 1998; Le Moigne et al., 2013), coupled with iron- and/or silicate-limitation of phytoplankton (Hiscock et al., 2003; Sosik & Olson, 2002) and enhanced grazing pressure (Becquevort et al., 2000). Mixed-layer NH_4^+ concentrations remained high between late summer and winter, given the 2017 and 2019 winter measurements, likely due to sustained heterotrophic NH_4^+ production in excess of NH_4^+ removal. This notion is supported by estimates of the residence time of NH_4^+. Using the NH_4^+ concentrations and ρNH_4^+ measured in late summer 2019 (Deary, 2020) and the equations in section 3.3.2, the *in situ* NH_4^+ pool would be depleted in 2 to 27 days (median of 5 days) without coincident NH_4^+ production. Further, the net decline in NH_4^+ concentration of 0.31 ± 0.97 µM between late summer and winter requires an average NH_4^+ production rate of 52.8 ± 25.0 nM/day given the observed rates of NH_4^+ assimilation and the result from equation 8. This estimate is remarkably similar to the only measurements of NH_4^+ regeneration available for the Southern Ocean, measured near the Antarctic Peninsula in summer (average of 55 nM day^{-1}; Goeyens et al., 1991).

By the early spring, NH_4^+ concentrations had declined (Fig. 13d), implicating increased photosynthetic activity – and thus nutrient assimilation – following the alleviation of light-limitation that results in the assimilation of nutrients introduced into surface waters in winter. This study postulates that any residual NH_4^+ remaining in late winter/early spring would have been consumed prior to significant NO_3^- drawdown because far less energy (i.e., light) is required for its assimilation (Dortch, 1990). Contrastingly, high NH_4^+ concentrations in late spring, which are most noticeable in the PFZ (Fig. 13e), are attributed to elevated heterotrophic

activity in response to high levels of regional phytoplankton growth driven by frontal upwelling of limiting nutrients (Becquevort et al., 2000; Mayzaud et al., 2002).

From these six transects of surface NH_4^+ concentrations across the Southern Ocean, a seasonal cycle for mixed-layer NH_4^+ south of the SAF is proposed (Fig. 13f). This proposal is consistent with previous characterizations of the early summer-to-autumn evolution of Southern Ocean NH_4^+ concentrations (i.e., from below detection due to phytoplankton assimilation to elevated due to net heterotrophy). However, it contradicts the hypothesis that NH_4^+ will subsequently decline due to persistent but low rates of photosynthesis that yield insufficient biomass to support elevated heterotrophy in autumn, thus driving a coincident decrease in photosynthetic and heterotrophic activity (Koike et al., 1986; Serebrennikova & Fanning, 2004). Instead, the data in section 4.6.1 evince a gradual decline in mixed-layer NH_4^+ concentrations from late summer through winter. This decline can be explained by heterotrophic NH_4^+ production outpacing NH_4^+ removal in late summer/autumn, with NH_4^+ regeneration then decreasing during winter to lower rates than the combined rate of NH_4^+ assimilation and oxidation. By late spring, NH_4^+ reaches concentrations similar to those observed in early summer as the improved growing conditions (i.e., elevated light and iron availability; Ellwood et al., 2008; Mtshali et al., 2019) allow phytoplankton to rapidly consume any NH_4^+ remaining at the end of winter and subsequently produced in spring. An exception to this scenario is elevated, localized NH_4^+ production near fronts, such as what was observed in late spring 2019, which likely resulted from biological activity supported by frontal upwelling of silicate- and iron-bearing Upper Circumpolar Deep Water (Prézelin et al., 2000).

5.3 IMPLICATIONS OF AMMONIUM ACCUMULATION

5.3.1 Potential for ammonium inhibition of nitrate uptake

The low rates of NO_3^- uptake characteristic of winter Southern Ocean surface waters have been attributed to light, temperature, and micronutrient (especially iron) limitation of phytoplankton growth (Martin et al., 1990; Reay et al., 2001; Strzepek et al., 2019; Sunda & Huntsman, 1997). Wintertime NO_3^- uptake may be further inhibited by the high NH_4^+ concentrations, as has been observed in the Southern Ocean previously (Goeyens et al., 1995; Philibert et al., 2015; Reay et al., 2001). Previous Southern Ocean studies have identified an inhibitory effect of NH_4^+ on NO_3^- uptake at NH_4^+ concentrations >1 μM (and occasionally between 0.5 μM and 1 μM; Cochlan, 1986; Cochlan et al., 2002; Kristiansen & Farbrot, 1991; Reay et al., 2001). Such concentrations were measured at a number of stations along the 2019 transects (Fig. 13b,c,e;

and in 2017 if inhibition occurs at NH_4^+ concentrations of 0.5 μM; Fig. 5a). If the seasonal accumulation of NH_4^+ inhibits NO_3^- drawdown, this amounts to an inefficiency in the biological pump. However, some culture studies report only a slight inhibition of NO_3^- uptake, even at high NH_4^+ concentrations (>>1 μM; Bagwell, 2009; Dortch, 1990 and references therein), while others have detected no influence of NH_4^+ on NO_3^- consumption (Rees et al., 1999), suggesting that this effect is not straightforward. In winter 2017, little evidence of NH_4^+ inhibition of NO_3^- uptake was observed – for example, the southward decrease in ρNO_3^- was not sharper than that of ρNH_4^+ despite the increase in NH_4^+ concentration, and no relationship between NH_4^+ concentration and the proportion of NO_3^--to-total N uptake was observed (i.e., the f-ratio, r = 0.28 including urea; n=7). Therefore, NH_4^+ inhibition of NO_3^- uptake is unlikely in open Southern Ocean surface waters, but may occur near fronts and/or the coasts of islands and Antarctica where NH_4^+ can accumulate to concentrations >>1 μM (Henley et al., 2017; Koike et al., 1986; Krell et al., 2005; Goeyens et al., 1995). In the case of coastal waters, the damping effect of NH_4^+ inhibition on the biological pump is only relevant if the NH_4^+ being consumed in lieu of NO_3^- derives from *in situ* regeneration rather than being supplied from land.

5.3.2 Palaeoceanographic proxies

NH_4^+ cycling in the Southern Ocean mixed layer may be important for palaeoceanographic proxies (Smart et al., 2020; Robinson et al., 2020), such as those that use the $\delta^{15}N$ of organic matter preserved in fossil foraminifer or diatom shells to infer the extent of upper ocean NO_3^- consumption in the past (and by extension, the role of Southern Ocean biology in determining atmospheric CO_2; e.g., Martínez-García et al., 2014; Studer et al., 2015). A recent ground-truthing study from the Southern Ocean showed that the $\delta^{15}N$ of foraminifer-bound organic N tracks the $\delta^{15}N$ of PON rather than NO_3^- (Smart et al., 2020), in contrast to results from the low-latitude ocean (Ren et al., 2012; Smart et al., 2015). Between summer and winter, the $\delta^{15}N$ of mixed-layer PON declines in the Southern Ocean (particularly in the AZ) due to enhanced mixed-layer NH_4^+ cycling (Fig. 9; Lourey et al., 2003); this decrease will subsequently be reflected in the $\delta^{15}N$ of the foraminifera that feed on PON (Smart et al., 2020) and the late summer/autumn diatom communities that consume proportionally more NH_4^+ relative to NO_3^- than in spring and early summer (Studer et al., 2015; Kemeny et al., 2018). Thus, a decrease in the $\delta^{15}N$ of fossil foraminifera or diatoms could reflect enhanced NH_4^+ consumption by the upper ocean ecosystem rather than a change in the extent of NO_3^- drawdown, although this will depend on the degree to which surface conditions in the different seasons are communicated to

the sediments (Smart et al., 2020). Further clarifying the seasonal mixed-layer NH_4^+ cycle in the Southern Ocean may thus aid interpretations of palaeoceanographic records.

5.3.3 Ocean ammonia emissions

The implications of NH_4^+ cycling extend beyond the upper ocean to the atmosphere. Ammonium aerosols that influence Earth's albedo through scattering and absorption of solar radiation and cloud formation (Tevlin & Murphy, 2019) are formed in the marine boundary layer from reactions of NH_3 gas with acidic species, usually sulfur derived from surface ocean dimethylsulfide emissions. The ocean is the largest natural source of NH_3 globally, however, the magnitude of the marine NH_3 source remains highly uncertain (Paulot et al., 2015). Surface ocean NH_4^+ concentrations play a central role in determining the sign and magnitude of the air-sea NH_3 flux, along with wind speed, surface ocean temperature, and pH. Therefore, the biogeochemical pathways that drive seasonality in surface ocean NH_4^+ concentrations are an important control on the remote Southern Ocean air-sea NH_3 flux, with implications for aerosol composition, cloud formation, and climate (Altieri et al., 2021).

5.4 LIMITATIONS TO THE RESEARCH AND FUTURE STUDIES

In this section, the limitations of the presented data are discussed and the implications of these limitations for the conclusions in section 5.1 and 5.2 are explored.

5.4.1 Ammonium concentration and uptake rate measurements

The adjustment factor for the measured fluorescence (equation 4 in Taylor et al., 2007) can be attained through an experiment (e.g., using the standard addition method of Saxberg & Kowalski, 1979), that is conducted with each batch of samples that are analysed, and typically results in higher NH_4^+ concentrations than if it were not used. In the seasonal dataset, all concentrations included the correction for the matrix effect, thereby changing the amount of analyte recovered in the analysis by 8±15%. The matrix effect, as described in section 3.3.1, was not accounted for in the winter 2017 NH_4^+ concentrations, since it was only measured on leg N. Typically, the matrix effect correction typically increases the NH_4^+ concentration, so if anything, the NH_4^+ accumulation that is presented in this study for winter 2017 is an underestimate, and the lack of matrix correction should not affect the evidence for or interpretation of NH_4^+ accumulation in the wintertime Southern Ocean that is presented in this dissertation.

Real-time NH_4^+ concentration measurements could have benefited the outcome of the uptake and oxidation experiments, since lower than expected NH_4^+ concentrations may result in over stimulating phytoplankton in tracer experiments (Lipschultz, 2008). However, given the K_m values listed in section 5.1.1 and the high ambient NH_4^+ concentrations measured in the PFZ and AZ, a stimulation effect could only be significant at the stations north of the SAF where the NH_4^+ concentrations were 10-100 nM, and even then, to a lesser extent for NH_4^+ oxidation than uptake given that ammonia oxidizers in the winter Southern Ocean become saturated at NH_4^+ concentrations of 100-200 nM (Mdutyana, 2021). The rates reported for the stations north of the SAF should therefore be considered "potential rates". However, since the focus is mainly on explaining the accumulation of NH_4^+ south of the SAF, having "potential" rather than "true" rates for the STZ and SAZ does not change the conclusions drawn.

On the other hand, isotope dilution (i.e., the dilution of $^{15}NH_4^+$ by co-occurring $^{14}NH_4^+$ regeneration) during the NH_4^+ uptake and oxidation experiments may have led to an underestimation of the rates (Glibert, 1982; Mdutyana, 2021). However, the short duration of the NH_4^+ uptake experiments (3 to 7.5 hours) would have rendered the effect of regeneration minor (Mdutyana et al., 2020). Moreover, the $^{15}NH_4^+$ additions were high (100 nM) relative to both the ambient NH_4^+ concentrations north of the SAF and the K_m values derived for NH_4^+ uptake and oxidation in the winter Southern Ocean (150-405 nM and 28-137 nM, respectively; Mdutyana, 2021), making a significant dilution effect unlikely (Lipschultz, 2008). Finally, at the stations south of the SAF, the ambient NH_4^+ concentrations were so high that even if the regeneration of $^{14}NH_4^+$ occurred at an elevated rate (e.g., 50 nM day^{-1}; as has been measured in the late-summer Southern Ocean when remineralization is expected to be elevated; Goeyens et al., 1991), the $^{15}N/^{14}N$ of the NH_4^+ pool would decrease by <1-2%. Thus, the potential effect of isotope dilution is likely minor.

5.4.2 Microscopy and flow cytometry

The microscopy method (see section 3.2.7) has some inherent limitations and drawbacks, including the uncertainty that may be introduced by varying taxonomic abilities (Culverhouse et al., 2003; Culverhouse, 2007). Although, this study was not concerned with classification beyond the order level, likely lessening the error related to taxonomic ability. The application of the technique in this study was further flawed due to the lack of replicate samples and the small volume of each sample that was settled (20 mL). Both of these would lessen the statistical

validity of the cell counts. However, for each sample, at least 100 cells were counted to ensure a statistically valid estimate (D. Walker, pers. comm.).

The relatively low magnification (200x) used in the microscopy method limited the cell sizes that could be reliably distinguished to those ≥15 µm, however cells <15 µm were enumerated using flow cytometry to account for this. Lastly, as mentioned in section 3.2.3, the community composition in winter is expected to be dominated by small cells and so a more statistically robust cell count for plankton >15 µm would not be expected to result in a substantial change in the data or interpretation.

Similarly, single replicates were analysed by flow cytometry for cell counts <15 µm. However, data acquisition was terminated when a minimum of 5000 and maximum of 10000 events were recorded, as is typical for the method, allowing for a statistically robust result. The samples were only analysed on the flow cytometer two years after collection and cell counts decline during storage, due to cell lysis, a decline in the magnitude of the fluorescence signal, or to the attachment of cells to sample tube walls, and the severity of this effect may be different for different microorganism groups (Kamiya et al., 2007; Marie et al., 2014). In fact, Kamiya et al. (2007) found that the abundance of marine bacteria in samples fixed with glutaraldehyde was <50% after 90 days, compared to counts taken immediately after sampling. However, Marie et al. (2014) found a less pronounced effect on eukaryotes, thus our heterotrophic prokaryotes may in fact be more abundant than measured, implying a higher degree of NH_4^+ production. For winter 2017 stations south of 53.0°S, a 50% higher heterotrophic abundance would result in a photosynthetic-to-heterotrophic cell ratio closer to one, thus implying a more even balance between auto- and heterotrophy. This would in fact provide a better explanation for why NH_4^+ concentrations are still high by the wintertime despite ongoing assimilation.

5.4.3 Sampling resolution and additional data

Increasing the number and spatial resolution of samples along the transect would have provided a more reliable view of each Southern Ocean zone without interpolation over expansive distances, e.g. 0.5° latitude. Due to logistical limitations during winter 2017, samples were only collected at eight CTD stations on leg N and four-hourly on leg S. However, as mentioned in section 3.3, samples were collected from the ship's underway system on the south- and northbound transects every two hours in 2018 and 2019. Further, good agreement was found in the spatial variation of NH_4^+ concentrations between the winter 2017 and winter 2019 cruises, thus providing confidence that the transect in winter 2017 provided a good

representation of the wintertime Southern Ocean, at least in the case of the nutrient concentrations. Finally, a higher spatial resolution *longitudinally* would provide more confidence in the scaling-up of this study's conclusions to the entire Southern Ocean and may be possible with a combination of ship-based and remote sensing techniques.

As has been discussed in section 5.2, the lack of measured rates of heterotrophic NH_4^+ production is a hinderance to the certainty in conclusions made in this study. Although, the estimated rate in section 4.6.2 is in agreement with the only measured rate of NH_4^+ production in the Southern Ocean (Goeyens et al., 1991). Measurements of heterotrophic grazing rates are difficult to acquire, methods of which are summarised in Pearce et al. (2010), therefore the use of assumptions and inferences to determine the degree of heterotrophic activity is necessary where these direct measurements do not exist, as is done in this dissertation. Although, the reliability of these inferences needs to be considered. Thus, measured NH_4^+ production rates from the Southern Ocean, especially from the wintertime (experiments which were conducted in 2019 by our group but are unpublished), would hugely benefit the research conducted here.

The plankton community composition and nutrient uptake rates for the 2018 and 2019 seasonal dataset would also be a valuable contribution to better understand the seasonal dynamics of the surface Southern Ocean (these were conducted and will be analysed in the future by other laboratory group members). Further, in understanding how the community composition currently affects or has affected the NH_4^+ pool prior to sampling, a better understanding of the preference or lack thereof for NH_4^+ by each phytoplankton group in section 4.5 is needed. Similarly, the implication of a large NH_4^+ pool for CO_2 drawdown can only be accurately explained if it is known whether high NH_4^+ concentrations (>0.5 µM) inhibit NO_3^- uptake, however this is still disputed in current literature.

6 CONCLUSION

This study, conducted in the Southern Ocean during the infrequently-sampled winter season, provides new insights into the internal cycling of N in the mixed layer of a globally-important region. Measurements of NO_3^-, NH_4^+, and urea uptake, NH_4^+ oxidation rates, δ^{15}N-PON, and the ratio of photosynthetic-to-heterotrophic cells to investigate NH_4^+ assimilation, and the relationship of VN_{tot} to VC, and measurements of plankton community composition were used to evaluate the potential for heterotrophic NH_4^+ production. Elevated NH_4^+ concentrations that persist in the winter mixed layer south of the SAF were attributed to sustained heterotrophic NH_4^+ production in excess of phytoplankton- and nitrifier-mediated NH_4^+ assimilation, driven

by temperature-, light-, and possibly iron-limitation of the NH_4^+ consumers. Further, it was concluded that heterotrophic bacteria are the main NH_4^+ producers in winter and that the contributions of DON degradation, nitrogen fixation, aerosol deposition, and sea-ice melt to the Southern Ocean's mixed-layer NH_4^+ pool are negligible. Measurements of heterotrophic NH_4^+ production rates are required to confirm the hypothesized seasonal cycle of NH_4^+ in the Southern Ocean mixed layer, and higher spatial resolution sampling of plankton community composition and N removal rates may help to explain local variability in NH_4^+ concentrations, particularly near the fronts.

From observations of surface NH_4^+ concentrations made between December 2018 and November 2019, it is suggested that the high-concentration NH_4^+ pool cannot be generated solely during winter. Instead, it is proposed here that NH_4^+ initially accumulates in late summer following the peak phytoplankton growing season, after which sustained heterotrophy throughout the autumn and winter prevents this NH_4^+ from being depleted until the early spring. The persistence of elevated NH_4^+ concentrations across the polar Southern Ocean between late summer and winter implies that the mixed layer is a biological source of CO_2 to the atmosphere for at least half the year, not only because NO_3^- drawdown is weak at this time (Arteaga et al., 2019; Johnson et al., 2017), but also because the ambient conditions allow for NH_4^+ accumulation.

There are additional implications of the observations in this study. For example, NH_4^+ concentrations >1 μM (and at times >0.5 μM) have been reported to inhibit NO_3^- uptake, including in the Southern Ocean (Cochlan, 1986; Goeyens et al., 1995; Philibert et al., 2015; Reay et al., 2001) and this may amount to an inefficiency in the biological pump. However, little evidence of this effect was observed in winter 2017. It is more likely that high surface ocean NH_4^+ concentrations would have palaeoceanographic and atmospheric implications. There is a possibility for modern surface NH_4^+ cycle studies to aid interpretations of palaeoceanographic records. Finally, due to the significant role of NH_4^+ concentrations in determining the sign and magnitude of the air-sea NH_3 flux, biogeochemical pathways that drive seasonality in surface ocean NH_4^+ concentrations are an important control on this flux in the Southern Ocean, with implications for aerosol composition, cloud formation, and climate (Altieri et al., 2021).

7 APPENDIX

7.1 COUPLING OF NPP AND N UPTAKE

Plotting the specific rate of total dissolved nitrogen uptake (V_{Ntot}) against that of inorganic carbon fixation (V_C) at each station provides a means of assessing the coupling between autotrophic N consumption and primary production (Fig. 15). If the data fall on a 1:1 line in this space, the implications are that 1) primary production is well represented by total N uptake (i.e., a potentially significant N source to phytoplankton has not been overlooked in designing these experiments) and 2) all measured N uptake can be attributed to phytoplankton. Deviations from the 1:1 relationship can thus provide valuable information about the biogeochemical functioning of the upper ocean ecosystem (Flynn et al., 2018; Mdutyana et al., 2020; Peng et al., 2018).

As discussed in section 5.1.2 of the main text, the bulk specific rates at the AZ stations fall slightly above the 1:1 line, with $V_{Ntot} > V_C$ (circles in Fig. 15). This can be interpreted to evince consumption of dissolved N (likely NH_4^+ and/or urea) by heterotrophic bacteria, which would occur in the absence of carbon fixation. Indeed, significant rates of NH_4^+ uptake by heterotrophic bacteria have been inferred previously for the winter Southern Ocean from a decoupling of NPP and total N uptake (Mdutyana et al., 2020). Values of V_{Ntot} in excess of V_C could alternately be due to the stimulation of phytoplankton NH_4^+ uptake (above the *in situ* rates) following $^{15}NH_4^+$ tracer addition (Lipschultz, 2008). However, the ambient NH_4^+ concentrations in the AZ were the highest of the transect, and $^{15}NH_4^+$ was added at only ~10% of the ambient concentration, which is unlikely to have stimulated V_{NH_4}.

For the STZ stations, the bulk values of V_C considerably exceed V_{Ntot} (triangles in Fig. 15). One interpretation of such a deviation is that some fraction of the measured NPP was supported by an N source that was not accounted for here (Mdutyana et al., 2020; Peng et al., 2018). However, V_{Ntot} in the STZ includes NO_3^-, NH_4^+ and urea uptake, the three species that typically fuel phytoplankton growth. A further potential N source is N_2 fixation, but the available data suggest that this pathway is limited in the open subtropical South Atlantic (Mather et al., 2008; Moore et al., 2009), as is atmospheric N deposition (Baker et al., 2003; Jickells et al., 2016; Yan et al., 2013). An alternate possibility, as has been suggested for oligotrophic subtropical waters elsewhere (Fawcett et al., 2018), is that phytoplankton growing under nutrient-limited conditions will fix carbon in excess of their stoichiometric requirements (and thus in excess of

1351 V_{Ntot}) and then exude it into the environment where it will ultimately contribute to the
1352 formation of transparent exopolymer particles (TEP; Alldredge et al., 1993; Chin et al., 1998;
1353 Corzo et al., 2000; Engel, 2004; Mari et al., 2017).While this possibility cannot be ruled out,
1354 the nutrient concentrations at the SAZ stations at the time of sampling (NO_3^- of 2.4-3.4 µM
1355 and PO_4^{3-} of 0.39-0.49 µM; Fig. 6a and b) were unlikely to be limiting to subtropical
1356 phytoplankton. A perhaps more plausible explanation, therefore, is that the apparent surface
1357 decoupling of V_C and V_{Ntot} may not hold over the entire mixed layer given the far stronger light
1358 dependence of photosynthesis compared to inorganic N uptake (particularly NH_4^+ and urea;
1359 Dortch, 1990), such that if depth-resolved data was available in this study, mixed-layer
1360 integrated V_C and V_{Ntot} might be coupled.

1361

8 REFERENCES

Aarnos, H., Ylöstalo, P., and Vähätalo, A.V., (2012). Seasonal phototransformation of dissolved organic matter to ammonium, dissolved inorganic carbon, and labile substrates supporting bacterial biomass across the Baltic Sea. *Journal of Geophysical Research: Biogeosciences*, 117(G1).

Alldredge, A.L., and Gotschalk, C., (1988). In situ settling behavior of marine snow 1. *Limnology and Oceanography*, 33(3), pp.339-351.

Altabet, M.A., (1988). Variations in nitrogen isotopic composition between sinking and suspended particles: Implications for nitrogen cycling and particle transformation in the open ocean. *Deep Sea Research Part A. Oceanographic Research Papers*, 35(4), pp.535-554.

Altieri, K.E., Spence, K.A.M., and Smith, S., (2021). Air-Sea Ammonia Fluxes Calculated From High-Resolution Summertime Observations Across the Atlantic Southern Ocean. *Geophysical Research Letters*, 48(9), p.e2020GL091963.

Amin, S.A., Moffett, J.W., Martens-Habbena, W., Jacquot, J.E., Han, Y., Devol, A., Ingalls, A.E., Stahl, D.A., and Armbrust, E.V., (2013). Copper requirements of the ammonia-oxidizing archaeon *Nitrosopumilus maritimus* SCM1 and implications for nitrification in the marine environment. *Limnology and Oceanography*, 58(6), pp.2037-2045.

Anderson, R.F., Ali, S., Bradtmiller, L.I., Nielsen, S.H.H., Fleisher, M.Q., Anderson, B.E., and Burckle, L.H., (2009). Wind-driven upwelling in the Southern Ocean and the deglacial rise in atmospheric CO_2. *Science*, 323(5920), pp.1443-1448.

Armstrong, R.A., (1999). An optimization-based model of iron-light-ammonium colimitation of nitrate uptake and phytoplankton growth. *Limnology and Oceanography*, 44(6), pp.1436-1446.

Arrigo, K.R., and McClain, C.R., (1994). Spring phytoplankton production in the western Ross Sea. *Science*, 266(5183), pp.261-263.

Arrigo, K. R., van Dijken, G. L., and Bushinsky, S. (2008). Primary production in the Southern Ocean, 1997–2006. *Journal of Geophysical Research*, 113(C8), C08004.

Arteaga, L.A., Pahlow, M., Bushinsky, S.M., and Sarmiento, J.L., (2019). Nutrient controls on export production in the Southern Ocean. *Global Biogeochemical Cycles*, 33(8), pp.942-956.

Atkinson, A., Ward, P., Hunt, B.P.V., Pakhomov, E.A., and Hosie, G.W., (2012). An overview of Southern Ocean zooplankton data: abundance, biomass, feeding and functional relationships. *CCAMLR Science*, 19, pp.171-218.

Assmy, P., Smetacek, V., Montresor, M., Klaas, C., Henjes, J., Strass, V.H., Arrieta, J.M., Bathmann, U., Berg, G.M., Breitbarth, E., and Cisewski, B., (2013). Thick-shelled, grazer-protected diatoms

decouple ocean carbon and silicon cycles in the iron-limited Antarctic Circumpolar Current. *Proceedings of the National Academy of Sciences*, 110(51), pp.20633-20638.

Baer, S.E., Connelly, T.L., Sipler, R.E., Yager, P.L., and Bronk, D.A., (2014). Effect of temperature on rates of ammonium uptake and nitrification in the western coastal Arctic during winter, spring, and summer. *Global Biogeochemical Cycles*, 28(12), pp.1455-1466.

Bagwell, J.E., (2009). Transcriptional Response of Nitrogen Uptake and Assimilation in Marine Diatoms; *Thalassiosira Pseudonana* and *Thalassiosira Weissflogii* (Doctoral dissertation, University of North Carolina Wilmington).

Baines, S.B., Twining, B.S., Brzezinski, M.A., Nelson, D.M., and Fisher, N.S., (2010). Causes and biogeochemical implications of regional differences in silicification of marine diatoms. *Global Biogeochemical Cycles*, 24(4).

Baird, M.E., Emsley, S.M., and Mcglade, J.M., (2001). Modelling the interacting effects of nutrient uptake, light capture and temperature on phytoplankton growth. *Journal of Plankton Research*, 23(8), pp.829-840.

Barlow, R.G., and Alberte, R.S., (1985). Photosynthetic characteristics of phycoerythrin-containing marine *Synechococcus* spp.. *Marine Biology,* 86, pp.63–74.

Bathmann, U.V., Scharek, R., Klaas, C., Dubischar, C.D., and Smetacek, V., (1997). Spring development of phytoplankton biomass and composition in major water masses of the Atlantic sector of the Southern Ocean. *Deep Sea Research Part II: Topical Studies in Oceanography*, 44(1-2), pp.51-67.

Becquevort, S., Menon, P., and Lancelot, C., (2000). Differences of the protozoan biomass and grazing during spring and summer in the Indian sector of the Southern Ocean. *Polar Biology*, 23(5), 309–320.

Behrenfeld, M.J., Hu, Y., O'Malley, R.T., Boss, E.S., Hostetler, C.A., Siegel, D.A., Sarmiento, J.L., Schulien, J., Hair, J.W., Lu, X., and Rodier, S., (2017). Annual boom–bust cycles of polar phytoplankton biomass revealed by space-based lidar. *Nature Geoscience*, 10(2), pp.118-122.

Belkin, I. M., and Gordon, A. L., (1996). Southern Ocean fronts from the Greenwich meridian to Tasmania. *Journal of Geophysical Research C: Oceans*, 101(C2), 3675–3696.

Bendschneider, K., and Robinson, R.J., (1952). A new spectrophotometric method for the determination of nitrite in sea water.

Bianchi, M., Feliatra, F., Tréguer, P., Vincendeau, M.A., and Morvan, J., (1997). Nitrification rates, ammonium and nitrate distribution in upper layers of the water column and in sediments of the Indian sector of the Southern Ocean. *Deep Sea Research Part II: Topical Studies in Oceanography*, 44(5), pp.1017-1032.

Billen, G., (1984). Heterotrophic utilization and regeneration of nitrogen. In *Heterotrophic activity in the sea*. NATO Conference Series (IV Marine Sciences), vol 15. Springer, Boston, MA.

Bouwman, A. F., Lee, D. S., Asman, W. A. H., Dentener, F. J., Van Der Hoek, K. W., and Olivier, J. G. J., (1997). A global high-resolution emission inventory for ammonia. *Global Biogeochemical Cycles*, 11(4), 561–587.

Boyd, P.W., Crossley, A.C., DiTullio, G.R., Griffiths, F.B., Hutchins, D.A., Queguiner, B., Sedwick, P.N., and Trull, T.W., (2001). Control of phytoplankton growth by iron supply and irradiance in the subantarctic Southern Ocean: Experimental results from the SAZ Project. *Journal of Geophysical Research: Oceans*, 106(C12), pp.31573-31583.

Boyd, P. W., Rynearson, T. A., Armstrong, E. A., Fu, F., Hayashi, K., Hu, Z., Hutchins, D. A., Kudela, R. M., Litchman, E., Mulholland, M. R., Passow, U., Strzepek, R. F., Whittaker, K. A., Yu, E., and Thomas, M. K., (2013). Marine Phytoplankton Temperature versus Growth Responses from Polar to Tropical Waters - Outcome of a Scientific Community-Wide Study. *PLoS ONE*, 8(5), pp.1–17.

Bracher, A. U., Kroon, B. M. A., and Lucas, M. I., (1999). Primary production, physiological state and composition of phytoplankton in the Atlantic sector of the Southern Ocean. *Marine Ecology Progress Series*, 190, pp.1–16.

Bradford-Grieve, J.M., Boyd, P.W., Chang, F.H., Chiswell, S., Hadfield, M., Hall, J.A., James, M.R., Nodder, S.D., and Shushkina, E.A., (1999). Pelagic ecosystem structure and functioning in the Subtropical Front region east of New Zealand in austral winter and spring 1993. *Journal of Plankton Research*, 21(3), pp.405-428.

Brandini, F.P., Boltovskoy, D., Piola, A., Kocmur, S., Röttgers, R., Abreu, P.C., and Lopes, R.M., (2000). Multiannual trends in fronts and distribution of nutrients and chlorophyll in the southwestern Atlantic (30–62°S). *Deep Sea Research Part I: Oceanographic Research Papers*, 47(6), pp.1015-1033.

Brightman, R.I., and Smith Jr, W.O., (1989). Photosynthesis-irradiance relationships of Antarctic phytoplankton during austral winter. *Marine Ecology Progress Series*, 53(2), pp.143-151.

Broecker, W.S., and Peng, T.H., (1992). Interhemispheric transport of carbon dioxide by ocean circulation. *Nature*, 356(6370), pp.587-589.

Brzezinski, M. A., (1988). Vertical distribution of ammonium in stratified oligotrophic waters. *Limnology and Oceanography,* 33(5), pp.1176–1182.

Brzezinski, M.A., Nelson, D.M., Franck, V.M., and Sigman, D.E., (2001). Silicon dynamics within an intense open-ocean diatom bloom in the Pacific sector of the Southern Ocean. *Deep Sea Research Part II: Topical Studies in Oceanography*, 48(19-20), pp.3997-4018.

Buongiorno Nardelli, B., Guinehut, S., Verbrugge, N., Cotroneo, Y., Zambianchi, E., and Iudicone, D., (2017). Southern Ocean mixed-layer seasonal and interannual variations from combined satellite and in situ data. *Journal of Geophysical Research: Oceans*, *122*(12), pp.10042-10060.

Campitelli E., (2019). metR: Tools for Easier Analysis of Meteorological Fields. R package version 0.5.0. https://CRAN.R-project.org/package=metR

Capone, D.G., Bronk, D.A., Mulholland, M.R., and Carpenter, E.J. eds., (2008). *Nitrogen in the marine environment*. Elsevier.

Carter, L., McCave, I.N., and Williams, M.J., (2008). Circulation and water masses of the Southern Ocean: a review. *Developments in earth and environmental sciences*, 8, pp.85-114.

Carvalho, F., Kohut, J., Oliver, M.J., and Schofield, O., (2017). Defining the ecologically relevant mixed-layer depth for Antarctica's coastal seas. *Geophysical Research Letters*, 44(1), pp.338-345.

Cavagna, A.J., Fripiat, F., Elskens, M., Mangion, P., Chirurgien, L., Closset, I., Lasbleiz, M., Florez-Leiva, L., Cardinal, D., Leblanc, K., and Fernandez, C., (2015). Production regime and associated N cycling in the vicinity of Kerguelen Island, Southern Ocean. *Biogeosciences*, 12(21), pp.6515-6528.

Cavalieri, D.J., and Parkinson, C.L., (2008). Antarctic sea ice variability and trends, 1979–2006. *Journal of Geophysical Research: Oceans*, 113(C7).

Cavender-Bares, K.K., Mann, E.L., Chisholm, S.W., Ondrusek, M.E., and Bidigare, R.R., (1999). Differential response of equatorial Pacific phytoplankton to iron fertilization. *Limnology and Oceanography*, 44(2), pp.237-246.

Chapman, C.C., Lea, M.A., Meyer, A., Sallée, J.B., and Hindell, M., (2020). Defining Southern Ocean fronts and their influence on biological and physical processes in a changing climate. *Nature Climate Change*, 10(3), pp.209-219.

Checkley Jr, D.M., and Miller, C.A., (1989). Nitrogen isotope fractionation by oceanic zooplankton. *Deep Sea Research Part A: Oceanographic Research Papers*, 36(10), pp.1449-1456.

Chisholm, S. W. (1992). Phytoplankton Size. In: *Primary Productivity and Biogeochemical Cycles in the Sea*, edited by: Falkowski, P.G., Woodhead, A.D., and Vivirito, K., Springer United States of America, pp.213–237.

Church, M.J., DeLong, E.F., Ducklow, H.W., Karner, M.B., Preston, C.M., and Karl, D.M., (2003). Abundance and distribution of planktonic Archaea and Bacteria in the waters west of the Antarctic Peninsula. *Limnology and Oceanography*, 48(5), pp.1893-1902.

Coale, K. H., Gordon, R. M., and Wang, X., (2005). The distribution and behaviour of dissolved and particulate iron and zinc in the Ross Sea and Antarctic circumpolar current along 170°W. *Deep-Sea Research Part I: Oceanographic Research Papers*, 52(2), pp.295–318.

Cochlan, W.P., (1986). Seasonal study of uptake and regeneration of nitrogen on the Scotian Shelf. *Continental Shelf Research*, 5(5), pp.555-577.

Cochlan, W.P., (2008). Nitrogen uptake in the Southern Ocean. In: *Nitrogen in the Marine Environment*, edited by: Capone, D.G., Bronk, D.A., Mulholland, M.R., and Carpenter, E.J., 2nd Edition, Academic Press, Elsevier, pp.569-596.

Cochlan, W.P., Bronk, D.A., and Coale, K.H., (2002). Trace metals and nitrogenous nutrition of Antarctic phytoplankton: experimental observations in the Ross Sea. *Deep Sea Research Part II: Topical Studies in Oceanography*, 49(16), pp.3365-3390.

Coello-Camba, A., and Agustí, S., (2017). Thermal thresholds of phytoplankton growth in polar waters and their consequences for a warming polar ocean. *Frontiers in Marine Science*, 4, p.168.

Cota, G.F., Smith, W.O., Nelson, D.M., Muench, R.D., and Gordon, L.I., (1992). Nutrient and biogenic particulate distributions, primary productivity and nitrogen uptake in the Weddell-Scotia Sea marginal ice zone during winter. *Journal of Marine Research*, 50(1), pp.155-181.

Culverhouse, P.F., (2007). Human and machine factors in algae monitoring performance. *Ecological Informatics*, 2(4), pp.361-366.

Culverhouse, P.F., Williams, R., Reguera, B., Herry, V., and González-Gil, S., (2003). Do experts make mistakes? A comparison of human and machine indentification of dinoflagellates. *Marine Ecology Progress Series*, 247, pp.17-25.

Daly, K. L., Smith, W. O., Johnson, G. C., DiTullio, G. R., Jones, D. R., Mordy, C. W., Feely, R. A., Hansell, D. A., and Zhang, J.-Z., (2001). Hydrography, nutrients, and carbon pools in the Pacific sector of the Southern Ocean: Implications for carbon flux. *Journal of Geophysical Research: Oceans*, 106(C4), pp.7107–7124.

Deary, A. (2020). A high-resolution study of the early- to late summer progression in primary production and carbon export potential in the Atlantic Southern Ocean. (Honours dissertation, University of Cape Town).

del Giorgio, P.A., and Cole, J.J., (1998). Bacterial growth efficiency in natural aquatic systems. *Annual Review of Ecology and Systematics*, 29(1), pp.503-541.

Dennett, M. R., Mathot, S., Caron, D. A., Smith, W. O., and Lonsdale, D. J., (2001). Abundance and distribution of phototrophic and heterotrophic nano- and microplankton in the southern Ross Sea. *Deep-Sea Research Part II: Topical Studies in Oceanography*, 48(19–20), pp.4019–4037.

Deppeler, S.L., and Davidson, A.T., (2017). Southern Ocean phytoplankton in a changing climate. *Frontiers in Marine Science*, 4, p.40.

Detmer, A.E., and Bathmann, U.V., (1997). Distribution patterns of autotrophic pico-and nanoplankton and their relative contribution to algal biomass during spring in the Atlantic sector of the Southern Ocean. *Deep Sea Research Part II: Topical Studies in Oceanography*, 44(1-2), pp.299-320.

DiFiore, P. J., Sigman, D. M., Trull, T. W., Lourey, M. J., Karsh, K., Cane, G., and Ho, R., (2006). Nitrogen isotope constraints on subantarctic biogeochemistry. *Journal of Geophysical Research: Oceans*, 111(8).

Dixon, G.K., and Syrett, P.J., (1988). The growth of dinoflagellates in laboratory cultures. *New Phytologist*, 109(3), pp.297-302.

Doney, S.C., Mahowald, N., Lima, I., Feely, R.A., Mackenzie, F.T., Lamarque, J.F., and Rasch, P.J., (2007). Impact of anthropogenic atmospheric nitrogen and sulfur deposition on ocean acidification and the inorganic carbon system. *Proceedings of the National Academy of Sciences*, 104(37), pp.14580-14585.

Dong, S., Sprintall, J., Gille, S.T., and Talley, L., (2008). Southern Ocean mixed-layer depth from Argo float profiles. *Journal of Geophysical Research: Oceans*, 113(C6).

Dortch, Q., (1990). The interaction between ammonium and nitrate uptake in phytoplankton. *Marine Ecology Progress Series*, 61(1), pp.183–201.

Dugdale, R. C., and Goering, J. J., (1967). Uptake of new and regenerated forms of nitrogen in primary productivity. *Limnology and Oceanography*, 12(2), pp.196–206.

Dugdale, R.C., and Wilkerson, F.P., (1986). The use of ^{15}N to measure nitrogen uptake in eutrophic oceans; experimental considerations 1, 2. *Limnology and Oceanography*, 31(4), pp.673-689.

Ellwood, M.J., Boyd, P.W., and Sutton, P., (2008). Winter-time dissolved iron and nutrient distributions in the Subantarctic Zone from 40–52°S; 155–160°E. *Geophysical Research Letters*, 35(11).

El-Sayed, S., (1984). Productivity of the Antarctic waters—a reappraisal. In: *Marine phytoplankton and productivity*, edited by: Holm-Hansen, O., Bolis, L., and Gilles, R., Springer, Berlin, Heidelberg, pp.19–34.

Emery, W.J., (1977). Antarctic polar frontal zone from Australia to the Drake Passage. *Journal of Physical Oceanography*, 7(6), pp.811-822.

Engel, A., (2004). Distribution of transparent exopolymer particles (TEP) in the northeast Atlantic Ocean and their potential significance for aggregation processes. *Deep Sea Research Part I: Oceanographic Research Papers*, 51(1), pp.83-92.

Eppley, R.W., and Peterson, B.J., (1979). Particulate organic matter flux and planktonic new production in the deep ocean. *Nature*, 282(5740), pp.677-680.

Fan, C., Glibert, P.M., and Burkholder, J.M., (2003). Characterization of the affinity for nitrogen, uptake kinetics, and environmental relationships for *Prorocentrum minimum* in natural blooms and laboratory cultures. *Harmful Algae*, 2(4), pp.283-299.

Fawcett, S. E., and Ward, B. B., (2011). Phytoplankton succession and nitrogen utilization during the development of an upwelling bloom. *Marine Ecology Progress Series*, 428, pp.13–31.

Fawcett, S.E., Lomas, M.W., Casey, J.R., Ward, B.B., and Sigman, D.M., (2011). Assimilation of upwelled nitrate by small eukaryotes in the Sargasso Sea. *Nature Geoscience*, 4(10), pp.717-722.

Fawcett, S.E., Lomas, M.W., Ward, B.B., and Sigman, D.M., (2014). The counterintuitive effect of summer-to-fall mixed layer deepening on eukaryotic new production in the Sargasso Sea. *Global Biogeochemical Cycles*, 28(2), pp.86-102.

Fawcett, S.E., Johnson, K.S., Riser, S.C., Van Oostende, N., and Sigman, D.M., (2018). Low-nutrient organic matter in the Sargasso Sea thermocline: a hypothesis for its role, identity, and carbon cycle implications. *Marine Chemistry*, 207, pp.108-123.

Fiala, M., and Oriol, L., (1990). Light-temperature interactions on the growth of Antarctic diatoms. *Polar Biology*, 10(8), pp.629-636.

Fiala, M., Semeneh, M., and Oriol, L., (1998). Size-fractionated phytoplankton biomass and species composition in the Indian sector of the Southern Ocean during austral summer. *Journal of Marine Systems*, 17(1-4), pp.179-194.

Fieux, M. (2017). The Planetary Ocean. Les Ulis: EDP Sciences.

Finkel, Z.V., Irwin, A.J., and Schofield, O., (2004). Resource limitation alters the 3/4 size scaling of metabolic rates in phytoplankton. *Marine Ecology Progress Series*, 273, pp.269-279.

Finley A., Banerjee S., and Hjelle Ø. (2017). MBA: Multilevel B-Spline Approximation. package version 0.0-9. https://CRAN.R-project.org/package=MBA

Forsythe, W.C., Rykiel Jr, E.J., Stahl, R.S., Wu, H.I., and Schoolfield, R.M., (1995). A model comparison for daylength as a function of latitude and day of year. *Ecological Modelling*, 80(1), pp.87-95.

Flynn, R.F., Burger, J.M., Pillay, K., and Fawcett, S.E., (2018). Wintertime rates of net primary production and nitrate and ammonium uptake in the southern Benguela upwelling system. *African Journal of Marine Science*, 40(3), pp.253-266.

Franck, V.M., Brzezinski, M.A., Coale, K.H., and Nelson, D.M., (2000). Iron and silicic acid concentrations regulate Si uptake north and south of the Polar Frontal Zone in the Pacific Sector of the Southern Ocean. *Deep Sea Research Part II: Topical Studies in Oceanography*, 47(15-16), pp.3315-3338.

Franck, V.M., Smith, G.J., Bruland, K.W., and Brzezinski, M.A., (2005). Comparison of size-dependent carbon, nitrate, and silicic acid uptake rates in high-and low-iron waters. *Limnology and Oceanography*, 50(3), pp.825-838.

Francois, R., Altabet, M.A., and Burckle, L.H., (1992). Glacial to interglacial changes in surface nitrate utilization in the Indian sector of the Southern Ocean as recorded by sediment $\delta^{15}N$. *Paleoceanography*, 7(5), pp.589-606.

Fransson, A., Chierici, M., Anderson, L., and David, R., (2004). Transformation of carbon and oxygen in the surface layer of the eastern Atlantic sector of the Southern Ocean. *Deep Sea Research Part II: Topical Studies in Oceanography*, 51(22-24), pp.2757-2772.

Frigstad, H., Andersen, T., Hessen, D.O., Naustvoll, L.J., Johnsen, T.M., and Bellerby, R.G., (2011). Seasonal variation in marine C: N: P stoichiometry: can the composition of seston explain stable Redfield ratios?. *Biogeosciences*, 8(10), pp.2917-2933.

Fripiat, F., Elskens, M., Trull, T.W., Blain, S., Cavagna, A.J., Fernandez, C., Fonseca-Batista, D., Planchon, F., Raimbault, P., Roukaerts, A., and Dehairs, F., (2015). Significant mixed layer nitrification in a natural iron-fertilized bloom of the Southern Ocean. *Global Biogeochemical Cycles*, 29(11), pp.1929-1943.

Fripiat, F., Martínez-García, A., Fawcett, S.E., Kemeny, P.C., Studer, A.S., Smart, S.M., Rubach, F., Oleynik, S., Sigman, D.M., and Haug, G.H., (2019). The isotope effect of nitrate assimilation in the Antarctic Zone: Improved estimates and paleoceanographic implications. *Geochimica et Cosmochimica Acta*, 247, pp.261-279.

Fripiat, F., Martínez-García, A., Marconi, D., Fawcett, S.E., Kopf, S.H., Luu, V.H., Rafter, P.A., Zhang, R., Sigman, D.M., and Haug, G.H., (2021). Nitrogen isotopic constraints on nutrient sources to the upper ocean. *Nature Geoscience*,14, pp.855–861.

Frölicher, T.L., Sarmiento, J.L., Paynter, D.J., Dunne, J.P., Krasting, J.P., and Winton, M., (2015). Dominance of the Southern Ocean in anthropogenic carbon and heat uptake in CMIP5 models. *Journal of Climate*, 28(2), pp.862-886.

Froneman, P.W., Ansorge, I.J., Pakhomov, E.A., and Lutjeharms, J.R.E., (1999). Plankton community structure in the physical environment surrounding the Prince Edward Islands (Southern Ocean). *Polar Biology*, 22(3), pp.145-155.

Fujiki, T., and Taguchi, S., (2002). Variability in chlorophyll a specific absorption coefficient in marine phytoplankton as a function of cell size and irradiance. *Journal of Plankton Research*, 24(9), pp.859-874.

Gao, Y., Kaufman, Y. J., Tanré, D., Kolber, D., and Falkowski, P. G. (2001). Seasonal distributions of aeolian iron fluxes to the global ocean. *Geophysical Research Letters*, 28(1), pp.29–32.

Gasol, J.M., and del Giorgio, P.A., (2000). Using flow cytometry for counting natural planktonic bacteria and understanding the structure of planktonic bacterial communities. *Scientia Marina*, 64(2), pp.197-224.

Glibert, P.M., (1982). Regional studies of daily, seasonal and size fraction variability in ammonium remineralization. *Marine Biology*, 70(2), pp.209-222.

Goericke, R., (1998). Response of phytoplankton community structure and taxon-specific growth rates to seasonally varying physical forcing in the Sargasso Sea off Bermuda. *Limnology and Oceanography*, 43(5), pp.921-935.

Goeyens, L., Tréguer, P., Lancelot, C., Mathot, S., Becquevort, S., Morvan, J., Dehairs, F., and Baeyens, W., (1991). Ammonium regeneration in the Scotia-Weddell Confluence area during spring 1988. *Marine Ecology Progress Series*, 78, pp.241-252.

Goeyens, L., Tréguer, P., Baumann, M. E. M., Baeyens, W., and Dehairs, F., (1995). The leading role of ammonium in the nitrogen uptake regime of Southern Ocean marginal ice zones. *Journal of Marine Systems*, 6(4), pp.345–361.

Gordon, A.L., Georgi, D.T., and Taylor, H.W., (1977). Antarctic polar front zone in the western Scotia Sea—Summer 1975. *Journal of Physical Oceanography*, 7(3), pp.309-328.

Granger, J., Sigman, D.M., Needoba, J.A., and Harrison, P.J., (2004). Coupled nitrogen and oxygen isotope fractionation of nitrate during assimilation by cultures of marine phytoplankton. *Limnology and Oceanography,* 49(5), pp.1763-1773.

Granger, J., Sigman, D.M., Rohde, M.M., Maldonado, M.T., and Tortell, P.D., (2010). N and O isotope effects during nitrate assimilation by unicellular prokaryotic and eukaryotic plankton cultures. *Geochimica et Cosmochimica Acta*, 74(3), pp.1030-1040.

Greene, R.M., Geider, R.J., and Falkowski, P.G., (1991). Effect of iron limitation on photosynthesis in a marine diatom. *Limnology and Oceanography*, 36(8), pp.1772-1782.

Grolemund, G., and Wickham, H., (2011). Dates and Times Made Easy with {lubridate}, *Journal of Statistical Software*, 40, pp.1-25.

Harrison, W.G., (1976). Nitrate metabolism of the red tide dinoflagellate *Gonyaulax polyedra* Stein. *Journal of Experimental Marine Biology and Ecology*, 21(3), pp.199-209.

Hasle, R.G., (1978). The inverted microscope method. *Phytoplankton manual*, pp.88-96.

Henley, S.F., Tuerena, R.E., Annett, A.L., Fallick, A.E., Meredith, M.P., Venables, H.J., Clarke, A., and Ganeshram, R.S., (2017). Macronutrient supply, uptake and recycling in the coastal ocean of the

west Antarctic Peninsula. *Deep Sea Research Part II: Topical Studies in Oceanography*, 139, pp.58-76.

Henley, S.F., Cavan, E.L., Fawcett, S.E., Kerr, R., Monteiro, T., Sherrell, R.M., Bowie, A.R., Boyd, P.W., Barnes, D.K., Schloss, I.R., Marshall, T., Flynn, R., and Smith, S., (2020). Changing biogeochemistry of the Southern Ocean and its ecosystem implications. *Frontiers in Marine Science*, 7, p.581.

Herbert, R.A., (1999). Nitrogen cycling in coastal marine ecosystems. *FEMS microbiology reviews*, 23(5), pp.563-590.

Hewes, C.D., Holm-Hansen, O., and Sakshaug, E., (1985). Alternate carbon pathways at lower trophic levels in the Antarctic food web. In: *Antarctic nutrient cycles and food webs*, edited by: Siegfried, W.R., Condy, P.R., and Laws, R.M., Springer, Berlin, Heidelberg, pp. 277-283.

Hewes, C.D., Sakshaug, E., Reid, F.M., and Holm-Hansen, O., (1990). Microbial autotrophic and heterotrophic eucaryotes in Antarctic waters: relationships between biomass and chlorophyll, adenosine triphosphate and particulate organic carbon. *Marine Ecology Progress Series*, pp.27-35.

Hiscock, M.R., Marra, J., Smith Jr, W.O., Goericke, R., Measures, C., Vink, S., Olson, R.J., Sosik, H.M., and Barber, R.T., (2003). Primary productivity and its regulation in the Pacific Sector of the Southern Ocean. *Deep Sea Research Part II: Topical Studies in Oceanography*, 50(3-4), pp.533-558.

Holm-Hansen, O., Mitchell, B.G., Hewes, C.D., and Karl, D.M., (1989). Phytoplankton blooms in the vicinity of Palmer Station, Antarctica. *Polar Biology*, 10(1), pp.49-57.

Holmes, R.M., Aminot, A., Kérouel, R., Hooker, B.A., and Peterson, B.J., (1999). A simple and precise method for measuring ammonium in marine and freshwater ecosystems. *Canadian Journal of Fisheries and Aquatic Sciences*, 56(10), pp.1801-1808.

Holzer, M., Primeau, F.W., DeVries, T., and Matear, R., (2014). The Southern Ocean silicon trap: Data-constrained estimates of regenerated silicic acid, trapping efficiencies, and global transport paths. *Journal of Geophysical Research: Oceans*, 119(1), pp.313-331.

Honjo, S., (2004). Particle export and the biological pump in the Southern Ocean. *Antarctic Science*, 16(4), pp.501-516.

Honjo, S., Francois, R., Manganini, S., Dymond, J., and Collier, R., (2000). Particle fluxes to the interior of the Southern Ocean in the Western Pacific sector along 170 W. *Deep Sea Research Part II: Topical Studies in Oceanography*, 47(15-16), pp.3521-3548.

Hooper, A.B., and Terry, K.R., (1974). Photoinactivation of ammonia oxidation in Nitrosomonas. *Journal of Bacteriology*, 119(3), pp.899-906.

Horak, R.E., Qin, W., Schauer, A.J., Armbrust, E.V., Ingalls, A.E., Moffett, J.W., Stahl, D.A., and Devol, A.H., (2013). Ammonia oxidation kinetics and temperature sensitivity of a natural marine community dominated by Archaea. *The ISME journal*, 7(10), pp.2023-2033.

Horrigan, S. G., and Springer, A. L., (1990). Oceanic and estuarine ammonium oxidation: Effects of light. *Limnology and Oceanography*, 35(2), pp.479–482.

Huang, K., Feng, Q., Zhang, Y., Ou, L., Cen, J., Lu, S., and Qi, Y., (2020). Comparative uptake and assimilation of nitrate, ammonium, and urea by dinoflagellate *Karenia mikimotoi* and diatom *Skeletonema costatum sl* in the coastal waters of the East China Sea. *Marine Pollution Bulletin*, *155*, p.111200.

Hudson, R.J., and Morel, F.M., (1993). Trace metal transport by marine microorganisms: implications of metal coordination kinetics. *Deep Sea Research Part I: Oceanographic Research Papers*, 40(1), pp.129-150.

Hutchins, D.A., Sedwick, P.N., DiTullio, G.R., Boyd, P.W., Queguiner, B., Griffiths, F.B., and Crossley, C., (2001). Control of phytoplankton growth by iron and silicic acid availability in the subantarctic Southern Ocean: Experimental results from the SAZ Project. *Journal of Geophysical Research: Oceans*, 106(C12), pp.31559-31572.

Iida, T., and Odate, T., (2014). Seasonal variability of phytoplankton biomass and composition in the major water masses of the Indian Ocean sector of the Southern Ocean. *Polar Science*, 8(3), pp.283-297.

Ishikawa, A., Wright, S.W., van den Enden, R., Davidson, A.T., and Marchant, H.J., (2002). Abundance, size structure and community composition of phytoplankton in the Southern Ocean in the austral summer 1999/2000. *Polar Biosciences*. 15, pp.11-26.

Ito, T., Woloszyn, M., and Mazloff, M., (2010). Anthropogenic carbon dioxide transport in the Southern Ocean driven by Ekman flow. *Nature*, 463(7277), pp.80-83.

Jacobson, D. M., and Anderson, D. M., (1996). Widespread phagocytosis of ciliates and other protists by marine mixotrophic and heterotrophic thecate dinoflagellates. *Journal of Phycology*, 32(2), 279–285.

Janssen, D.J., Sieber, M., Ellwood, M.J., Conway, T.M., Barrett, P.M., Chen, X., de Souza, G.F., Hassler, C.S., and Jaccard, S.L., (2020). Trace metal and nutrient dynamics across broad biogeochemical gradients in the Indian and Pacific sectors of the Southern Ocean. *Marine Chemistry*, 221, p.103773.

Jeong, H.J., and Latz, M.I., (1994). Growth and grazing rates of the heterotrophic dinoflagellates *Protoperidinium* spp. on red tide dinoflagellates. *Marine Ecology Progress Series*, 106, pp.173-173.

1718 Jiang, H.B., Fu, F.X., Rivero-Calle, S., Levine, N.M., Sañudo-Wilhelmy, S.A., Qu, P.P., Wang, X.W.,
1719 Pinedo-Gonzalez, P., Zhu, Z., and Hutchins, D.A., (2018). Ocean warming alleviates iron limitation of
1720 marine nitrogen fixation. *Nature Climate Change*, 8(8), pp.709-712.

1721 Johnson, K.S., Plant, J.N., Dunne, J.P., Talley, L.D., and Sarmiento, J.L., (2017). Annual nitrate
1722 drawdown observed by SOCCOM profiling floats and the relationship to annual net community
1723 production. *Journal of Geophysical Research: Oceans*, 122(8), pp.6668-6683.

1724 Jones, R.D., Morita, R.Y., Koops, H.P., and Watson, S.W., (1988). A new marine ammonium-oxidizing
1725 bacterium, *Nitrosomonas cryotolerans* sp. nov. *Canadian Journal of Microbiology*, 34(10), pp.1122-
1726 1128.

1727 Joubert, W. R., Thomalla, S. J., Waldron, H. N., Lucas, M. I., Boye, M., Le Moigne, F. A. C., Planchon,
1728 F., and Speich, S., (2011). Nitrogen uptake by phytoplankton in the Atlantic sector of the Southern
1729 Ocean during late austral summer. *Biogeosciences*, 8(10), pp.2947–2959.

1730 Kamiya, E., Izumiyama, S., Nishimura, M., Mitchell, J.G., and Kogure, K., (2007). Effects of fixation
1731 and storage on flow cytometric analysis of marine bacteria. *Journal of Oceanography*, 63(1), pp.101-
1732 112.

1733 Kassambara A., (2019). ggpubr: 'ggplot2' Based Publication Ready Plots. R package version 0.2.4.
1734 https://CRAN.R-project.org/package=ggpubr

1735 Kattner, G., Thomas, D.N., Haas, C., Kennedy, H., and Dieckmann, G.S., (2004). Surface ice and gap
1736 layers in Antarctic sea ice: highly productive habitats. *Marine Ecology Progress Series*, 277, pp.1-12.

1737 Kelley, D., and Richards, C., (2020). oce: Analysis of Oceanographic Data. R package version 1.2-0.
1738 https://CRAN.R-project.org/package=oce

1739 Kemeny, P.C., Kast, E.R., Hain, M.P., Fawcett, S.E., Fripiat, F., Studer, A.S., Martínez-García, A.,
1740 Haug, G.H., and Sigman, D.M., (2018). A seasonal model of nitrogen isotopes in the ice age Antarctic
1741 Zone: Support for weakening of the Southern Ocean upper overturning cell. *Paleoceanography and*
1742 *Paleoclimatology*, 33(12), pp.1453-1471.

1743 Kirchman, D. L., (1994). The Uptake of Inorganic Nutrients by Heterotrophic Bacteria. *Microbial*
1744 *Ecology,* 28(2), pp.255–271.

1745 Kitzinger, K., Padilla, C.C., Marchant, H.K., Hach, P.F., Herbold, C.W., Kidane, A.T., Könneke, M.,
1746 Littmann, S., Mooshammer, M., Niggemann, J., and Petrov, S., (2019). Cyanate and urea are substrates
1747 for nitrification by Thaumarchaeota in the marine environment. *Nature Microbiology*, 4(2), pp.234-
1748 243.

Klawonn, I., Bonaglia, S., Whitehouse, M.J., Littmann, S., Tienken, D., Kuypers, M.M., Brüchert, V., and Ploug, H., (2019). Untangling hidden nutrient dynamics: rapid ammonium cycling and single-cell ammonium assimilation in marine plankton communities. *The ISME journa*l, 13(8), pp.1960-1974.

Knapp, A.N., Dekaezemacker, J., Bonnet, S., Sohm, J.A., and Capone, D.G., (2012). Sensitivity of *Trichodesmium erythraeum* and *Crocosphaera watsonii* abundance and N2 fixation rates to varying NO_3^- and PO_4^{3-} concentrations in batch cultures. *Aquatic microbial ecology*, 66(3), pp.223-236.

Kobayashi, F., and Takahashi, K., (2002). Distribution of diatoms along the equatorial transect in the western and central Pacific during the 1999 La Niña conditions. *Deep Sea Research Part II: Topical Studies in Oceanography*, 49(13-14), pp.2801-2821.

Koike, I., Holm-Hansen, O., and Biggs, D. C., (1986). Phytoplankton With Special Reference To Ammonium Cycling. *Marine Ecology*, 30, pp.105–116.

Kopczyńska, E. E., Savoye, N., Dehairs, F., Cardinal, D., and Elskens, M., (2007). Spring phytoplankton assemblages in the Southern Ocean between Australia and Antarctica. *Polar Biology*, 31(1), pp.77–88.

Kottmeier, S.T., and Sullivan, C.W., (1987). Late winter primary production and bacterial production in sea ice and seawater west of the Antarctic Peninsula. *Marine Ecology Progress Series*, 36, pp.287-298.

Krell, A., Schnack-Schiel, S.B., Thomas, D.N., Kattner, G., Zipan, W., and Dieckmann, G.S., (2005). Phytoplankton dynamics in relation to hydrography, nutrients and zooplankton at the onset of sea ice formation in the eastern Weddell Sea (Antarctica). *Polar Biology*, 28(9), pp.700-713.

Kristiansen, S., and Farbrot, T., (1991). Nitrogen uptake rates in phytoplankton and ice algae in the Barents Sea. *Polar Research*, 10(1), pp.187-192.

Kustka, A.B., Sañudo-Wilhelmy, S.A., Carpenter, E.J., Capone, D., Burns, J., and Sunda, W.G., (2003). Iron requirements for dinitrogen-and ammonium-supported growth in cultures of Trichodesmium (IMS 101): Comparison with nitrogen fixation rates and iron: Carbon ratios of field populations. *Limnology and Oceanography*, 48(5), pp.1869-1884.

La Roche, J., (1983). Ammonium regeneration: its contribution to phytoplankton nitrogen requirements in a eutrophic environment. *Marine Biology*, 75(2–3), pp.231–240.

Landry, M.R., Selph, K.E., Brown, S.L., Abbott, M.R., Measures, C.I., Vink, S., Allen, C.B., Calbet, A., Christensen, S., and Nolla, H., (2002). Seasonal dynamics of phytoplankton in the Antarctic Polar Front region at 170°W. *Deep Sea Research Part II: Topical Studies in Oceanography*, 49(9-10), pp.1843-1865.

Langlais, C., Rintoul, S., and Schiller, A., (2011). Variability and mesoscale activity of the Southern Ocean fronts: Identification of a circumpolar coordinate system. *Ocean Modelling*, 39(1-2), pp.79-96.

Laubscher, R.K., Perissinotto, R., and McQuaid, C.D., (1993). Phytoplankton production and biomass at frontal zones in the Atlantic sector of the Southern Ocean. *Polar Biology*, 13(7), pp.471-481.

Lauderdale, J.M., Garabato, A.C.N., Oliver, K.I., Follows, M.J., and Williams, R.G., (2013). Wind-driven changes in Southern Ocean residual circulation, ocean carbon reservoirs and atmospheric CO_2. *Climate dynamics*, 41(7-8), pp.2145-2164.

Lee, S.H., Joo, H.M., Liu, Z., Chen, J., and He, J., (2012). Phytoplankton productivity in newly opened waters of the Western Arctic Ocean. *Deep Sea Research Part II: Topical Studies in Oceanography*, 81, pp.18-27.

Lee, S.H., Yun, M.S., Kim, B.K., Joo, H., Kang, S.H., Kang, C.K., and Whitledge, T.E., (2013). Contribution of small phytoplankton to total primary production in the Chukchi Sea. *Continental Shelf Research*, 68, pp.43-50.

Legrand, M., Ducroz, F., Wagenbach, D., Mulvaney, R., and Hall, J., (1998). Ammonium in coastal Antarctic aerosol and snow: Role of polar ocean and penguin emissions. *Journal of Geophysical Research: Atmospheres*, 103(D9), pp.11043-11056.

Lehette, P., Tovar-Sánchez, A., Duarte, C.M., and Hernández-León, S., (2012). Krill excretion and its effect on primary production. *Marine Ecology Progress Series*, 459, pp.29-38.

Le Moigne, F. A., Boye, M., Masson, A., Corvaisier, R., Grossteffan, E., Gueneugues, A., Pondaven, P., Le Moigne, F. A. C., Boye, M., Corvaisier, R., Guéneugues, A., and Pondaven, P., (2013). Description of the biogeochemical features of the subtropical southeastern Atlantic and the Southern Ocean south of South Africa during the austral summer of the International Polar Year. *European Geosciences Union*, 10(10), pp.281–295.

Lin, C. T., Jickells, T. D., Baker, A. R., Marca, A., and Johnson, M. T., (2016). Aerosol isotopic ammonium signatures over the remote Atlantic Ocean. *Atmospheric Environment*, 133, pp.165–169.

Lipschultz, F., (2008). Isotope tracer methods for studies of the marine nitrogen cycle. In: *Nitrogen in the Marine Environment*, edited by: Capone, D.G., Bronk, D.A., Mulholland, M.R., and Carpenter, E.J., 2nd Edition, Academic Press, Elsevier, pp.1345-1384.

Llort, J., Lévy, M., Sallée, J.B., and Tagliabue, A., (2019). Nonmonotonic response of primary production and export to changes in mixed-layer depth in the Southern Ocean. *Geophysical Research Letters*, 46(6), pp.3368-3377.

Lomas, M.W., Baer, S.E., Acton, S., and Krause, J.W., (2019). Pumped up by the cold: elemental quotas and stoichiometry of cold-water diatoms. *Frontiers in Marine Science*, 6, p.286.

Longhurst, A. R., (1998). Ecological Geography of the Sea. Academic Press, San Diego, CA.

Lourey, M. J., Trull, T. W., and Sigman, D. M., (2003). Sensitivity of $\delta^{15}N$ of nitrate, surface suspended and deep sinking particulate nitrogen to seasonal nitrate depletion in the Southern Ocean. *Global Biogeochemical Cycles*, 17(3), pp.1081.

Lu, S., Liu, X., Liu, C., Cheng, G., and Shen, H., (2020). Influence of photoinhibition on nitrification by ammonia-oxidizing microorganisms in aquatic ecosystems. *Reviews in Environmental Science and Bio/Technology*, pp.1-12.

Lutjeharms, J.R.E., (1985). Location of frontal systems between Africa and Antarctica: some preliminary results. *Deep Sea Research Part A. Oceanographic Research Papers*, 32(12), pp.1499-1509.

Lutjeharms, J.R.E., and Ansorge, I.J., (2001). The Agulhas return current. *Journal of Marine Systems*, 30(1-2), pp.115-138.

Lutjeharms, J. R. E., and Valentine, H. R., (1984). Southern ocean thermal fronts south of Africa. *Deep Sea Research Part A, Oceanographic Research Papers*, 31(12), 1461–1475.

Lutjeharms, J.R.E., and Van Ballegooyen, R.C., (1988). Anomalous upstream retroflection in the Agulhas Current. *Science*, 240(4860), pp.1770-1770.

Machu, E., and Garçon, V., (2001). Phytoplankton seasonal distribution from SeaWiFS data in the Agulhas Current system. *Journal of Marine Research*, 59(5), pp.795-812.

Macko, S.A., Estep, M.L.F., Engel, M.H., and Hare, P.E., (1986). Kinetic fractionation of stable nitrogen isotopes during amino acid transamination. *Geochimica et Cosmochimica Acta*, 50(10), pp.2143-2146.

Maldonado, M.T., Allen, A.E., Chong, J.S., Lin, K., Leus, D., Karpenko, N., and Harris, S.L., (2006). Copper-dependent iron transport in coastal and oceanic diatoms. *Limnology and Oceanography*, 51(4), pp.1729-1743.

Marie, D., Partensky, F., Jacquet, S., and Vaulot, D., (1997). Enumeration and cell cycle analysis of natural populations of marine picoplankton by flow cytometry using the nucleic acid stain SYBR Green I. *Appl. Environ. Microbiol.*, 63(1), pp.186-193.

Marie, D., Simon, N., and Vaulot, D., (2005). Phytoplankton cell counting by flow cytometry. *Algal Culturing Techniques*, 1, pp.253-267.

Marie, D., Rigaut-Jalabert, F., and Vaulot, D., (2014). An improved protocol for flow cytometry analysis of phytoplankton cultures and natural samples. *Cytometry Part A*, 85(11), pp.962-968.

Marinov, I., Gnanadesikan, A., Toggweiler, J.R., and Sarmiento, J.L., (2006). The southern ocean biogeochemical divide. *Nature*, 441(7096), pp.964-967.

Martin, J.H., Fitzwater, S.E., and Gordon, R.M., (1990). Iron deficiency limits phytoplankton growth in Antarctic waters. *Global Biogeochemical Cycles*, 4(1), pp.5-12.

Martínez-García, A., Sigman, D.M., Ren, H., Anderson, R.F., Straub, M., Hodell, D.A., Jaccard, S.L., Eglinton, T.I., and Haug, G.H., (2014). Iron fertilization of the Subantarctic Ocean during the last ice age. *Science*, 343(6177), pp.1347-1350.

Mayzaud, P., Razouls, S., Errhif, A., Tirelli, V., and Labat, J.P., (2002). Feeding, respiration and egg production rates of copepods during austral spring in the Indian sector of the Antarctic Ocean: role of the zooplankton community in carbon transformation. *Deep Sea Research Part I: Oceanographic Research Papers*, 49(6), pp.1027-1048.

McCartney, M.S., (1979). Subantarctic mode water. Woods Hole Oceanographic Institution.

McIlvin, M.R., and Altabet, M.A., (2005). Chemical conversion of nitrate and nitrite to nitrous oxide for nitrogen and oxygen isotopic analysis in freshwater and seawater. *Analytical Chemistry*, 77(17), pp.5589-5595.

McIlvin, M.R., and Casciotti, K.L., (2011). Technical updates to the bacterial method for nitrate isotopic analyses. *Analytical Chemistry*, 83(5), pp.1850-1856.

Mdutyana, M., Thomalla, S.J., Philibert, R., Ward, B.B., and Fawcett, S.E., (2020). The seasonal cycle of nitrogen uptake and nitrification in the Atlantic sector of the Southern Ocean. *Global Biogeochemical Cycles*, 34(7), p.e2019GB006363.

Mdutyana, M., (2021). Mixed layer nitrogen cycling in the Southern Ocean: seasonality, kinetics, and biogeochemical implications. (PhD thesis, University of Cape Town).

Mei, Z.P., Finkel, Z.V., and Irwin, A.J., (2009). Light and nutrient availability affect the size-scaling of growth in phytoplankton. *Journal of Theoretical Biology*, 259(3), pp.582-588.

Mengesha, S., Dehairs, F., Fiala, M., Elskens, M., and Goeyens, L., (1998). Seasonal variation of phytoplankton community structure and nitrogen uptake regime in the Indian Sector of the Southern Ocean. *Polar Biology*, 20(4), pp.259–272.

Möbius, J., (2013). Isotope fractionation during nitrogen remineralization (ammonification): Implications for nitrogen isotope biogeochemistry. *Geochimica et Cosmochimica Acta*, 105, pp.422-432.

Mongin, M., Nelson, D.M., Pondaven, P., and Tréguer, P., (2006). Simulation of upper-ocean biogeochemistry with a flexible-composition phytoplankton model: C, N and Si cycling and Fe limitation in the Southern Ocean. *Deep Sea Research Part II: Topical Studies in Oceanography*, 53(5-7), pp.601-619.

Moore, J.K., Abbott, M.R., Richman, J.G., Smith, W.O., Cowles, T.J., Coale, K.H., Gardner, W.D., and Barber, R.T., (1999). SeaWiFS satellite ocean color data from the Southern Ocean. *Geophysical Research Letters*, 26(10), pp.1465-1468.

Moore, C.M., Mills, M.M., Achterberg, E.P., Geider, R.J., LaRoche, J., Lucas, M.I., McDonagh, E.L., Pan, X., Poulton, A.J., Rijkenberg, M.J., and Suggett, D.J., (2009). Large-scale distribution of Atlantic nitrogen fixation controlled by iron availability. *Nature Geoscience*, 2(12), pp.867-871.

Mordy, C.W., Penny, D.M., and Sullivan, C.W., (1995). Spatial distribution of bacterioplankton biomass and production in the marginal ice-edge zone of the Weddell-Scotia Sea during austral winter. *Marine Ecology Progress Series*, 122, pp.9-19.

Moreau, S., Boyd, P.W., and Strutton, P.G., (2020). Remote assessment of the fate of phytoplankton in the Southern Ocean sea-ice zone. *Nature Communications*, 11(1), pp.1-9.

Morel, F.M., Hudson, R.J., and Price, N.M., (1991). Limitation of productivity by trace metals in the sea. *Limnology and Oceanography*, 36(8), pp.1742-1755.

Mtshali, T.N., van Horsten, N.R., Thomalla, S.J., Ryan-Keogh, T.J., Nicholson, S.A., Roychoudhury, A.N., Bucciarelli, E., Sarthou, G., Tagliabue, A., and Monteiro, P.M., (2019). Seasonal depletion of the dissolved iron reservoirs in the sub-Antarctic zone of the Southern Atlantic Ocean. *Geophysical Research Letters*, 46(8), pp.4386-4395.

Munk, W.H., and Riley, G., (1952). Absorption of nutrients by aquatic plants. *Journal of Marine Research,* 11, pp. 215-240.

Murphy, J., and Riley, J.P., (1962). A modified single solution method for the determination of phosphate in natural waters. *Analytica chimica acta*, 27, pp.31-36.

Nelson, D.M., Brzezinski, M.A., Sigmon, D.E., and Franck, V.M., (2001). A seasonal progression of Si limitation in the Pacific sector of the Southern Ocean. *Deep Sea Research Part II: Topical Studies in Oceanography*, 48(19-20), pp.3973-3995.

Olson, R.J., (1981). Differential photoinhibition of marine nitrifying bacteria: a possible mechanism for the formation of the primary nitrite maximum. *Journal of Marine Research*, 39(2), pp.227-238.

Orsi, A. H., Whitworth, T., and Nowlin, W. D., (1995). On the meridional extent and fronts of the Antarctic Circumpolar Current. *Deep-Sea Research Part I: Oceanographic Research Papers*, 42(5), pp.641–673.

Owens, N.J.P., Priddle, J., and Whitehouse, M.J., (1991). Variations in phytoplanktonic nitrogen assimilation around South Georgia and in the Bransfield Strait (Southern Ocean). *Marine Chemistry*, 35(1-4), pp.287-304.

Pachiadaki, M.G., Sintes, E., Bergauer, K., Brown, J.M., Record, N.R., Swan, B.K., Mathyer, M.E., Hallam, S.J., Lopez-Garcia, P., Takaki, Y., and Nunoura, T., (2017). Major role of nitrite-oxidizing bacteria in dark ocean carbon fixation. *Science*, 358(6366), pp.1046-1051.

Painter, S.C., Patey, M.D., Tarran, G.A., and Torres-Valdés, S., (2014). Picoeukaryote distribution in relation to nitrate uptake in the oceanic nitracline. *Aquatic Microbial Ecology*, 72(3), pp.195-213.

Palenik, B., Brahamsha, B., Larimer, F. W., Land, M., Hauser, L., Chain, P., Lamerdin, J., Regala, W., Allen, E. E., McCarren, J., Paulsen, I., Dufresne, A., Partensky, F., Webb, E. A., and Waterbury, J., (2003). The genome of a motile marine *Synechococcus*. *Nature*, 424(6952), pp.1037–1042.

Palter, J.B., Sarmiento, J.L., Gnanadesikan, A., Simeon, J., and Slater, R.D., (2010). Fueling export production: nutrient return pathways from the deep ocean and their dependence on the Meridional Overturning Circulation. *Biogeosciences*, 7(11), pp.3549-3568.

Park, Y.H., Charriaud, E., and Fieux, M., (1998). Thermohaline structure of the Antarctic surface water/winter water in the Indian sector of the Southern Ocean. *Journal of Marine Systems*, 17(1-4), pp.5-23.

Paulot, F., Jacob, D. J., Johnson, M. T., Bell, T. G., Baker, A. R., Keene, W. C., Lima, I. D., Doney, S. C., and Stock, C. A., (2015). Global oceanic emission of ammonia: Constraints from seawater and atmospheric observations. *Global Biogeochemical Cycles*, 29(8), pp.1165–1178.

Pausch, F., Bischof, K., and Trimborn, S., (2019). Iron and manganese co-limit growth of the Southern Ocean diatom Chaetoceros debilis. *PloS ONE*, 14(9), p.e0221959.

Pearce, I., Davidson, A. T., Thomson, P. G., Wright, S., and van den Enden, R., (2010). Marine microbial ecology off East Antarctica (30 - 80°E): Rates of bacterial and phytoplankton growth and grazing by heterotrophic protists. *Deep-Sea Research Part II: Topical Studies in Oceanography*, 57(9–10), pp.849–862.

Peng, X., Fuchsman, C.A., Jayakumar, A., Oleynik, S., Martens-Habbena, W., Devol, A.H., and Ward, B.B., (2015). Ammonia and nitrite oxidation in the Eastern Tropical North Pacific. *Global Biogeochemical Cycles*, 29(12), pp.2034-2049.

Peng, X., Fawcett, S.E., Van Oostende, N., Wolf, M.J., Marconi, D., Sigman, D.M., and Ward, B.B., (2018). Nitrogen uptake and nitrification in the subarctic North Atlantic Ocean. *Limnology and Oceanography*, 63(4), pp.1462-1487.

Philibert, R., Waldron, H., and Clark, D., (2015). A geographical and seasonal comparison of nitrogen uptake by phytoplankton in the Southern Ocean. *Ocean Science*, 11(2), pp.251-267.

Plate, T., and Heiberger, R., (2019). abind: Combine multi-dimensional arrays. R package version 1.1. https://cran.r-project.org/web/packages/abind

Pollard, R.T., Lucas, M.I., and Read, J.F., (2002). Physical controls on biogeochemical zonation in the Southern Ocean. *Deep Sea Research Part II: Topical Studies in Oceanography*, 49(16), pp.3289-3305.

Pomeroy, L. R., and Wiebe, W. J., (2001). Temperature and substrates as interactive limiting factors for marine heterotrophic bacteria. *Aquatic Microbial Ecology*, 23(2), pp.187–204.

Pondaven, P., Ragueneau, O., Tréguer, P., Hauvespre, A., Dezileau, L., and Reyss, J.L., (2000). Resolving the 'opal paradox' in the Southern Ocean. *Nature*, 405(6783), pp.168-172.

Popp, B.N., Trull, T., Kenig, F., Wakeham, S.G., Rust, T.M., Tilbrook, B., Griffiths, B., Wright, S.W., Marchant, H.J., Bidigare, R.R., and Laws, E.A., (1999). Controls on the carbon isotopic composition of Southern Ocean phytoplankton. *Global Biogeochemical Cycles*, 13(4), pp.827-843.

Prézelin, B.B., Hofmann, E.E., Mengelt, C., and Klinck, J.M., (2000). The linkage between Upper Circumpolar Deep Water (UCDW) and phytoplankton assemblages on the west Antarctic Peninsula continental shelf. *Journal of Marine Research*, 58(2), pp.165-202.

Price, N.M., Ahner, B.A., and Morel, F.M., (1994). The equatorial Pacific Ocean: Grazer-controlled phytoplankton populations in an iron-limited ecosystem 1. *Limnology and Oceanography*, 39(3), pp.520-534.

Primeau, F. W., Holzer, M., and DeVries, T., (2013). Southern Ocean nutrient trapping and the efficiency of the biological pump. *Journal of Geophysical Research: Oceans*, 118(5), pp.2547–2564.

R Core Team, (2020). R: A language and environment for statistical computing. R Foundation for Statistical Computing, Vienna, Austria. https://www.R-project.org/.

Raven, J.A., (1988). The iron and molybdenum use efficiencies of plant growth with different energy, carbon and nitrogen sources. *New Phytologist*, 109(3), pp.279-287.

Read, J.F., Pollard, R.T., and Bathmann, U., (2002). Physical and biological patchiness of an upper ocean transect from South Africa to the ice edge near the Greenwich Meridian. *Deep Sea Research Part II: Topical Studies in Oceanography*, 49(18), pp.3713-3733.

Reay, D. S., Priddle, J., Nedwell, D. B., Whitehouse, M. J., Ellis-Evans, J. C., Deubert, C., and Connelly, D. P., (2001). Regulation by low temperature of phytoplankton growth and nutrient uptake in the Southern Ocean. *Marine Ecology Progress Series*, 219(1990), pp.51–64.

Rees, A., Woodward, M., and Joint, I., (1999). Measurement of nitrate and ammonium uptake at ambient concentrations in oligotrophic waters of the North-East Atlantic Ocean. *Marine Ecology Progress Series*, 187, pp.295-300.

Rembauville, M., Briggs, N., Ardyna, M., Uitz, J., Catala, P., Penkerc'h, C., Poteau, A., Claustre, H., and Blain, S., (2017). Plankton assemblage estimated with BGC-Argo floats in the Southern Ocean:

Implications for seasonal successions and particle export. *Journal of Geophysical Research: Oceans*, 122(10), pp.8278-8292.

Ren, H., Sigman, D.M., Thunell, R.C., and Prokopenko, M.G., (2012). Nitrogen isotopic composition of planktonic foraminifera from the modern ocean and recent sediments. *Limnology and Oceanography*, 57(4), pp.1011-1024.

Revilla, M., Alexander, J., and Glibert, P.M., (2005). Urea analysis in coastal waters: comparison of enzymatic and direct methods. *Limnology and Oceanography: Methods*, 3(7), pp.290-299.

Richardson, T.L., and Jackson, G.A., (2007). Small phytoplankton and carbon export from the surface ocean. *Science*, 315(5813), pp.838-840.

Rintoul, S.R., and Trull, T.W., (2001). Seasonal evolution of the mixed layer in the Subantarctic Zone south of Australia. *Journal of Geophysical Research: Oceans*, 106(C12), pp.31447-31462.

Robinson, R.S., Jones, C.A., Kelly, R.P., Love, A., Closset, I., Rafter, P.A., and Brzezinski, M., (2020). A Test of the Diatom-Bound Paleoproxy: Tracing the Isotopic Composition of Nutrient-Nitrogen Into Southern Ocean Particles and Sediments. *Global Biogeochemical Cycles*, 34(10), p.e2019GB006508.

Rodrigues, R.M., and Williams, P.J.L.B., (2001). Heterotrophic bacterial utilization of nitrogenous and nonnitrogenous substrates, determined from ammonia and oxygen fluxes. *Limnology and Oceanography*, 46(7), pp.1675-1683.

Sallée, J.B., Speer, K.G., and Rintoul, S.R., (2010). Zonally asymmetric response of the Southern Ocean mixed-layer depth to the Southern Annular Mode. *Nature Geoscience*, 3(4), pp.273-279.

Sambrotto, R.N., and Mace, B.J., (2000). Coupling of biological and physical regimes across the Antarctic Polar Front as reflected by nitrogen production and recycling. *Deep Sea Research Part II: Topical Studies in Oceanography*, 47(15-16), pp.3339-3367.

Santoro, A.E., Sakamoto, C.M., Smith, J.M., Plant, J.N., Gehman, A.L., Worden, A.Z., Johnson, K.S., Francis, C.A., and Casciotti, K.L., (2013). Measurements of nitrite production in and around the primary nitrite maximum in the central California Current. *Biogeosciences*, 10(11), pp.7395-7410.

Sarmiento, J.L., and Orr, J.C., (1991). Three-dimensional simulations of the impact of Southern Ocean nutrient depletion on atmospheric CO_2 and ocean chemistry. *Limnology and Oceanography*, 36(8), pp.1928-1950.

Sarmiento, J.L., and Toggweiler, J.R., (1984). A new model for the role of the oceans in determining atmospheric pCO_2. *Nature*, 308(5960), pp.621-624.

Sarmiento, J. L., Gruber, N., Brzezinski, M. A., and Dunne, J. P., (2004). High-latitude controls of thermocline nutrients and low latitude biological productivity. *Nature*, 427(6969), pp.56–60.

Savoye, N., Dehairs, F., Elskens, M., Cardinal, D., Kopczyńska, E.E., Trull, T.W., Wright, S., Baeyens, W., and Griffiths, F.B., (2004). Regional variation of spring N-uptake and new production in the Southern Ocean. *Geophysical Research Letters*, 31(3), pp.L03301.

Saxberg, B.E., and Kowalski, B.R., (1979). Generalized standard addition method. *Analytical Chemistry*, 51(7), pp.1031-1038.

Schaafsma, F. L., Cherel, Y., Flores, H., van Franeker, J. A., Lea, M. A., Raymond, B., and van de Putte, A. P., (2018). Review: the energetic value of zooplankton and nekton species of the Southern Ocean. *Marine Biology*, 165(8), pp.1–35.

Scharek, R., Smetacek, V., Fahrbach, E., Gordon, L.I., Rohardt, G., and Moore, S., (1994). The transition from winter to early spring in the eastern Weddell Sea, Antarctica: plankton biomass and composition in relation to hydrography and nutrients. *Deep Sea Research Part I: Oceanographic Research Papers*, 41(8), pp.1231-1250.

Schön, G. H., and Engel, H., (1962). Der Einflußdes Lichtes auf Nitrosomonas europaea Win. *Archiv Für Mikrobiologie*, 42(4), pp.415–428.

Sedwick, P. N., Bowie, A. R., and Trull, T. W., (2008). Dissolved iron in the Australian sector of the Southern Ocean (CLIVAR SR3 section): Meridional and seasonal trends. *Deep-Sea Research Part I: Oceanographic Research Papers*, 55(8), pp.911–925.

Semeneh, M., Dehairs, F., Elskens, M., Baumann, M. E. M., Kopczynska, E. E., Lancelot, C., and Goeyens, L., (1998). Nitrogen uptake regime and phytoplankton community structure in the Atlantic and Indian sectors of the Southern Ocean. *Journal of Marine Systems*, 17(1–4), pp.159–177.

Serebrennikova, Y. M., and Fanning, K. A., (2004). Nutrients in the Southern Ocean GLOBEC region: Variations, water circulation, and cycling. *Deep-Sea Research Part II: Topical Studies in Oceanography*, 51(17–19), pp.1981–2002.

Shadwick, E.H., Trull, T.W., Tilbrook, B., Sutton, A.J., Schulz, E., and Sabine, C.L., (2015). Seasonality of biological and physical controls on surface ocean CO_2 from hourly observations at the Southern Ocean Time Series site south of Australia. *Global Biogeochemical Cycles*, 29(2), pp.223-238.

Shafiee, R.T., Snow, J.T., Zhang, Q., and Rickaby, R.E., (2019). Iron requirements and uptake strategies of the globally abundant marine ammonia-oxidising archaeon, *Nitrosopumilus maritimus* SCM1. *The ISME journal*, 13(9), pp.2295-2305.

Shiozaki, T., Fujiwara, A., Ijichi, M., Harada, N., Nishino, S., Nishi, S., Nagata, T., and Hamasaki, K., (2018). Diazotroph community structure and the role of nitrogen fixation in the nitrogen cycle in the Chukchi Sea (western Arctic Ocean). *Limnology and Oceanography*, 63(5), pp.2191-2205.

Sigman, D. M., Altabet, M. A., McCorkle, D. C., Francois, R., and Fischer, G., (1999). The δ ^{15}N of nitrate in the southern ocean: Consumption of nitrate in surface waters. *Global Biogeochemical Cycles*, 13(4), pp.1149–1166.

Sigman, D.M., Altabet, M.A., McCorkle, D.C., Francois, R., and Fischer, G., (2000). The δ15N of nitrate in the Southern Ocean: Nitrogen cycling and circulation in the ocean interior. *Journal of Geophysical Research: Oceans*, 105(C8), pp.19599-19614.

Sigman, D.M., and Boyle, E.A., (2000). Glacial/interglacial variations in atmospheric carbon dioxide. *Nature*, 407(6806), pp.859-869.

Silfer, J.A., Engel, M.H., and Macko, S.A., (1992). Kinetic fractionation of stable carbon and nitrogen isotopes during peptide bond hydrolysis: experimental evidence and geochemical implications. *Chemical Geology: Isotope Geoscience section*, 101(3-4), pp.211-221.

Sipler, R.E., and Bronk, D.A., (2015). Dynamics of dissolved organic nitrogen. *Biogeochemistry of Marine Dissolved Organic Matte*r, pp.127-232.

Sloyan, B.M., and Rintoul, S.R., (2001). The Southern Ocean limb of the global deep overturning circulation. *Journal of Physical Oceanography*, 31(1), pp.143-173.

Smart, S. M., Fawcett, S. E., Thomalla, S. J., Weigand, M. A., Reason, C. J. C., and Sigman, D. M., (2015). Isotopic evidence for nitrification in the Antarctic winter mixed layer. *Global Biogeochemical Cycles*, 29(4), pp.427–445.

Smart, S.M., Fawcett, S.E., Ren, H., Schiebel, R., Tompkins, E.M., Martínez-García, A., Stirnimann, L., Roychoudhury, A., Haug, G.H., and Sigman, D.M., (2020). The Nitrogen Isotopic Composition of Tissue and Shell-Bound Organic Matter of Planktic Foraminifera in Southern Ocean Surface Waters. *Geochemistry, Geophysics, Geosystems*, 21(2), pp.e2019GC008440.

Smith, J. M., Chavez, F. P., and Francis, C. A., (2014). Ammonium Uptake by Phytoplankton Regulates Nitrification in the Sunlit Ocean. *PLoS ONE*, *9*(9), pp.e108173.

Smith Jr, W.O., and Harrison, W.G., (1991). New production in polar regions: the role of environmental controls. *Deep Sea Research Part A. Oceanographic Research Papers*, 38(12), pp.1463-1479.

Smith Jr, W.O., and Lancelot, C., (2004). Bottom-up versus top-down control in phytoplankton of the Southern Ocean. *Antarctic Science*, 16(4), pp.531.

Smith Jr, W.O., Marra, J., Hiscock, M.R., and Barber, R.T., (2000). The seasonal cycle of phytoplankton biomass and primary productivity in the Ross Sea, Antarctica. *Deep Sea Research Part II: Topical Studies in Oceanography*, 47(15-16), pp.3119-3140.

Smetacek, V., Assmy, P., and Henjes, J., (2004). The role of grazing in structuring Southern Ocean pelagic ecosystems and biogeochemical cycles. *Antarctic Science*, 16(4), pp.541-558.

Soares, M.A., Bhaskar, P.V., Naik, R.K., Dessai, D., George, J., Tiwari, M., and Anilkumar, N., (2015). Latitudinal $\delta^{13}C$ and $\delta^{15}N$ variations in particulate organic matter (POM) in surface waters from the Indian ocean sector of Southern Ocean and the Tropical Indian Ocean in 2012. *Deep Sea Research Part II: Topical Studies in Oceanography*, 118, pp.186-196.

Sokolov, S., and Rintoul, S.R., (2007). On the relationship between fronts of the Antarctic Circumpolar Current and surface chlorophyll concentrations in the Southern Ocean. *Journal of Geophysical Research: Oceans*, 112(C7).

Sokolov, S., and Rintoul, S.R., (2009). Circumpolar structure and distribution of the Antarctic Circumpolar Current fronts: 2. Variability and relationship to sea surface height. *Journal of Geophysical Research: Oceans*, 114(C11).

Sosik, H.M., and Olson, R.J., (2002). Phytoplankton and iron limitation of photosynthetic efficiency in the Southern Ocean during late summer. *Deep Sea Research Part I: Oceanographic Research Papers*, 49(7), pp.1195-1216.

Squire, V.A., (1998). The marginal ice zone. *Physics of ice-covered seas*, 1, pp.381-446.

Steinberg, D.K., and Saba, G.K., (2008). Nitrogen consumption and metabolism in marine zooplankton. In: *Nitrogen in the marine environment,* edited by: Capone, D.G., Bronk, D.A., Mulholland, M.R., and Carpenter, E.J., 2nd Edition, Academic Press, Elsevier, pp.1135-1196.

Strickland, J.D.H., and Parsons, T.R., (1972). A practical handbook of seawater analysis.

Strzepek, R.F., Boyd, P.W., and Sunda, W.G., (2019). Photosynthetic adaptation to low iron, light, and temperature in Southern Ocean phytoplankton. *Proceedings of the National Academy of Sciences*, 116(10), pp.4388-4393.

Studer, A.S., Sigman, D.M., Martínez-García, A., Benz, V., Winckler, G., Kuhn, G., Esper, O., Lamy, F., Jaccard, S.L., Wacker, L., and Oleynik, S., (2015). Antarctic Zone nutrient conditions during the last two glacial cycles. *Paleoceanography*, 30(7), pp.845-862.

Sunda, W.G., and Huntsman, S.A., (1997). Interrelated influence of iron, light and cell size on marine phytoplankton growth. *Nature*, 390(6658), pp.389-392.

Tagliabue, A., Mtshali, T., Aumont, O., Bowie, A.R., Klunder, M.B., Roychoudhury, A.N., and Swart, S., (2012). A global compilation of dissolved iron measurements: focus on distributions and processes in the Southern Ocean. *Biogeosciences*, 9(6), pp.2333-2349.

Tagliabue, A., Sallée, J.B., Bowie, A.R., Lévy, M., Swart, S., and Boyd, P.W., (2014). Surface-water iron supplies in the Southern Ocean sustained by deep winter mixing. *Nature Geoscience*, *7*(4), pp.314-320.

Takao, S., Hirawake, T., Wright, S.W., and Suzuki, K., (2012). Variations of net primary productivity and phytoplankton community composition in the Indian sector of the Southern Ocean as estimated from ocean color remote sensing data. *Biogeosciences*, 9(10), pp.3875-3890.

Takeda, S., (1998). Influence of iron availability on nutrient consumption ratio of diatoms in oceanic waters. *Nature*, 393(6687), pp.774-777.

Talmy, D., Martiny, A.C., Hill, C., Hickman, A.E., and Follows, M.J., (2016). Microzooplankton regulation of surface ocean POC: PON ratios. *Global Biogeochemical Cycles*, 30(2), pp.311-332.

Taylor, B.W., Keep, C.F., Hall Jr, R.O., Koch, B.J., Tronstad, L.M., Flecker, A.S., and Ulseth, A.J., (2007). Improving the fluorometric ammonium method: matrix effects, background fluorescence, and standard additions. *Journal of the North American Benthological Society*, 26(2), pp.167-177.

Tevlin, A.G., and Murphy, J.G., (2019). Atmospheric Ammonia: Measurements, Modeling, and Chemistry–Climate Interactions. *Advances In Atmospheric Chemistry-Volume 2: Organic Oxidation And Multiphase Chemistry*, *2*, p.1.

Thomalla, S.J., Waldron, H.N., Lucas, M.I., Read, J.F., Ansorge, I.J., and Pakhomov, E., (2011). Phytoplankton distribution and nitrogen dynamics in the southwest indian subtropical gyre and Southern Ocean waters. *Ocean Science*, 7(1), pp.113-127.

Tilzer, M.M., and Dubinsky, Z., (1987). Effects of temperature and day length on the mass balance of Antarctic phytoplankton. *Polar Biology*, 7(1), pp.35-42.

Timmermans, K.R., Van Leeuwe, M.A., De Jong, J.T.M., McKay, R.M.L., Nolting, R.F., Witte, H.J., Van Ooyen, J., Swagerman, M.J.W., Kloosterhuis, H., and De Baar, H.J., (1998). Iron stress in the Pacific region of the Southern Ocean: evidence from enrichment bioassays. *Marine Ecology Progress Series*, 166, pp.27-41.

Timmermans, K.R., Van Der Wagt, B., and De Baar, H.J., (2004). Growth rates, half-saturation constants, and silicate, nitrate, and phosphate depletion in relation to iron availability of four large, open-ocean diatoms from the Southern Ocean. *Limnology and Oceanography*, 49(6), pp.2141-2151.

Tolar, B.B., Ross, M.J., Wallsgrove, N.J., Liu, Q., Aluwihare, L.I., Popp, B.N., and Hollibaugh, J.T., (2016). Contribution of ammonia oxidation to chemoautotrophy in Antarctic coastal waters. *ISME Journal*, 10(11), pp.2605–2619.

Tréguer, P., and Jacques, G., (1992). Review Dynamics of nutrients and phytoplankton, and fluxes of carbon, nitrogen and silicon in the Antarctic Ocean. In: *Weddell Sea Ecology*, edited by: Hempel, G., Springer, Berlin, Heidelberg, pp.149-162.

Trull, T.W., Bray, S.G., Manganini, S.J., Honjo, S., and Francois, R., (2001). Moored sediment trap measurements of carbon export in the Subantarctic and Polar Frontal Zones of the Southern Ocean, south of Australia. *Journal of Geophysical Research: Oceans*, 106(C12), pp.31489-31509.

Trull, T.W., Davies, D., and Casciotti, K., (2008). Insights into nutrient assimilation and export in naturally iron-fertilized waters of the Southern Ocean from nitrogen, carbon and oxygen isotopes. *Deep Sea Research Part II: Topical Studies in Oceanography*, 55(5-7), pp.820-840.

Tupas, L., and Koike, I., (1990). Amino acid and ammonium utilization by heterotrophic marine bacteria grown in enriched seawater. *Limnology and Oceanography*, 35(5), 1145–1155.

Utermöhl, H., (1958). Zur vervollkommnung der quantitativen phytoplankton-methodik: mit 1 Tabelle und 15 abbildungen im Text und auf 1 Tafel. *Internationale Vereinigung für theoretische und angewandte Limnologie: Mitteilungen*, 9(1), pp.1-38.

Vaulot, D., Courties, C., and Partensky, F., (1989). A simple method to preserve oceanic phytoplankton for flow cytometric analyses. *Cytometry: The Journal of the International Society for Analytical Cytology*, 10(5), pp.629-635.

Venkataramana, V., Anilkumar, N., Naik, R.K., Mishra, R.K., and Sabu, P., (2019). Temperature and phytoplankton size class biomass drives the zooplankton food web dynamics in the Indian Ocean sector of the Southern Ocean. *Polar Biology*, 42(4), pp.823-829.

Viljoen, J.J., Weir, I., Fietz, S., Cloete, R., Loock, J., Philibert, R., and Roychoudhury, A.N., (2019). Links between the phytoplankton community composition and trace metal distribution in summer surface waters of the Atlantic southern ocean. *Frontiers in Marine Science*, 6, p.295.

Volk, T., and Hoffert, M.I., (1985). Ocean carbon pumps: Analysis of relative strengths and efficiencies in ocean-driven atmospheric CO_2 changes. *The carbon cycle and atmospheric CO_2: natural variations Archean to present*, 32, pp.99-110.

Wadley, M.R., Jickells, T.D., and Heywood, K.J., (2014). The role of iron sources and transport for Southern Ocean productivity. *Deep Sea Research Part I: Oceanographic Research Papers*, 87, pp.82-94.

Wan, X.S., Sheng, H.X., Dai, M., Zhang, Y., Shi, D., Trull, T.W., Zhu, Y., Lomas, M.W., and Kao, S.J., (2018). Ambient nitrate switches the ammonium consumption pathway in the euphotic ocean. *Nature Communications*, 9(1), pp.1-9.

Ward, B. B., (1985). Light and substrate concentration relationships with marine ammonium assimilation and oxidation rates. *Marine Chemistry*, 16(4), pp.301–316.

Ward, B.B., (2005). Temporal variability in nitrification rates and related biogeochemical factors in Monterey Bay, California, USA. *Marine Ecology Progress Series*, 292, pp.97-109.

Weber, L.H., and El-Sayed, S.Z., (1987). Contributions of the net, nano-and picoplankton to the phytoplankton standing crop and primary productivity in the Southern Ocean. *Journal of Plankton Research*, 9(5), pp.973-994.

Wei, T., and Simko, V., (2017). R package "corrplot": Visualization of a Correlation Matrix (Version 0.84). https://github.com/taiyun/corrplot

Weir, I., Fawcett, S., Smith, S., Walker, D., Bornman, T., and Fietz, S., (2020). Winter biogenic silica and diatom distributions in the Indian sector of the Southern Ocean. *Deep Sea Research Part I: Oceanographic Research Papers*, 166, p.103421.

Welschmeyer, N.A., (1994). Fluorometric analysis of chlorophyll a in the presence of chlorophyll b and pheopigments. *Limnology and Oceanography*, 39(8), pp.1985-1992.

Wickham, H., (2016). ggplot2: Elegant Graphics for Data Analysis. Springer-Verlag New York. ISBN 978-3-319-24277-4, https://ggplot2.tidyverse.org

Wickham, H., and Seidel, D., (2020). scales: scale functions for visualisation, R package version 1.1.1, https://CRAN.R-project.org/package=scales

Wood, S., (2017). Generalized Additive Models: An Introduction with R, 2nd edition, Chapman and Hall/CRC.

Xu, G., Chen, L., Zhang, M., Zhang, Y., Wang, J., and Lin, Q., (2019). Year-round records of bulk aerosol composition over the Zhongshan Station, Coastal East Antarctica. *Air Quality, Atmosphere & Health*, 12(3), pp.271-288.

Yool, A., Martin, A.P., Fernández, C., and Clark, D.R., (2007). The significance of nitrification for oceanic new production. *Nature*, 447(7147), pp.999-1002.

Zakem, E. J., Al-Haj, A., Church, M. J., Van Dijken, G. L., Dutkiewicz, S., Foster, S. Q., Fulweiler, R. W., Mills, M. M., and Follows, M. J., (2018). Ecological control of nitrite in the upper ocean. *Nature Communications*, 9(1), pp.1–13.

Zhang, Y., Qin, W., Hou, L., Zakem, E.J., Wan, X., Zhao, Z., Liu, L., Hunt, K.A., Jiao, N., Kao, S.J., and Tang, K., (2020). Nitrifier adaptation to low energy flux controls inventory of reduced nitrogen in the dark ocean. *Proceedings of the National Academy of Sciences*, 117(9), pp.4823-4830.

Zhou, J., Delille, B., Kaartokallio, H., Kattner, G., Kuosa, H., Tison, J.L., Autio, R., Dieckmann, G.S., Evers, K.U., Jørgensen, L., and Kennedy, H., (2014). Physical and bacterial controls on inorganic nutrients and dissolved organic carbon during a sea ice growth and decay experiment. *Marine Chemistry*, 166, pp.59-69.